

PERFORMANCE MODELING AND ANALYSIS OF THE INTERPLAY AMONG TCP, ACTIVE QUEUE MANAGEMENT AND WIRELESS LINK ADAPTATION

A DISSERTATION SUBMITTED TO
THE GRADUATE SCHOOL OF ENGINEERING AND SCIENCE
OF BILKENT UNIVERSITY
IN PARTIAL FULFILLMENT OF THE REQUIREMENTS FOR
THE DEGREE OF
DOCTOR OF PHILOSOPHY
IN
ELECTRICAL AND ELECTRONICS ENGINEERING

By
Onur Öztürk
September, 2015

PERFORMANCE MODELING AND ANALYSIS OF THE INTER-
PLAY AMONG TCP, ACTIVE QUEUE MANAGEMENT AND
WIRELESS LINK ADAPTATION

By Onur Öztürk

September, 2015

We certify that we have read this thesis and that in our opinion it is fully adequate,
in scope and in quality, as a dissertation for the degree of Doctor of Philosophy.

Prof. Dr. Nail Akar (Advisor)

Prof. Dr. Ezhan Karahan

Prof. Dr. Murat Alanyalı

Prof. Dr. Erdal Arıkan

Asst. Prof. Dr. Mehmet Köseoglu

Approved for the Graduate School of Engineering and Science:

Prof. Dr. Levent Onural
Director of the Graduate School

ABSTRACT

PERFORMANCE MODELING AND ANALYSIS OF THE INTERPLAY AMONG TCP, ACTIVE QUEUE MANAGEMENT AND WIRELESS LINK ADAPTATION

Onur Öztürk

Ph.D. in Electrical and Electronics Engineering

Advisor: Prof. Dr. Nail Akar

September, 2015

We propose a novel workload-dependent queuing model of a wireless router link which employs active queue management and is offered with a number of persistent TCP flows. As opposed to existing work that focus only on the average queue occupancy as the performance metric of interest, the proposed analytical method obtains the more informative steady-state queue occupancy distribution of the wireless link. With the intention of maximizing TCP throughput, this analytical method is used to study traffic agnostic link adaptation schemes with and without hybrid ARQ.

Moreover, a novel cross-layer queue-aware link adaptation scheme is proposed to improve the TCP throughput relative to the case where adaptive modulation and coding decisions are made based solely on the physical layer parameters. A fixed-point analytical model is proposed to obtain the aggregate TCP throughput attained at wireless links employing active queue management and queue-aware link adaptation. Allowing packet retransmissions and generalizing the scope from a single link to a network of such links, we propose an energy efficient queue-aware link adaptation scheme with hybrid ARQ which jointly adapts the transmission power and rate of the wireless links based on the queue occupancy levels and the channel conditions. Furthermore, we provide a fixed-point analytical method for such networks.

Keywords: Link Adaptation, Adaptive Modulation and Coding, Wireless Networks, TCP, Cross-layer Queuing Analysis, Queue Awareness, Active Queue Management.

ÖZET

TCP, ETKİN KUYRUK YÖNETİMİ VE KABLOSUZ BAĞ UYARLAMASI ARASINDAKİ ETKİLEŞİMİN PERFORMANS MODELLEMESİ VE ÇÖZÜMLEMESİ

Onur Öztürk

Elektrik ve Elektronik Mühendisliği, Doktora

Tez Danışmanı: Prof. Dr. Nail Akar

Eylül, 2015

Etkin kuyruk yönetimi kullanan ve kendisine belirli bir sayıda sürekli TCP akışı sunulan bir kablosuz yönlendirici için, iş yükü bağımlı yeni bir kuyruk modeli önerilmiştir. Önerilen bu çözümlemeli yöntem, başarımlı ölçütü olarak sadece ortalama kuyruk doluluğunu alan mevcut çalışmaların aksine kablosuz bağın daha çok bilgi barındıran kararlı haldeki kuyruk doluluğu dağılımını elde etmektedir. TCP iş çıkarma yeteneğini ençoklamak amacıyla, bu çözümlemeli yöntem, melez otomatik tekrar talebinde bulunan ve bulunmayan iki trafik agnostik bağ uyarlama tekniğini çalışmak için kullanılmıştır.

Ayrıca, uyarlanırlı kipleme ve kodlama kararlarının sadece fiziksel katman parametrelerine göre verildiği duruma göre TCP iş çıkarma yeteneğini iyileştirecek katmanlar arası çalışan ve kuyruk farkındalıklı yeni bir bağ uyarlama tekniği önerilmiştir. Etkin kuyruk yönetimi ve kuyruk farkındalığını kullanan kablosuz bağlarda erişilen yekün TCP iş çıkarma yeteneğini elde etmek için sabit noktalı bir çözümleme önerilmiştir. Paket yeniden gönderimlerine izin vererek ve kapsamı tek bir bağdan böylesi bağların oluşturduğu bir ağa genelleştirerek, kuyruk doluluğu ve kanal durumuna göre gönderim gücünü ve hızını birlikte uyarlayan enerji etkin, melez otomatik tekrar talepli ve kuyruk farkındalıklı yeni bir bağ uyarlama tekniği önerilmiştir. Buna ek olarak, böylesi ağlar için sabit döngülü ve çözümlemeli bir yöntem önerilmiştir.

Anahtar sözcükler: Bağ Uyarlaması, Uyarlanırlı Kipleme ve Kodlama, Kablosuz Ağlar, TCP, Katmanlar Arası Kuyruk Çözümlemesi, Kuyruk Farkındalığı, Etkin Kuyruk Yönetimi.

Acknowledgement

I would like to express my deepest gratitude to Dr. Nail Akar for his constant and invaluable guidance throughout my graduate studies. I have been extremely fortunate to have such an encouraging and caring supervisor who has become more of a mentor to me in the meantime.

Dedicated to my beloved wife, Deniz...

Contents

List of Abbreviations and Acronyms	xv
1 Introduction	1
1.1 Motivation and Objectives of the Thesis	1
1.2 Scope of the Thesis	2
1.3 Contribution of the Thesis	4
1.3.1 Traffic-Agnostic Link Adaptation (TAGLA)	5
1.3.2 Traffic-Agnostic Link Adaptation with HARQ (TAGLAWH)	6
1.3.3 Queue-Aware Link Adaptation (QAWLA)	7
1.3.4 Energy Efficient Queue-Aware Link Adaptation with HARQ (EnQAWLAWH)	9
1.4 List of Publications	12
1.5 Organization of the Thesis	12
2 Background	14
2.1 Transmission Control Protocol (TCP)	14
2.2 Active Queue Management (AQM)	17
2.3 LTE and WiMAX	19
2.4 Link Adaptation (LA)	21
2.5 Green Communications	26
3 Traffic-Agnostic Link Adaptation (TAGLA)	28
3.1 Problem Description	28
3.2 Analytical Model	29
3.2.1 Workload-Dependent $M(x)/G/1$ Queue	29
3.2.2 Equation-Based TCP Model	31

3.2.3	Active Queue Management	32
3.2.4	Proposed Model	32
3.3	Model Validation	37
3.4	Cross Layer Framework	42
4	Traffic-Agnostic Link Adaptation with HARQ (TAGLAWH)	56
4.1	Problem Description	56
4.2	Analytical Model	57
4.2.1	$M(x)/G/1$ Queuing Model	58
4.2.2	Approximate Resequencing Delay Model	62
4.3	Numerical Results	64
5	Queue-Aware Link Adaptation (QAWLA)	72
5.1	Problem Description	72
5.2	Dual-Regime Wireless Link	73
5.3	Fixed-Point Analytical Model of DRWL	76
5.4	Wireless Link and Traffic Scenarios	82
5.5	Validation of the Analytical Model	85
5.6	Performance Evaluation of QAWLA	89
6	Energy Efficient Queue-Aware Link Adaptation with HARQ (EnQAWLAWH)	98
6.1	Problem Description	98
6.2	Analytical Model	99
6.2.1	Analytical Model of DRWN	103
6.2.2	Approximate DRWL Resequencing Delay Model	107
6.2.3	Network Performance Metrics	110
6.3	Validation of the Analytical Model	113
6.4	Performance Evaluation of EnQAWLAWH	125
7	Conclusion	138

List of Figures

1.1	Illustration of the LA framework presented in this thesis.	3
1.2	Methodology of this thesis.	4
1.3	Categorization of the LA schemes presented in this thesis.	12
2.1	Packet drop probability function of the GRED AQM scheme used in this thesis.	18
3.1	ns-3 simulation topology.	37
3.2	Queue occupancy PMF u_k for three values of N for Scenario A: $(D_L, D_F, D_{R_i}) = (5, 0, 5)$ ms.	39
3.3	Queue occupancy PMF u_k for three values of N for Scenario B: $(D_L, D_F, D_{R_i}) = (15, 0, 5 + 5[i/(N/10)])$ ms.	40
3.4	Queue occupancy PMF u_k for Scenario B with $N = 10$ and $r_L =$ 0.9 Mbps.	41
3.5	Queue occupancy PMF u_k for Scenario C: $(D_L, D_F, D_{R_i}) =$ $(5, 5, 10)$ ms with $PER_{m,s} = 0.1$ for three different N values. . . .	43
3.6	Queue occupancy PMF u_k for Scenario C: $(D_L, D_F, D_{R_i}) =$ $(5, 5, 10)$ ms with $PER_{m,s} = 0.01$ for three different N values. . .	44
3.7	Queue occupancy PMF u_k for Scenario C: $(D_L, D_F, D_{R_i}) =$ $(5, 5, 10)$ ms with $PER_{m,s} = 0.001$ for three different N values. . .	45
3.8	Simulated FER $FER_{m,s}$ for the AWGN channel.	46
3.9	Simulated FER $FER_{m,s}$ for the ITU-A channel.	47
3.10	Optimum MCS selection for the AWGN channel as a function of SNR level SNR_s for scenarios $SF_{1,160}$, $SF_{4,160}$ and $SF_{16,160}$ cor- responding to $RTT_{0,i} = 160$ ms and $N = 1$, $N = 4$, $N = 16$, respectively.	49

3.11	Average aggregate TCP throughput achieved by the <i>optimum policy</i> and <i>TAGLA</i> averaged over SNR_s for each scenario of Table 3.2 for the AWGN channel.	50
3.12	Average aggregate TCP throughput achieved by the <i>optimum policy</i> and <i>TAGLA</i> averaged over SNR_s for each scenario of Table 3.3 for the ITU-A channel.	51
3.13	Average normalized aggregate TCP throughput achieved by <i>TAGLA</i> averaged over SNR_s for scenarios G_{all} , G_{low} , and G_{high} for the AWGN channel.	54
3.14	Average normalized aggregate TCP throughput achieved by <i>TAGLA</i> averaged over SNR_s for scenarios G_{all} , G_{low} , and G_{high} for the ITU-A channel.	55
4.1	Simulated FER $FER_{m,s,z}$ for $Z = 3$ maximum number of allowed retransmissions and the ITU Vehicular-A channel.	65
4.2	Probability of failure in the first transmission $P_{m,s,0}$ of TAGLAWH for varying SNR values SNR_s and threshold parameter th_P	67
4.3	Normalized aggregate TCP throughput of TAGLAWH averaged over all SNR values SNR_s for varying traffic scenarios $S_{N,F}$ and threshold parameter th_P , and for $Z = 3$ maximum number of allowed retransmissions.	69
4.4	Average and minimum (worst case) normalized aggregate TCP throughput of TAGLAWH taken over all SNR values SNR_s and traffic scenarios $S_{N,F}$ for varying threshold parameter th_P and maximum number of allowed retransmissions Z	70
4.5	Average and maximum (worst case) mean resequencing delay $X_{m,s}$ of TAGLAWH taken over all SNR values SNR_s and traffic scenarios $S_{N,F}$ for varying threshold parameter th_P and maximum number of allowed retransmissions Z	71
5.1	Illustration of DRWL with the x -axis representing the queue occupancy x	75
5.2	Simulated PER $per_{m,s}$ for different values of the MCS index m and the AWGN channel.	83

5.3	Simulated PER $per_{m,s}$ for different values of the MCS index m and the ITU-A channel.	84
5.4	ns-3 simulation topology.	85
5.5	The empirical queue occupancy PMF u_k for the scenario with $idx = 2$ for varying $B \in \{10, 20, 30\}$, all having the same fixed-point solution with a queue occupancy level of 3.9049 packets. . .	89
5.6	The empirical queue occupancy PMF u_k for scenarios with $idx \in \{3, 4, 11, 13, 14, 18\}$ and $B = 20$. Analytical results are also depicted.	90
5.7	Mean normalized aggregate TCP throughput $\mathbf{T_M}$ of TAGLA and QAWLA as a function of th_{PER} with $H \in \{10, 100, 1000\}$ and $B \in \{20, 30, 40\}$ for the AWGN channel.	92
5.8	Mean normalized aggregate TCP throughput $\mathbf{T_M}$ of TAGLA and QAWLA as a function of th_{PER} with $H \in \{10, 100, 1000\}$ and $B \in \{20, 30, 40\}$ for the ITU-A channel.	93
5.9	Mean normalized aggregate TCP throughput $\mathbf{T_M}$ of TAGLA and QAWLA as a function of th_{PER} with $H = 100$ and $B = 20$ for the AWGN channel.	94
5.10	Mean normalized aggregate TCP throughput $\mathbf{T_M}$ of TAGLA and QAWLA as a function of th_{PER} with $H = 100$ and $B = 20$ for the ITU-A channel.	95
5.11	Worst case normalized aggregate TCP throughput $\mathbf{T_W}$ of TAGLA and QAWLA as a function of th_{PER} with $H = 100$ and $B = 20$ for the AWGN channel.	96
5.12	Worst case normalized aggregate TCP throughput $\mathbf{T_W}$ of TAGLA and QAWLA as a function of th_{PER} with $H = 100$ and $B = 20$ for the ITU-A channel.	96
6.1	Illustration of DRWL with the x -axis representing the queue occupancy x	102
6.2	Simulated FER $fer_{m,s,z}$ for $Z = 3$ maximum number of allowed retransmissions and the AWGN channel.	114
6.3	ns-3 simulation topology.	118
6.4	Topology A chosen for the performance evaluation of DRWN. . .	125
6.5	Topology B chosen for the performance evaluation of DRWN. . .	126

6.6	$\Theta(0.75)$ averaged over two topologies and three SNR_2 values for the EnQAWLAWH(B, Ω, th_P, Z) = (.,.,0.25,3) scheme.	127
6.7	CDF of Θ of Topology A and B with links having randomized SNR_2 for various values of β for the EnQAWLAWH(B, Ω, th_P, Z) = (4C,3,0.25,3) scheme.	128
6.8	CDF of E_pBRP of Topology A and B with links having randomized SNR_2 for the EnQAWLAWH(B, Ω, th_P, Z) = (4C,3,0.25,3) scheme.	129
6.9	CDF of $FRTT_n$ of Topology A with randomized flow routes for various values of N and SNR_2 for the EnQAWLAWH(B, Ω, th_P, Z) = (4C,3,0.25,3) scheme. Mean value of $FRTT_n$ for each CDF is annotated inside the corresponding legend box.	131
6.10	CDF of $FRTT_n$ of Topology B with randomized flow routes for various values of N and SNR_2 for the EnQAWLAWH(B, Ω, th_P, Z) = (4C,3,0.25,3) scheme. Mean value of $FRTT_n$ for each CDF is annotated inside the corresponding legend box.	132
6.11	CDF of $FPLR_n$ of Topology A with randomized flow routes for various values of N and SNR_2 for the EnQAWLAWH(B, Ω, th_P, Z) = (4C,3,0.25,3) scheme. Mean value of $FPLR_n$ for each CDF is annotated inside the corresponding legend box.	133
6.12	CDF of $FPLR_n$ of Topology B with randomized flow routes for various values of N and SNR_2 for the EnQAWLAWH(B, Ω, th_P, Z) = (4C,3,0.25,3) scheme. Mean value of $FPLR_n$ for each CDF is annotated inside the corresponding legend box.	134
6.13	CDF of Θ of Topology A with randomized flow routes for various values of N , β and SNR_2 for the EnQAWLAWH(B, Ω, th_P, Z) = (4C,3,0.25,3) scheme. Mean value of Θ for each CDF is annotated inside the corresponding legend box.	136
6.14	CDF of Θ of Topology B with randomized flow routes for various values of N , β and SNR_2 for the EnQAWLAWH(B, Ω, th_P, Z) = (4C,3,0.25,3) scheme. Mean value of Θ for each CDF is annotated inside the corresponding legend box.	137

List of Tables

3.1	Modulation and coding schemes of IEEE 802.16 used in this study.	43
3.2	Scenarios $SF_{N,F}$ and $SU_{N,F}$ indexed by increasing throughput of <i>optimum policy</i> for the AWGN channel.	52
3.3	Scenarios $SF_{N,F}$ and $SU_{N,F}$ indexed by increasing throughput of <i>optimum policy</i> for the ITU-A channel.	53
4.1	Modulation and coding schemes of IEEE 802.16 used in this study.	64
4.2	Resequencing delay validation test cases and results for $Z = 3$. Results are presented with the 99% confidence intervals.	66
5.1	Modulation and coding schemes of IEEE 802.16 used in this study.	82
5.2	The list of eighteen traffic scenarios indexed with <i>idx</i> used for validation of the fixed-point analytical model proposed for DRWL for the ITU-A channel model.	86
5.3	Aggregate TCP throughput T obtained with ns-3 simulations and the fixed-point analytical model for $B = 10$. Results for ns-3 simulations are presented with the 99% confidence intervals. . . .	87
5.4	Aggregate TCP throughput T obtained with ns-3 simulations and the fixed-point analytical model for $B = 20$. Results for ns-3 simulations are presented with the 99% confidence intervals. . . .	88
5.5	Aggregate TCP throughput T obtained with ns-3 simulations and the fixed-point analytical model for $B = 30$. Results for ns-3 simulations are presented with the 99% confidence intervals. . . .	88
5.6	Comparison of the mean ($\mathbf{T_M}$) and the worst case ($\mathbf{T_W}$) normalized aggregate TCP throughput performances of TAGLA and QAWLA for the AWGN and the ITU-A channels.	97

6.1	Modulation and coding schemes of IEEE 802.16 used in this study.	113
6.2	DRWL resequencing delay validation test cases and results for $Z = 3$. Results are presented with the 99% confidence intervals.	116
6.3	The list of eighteen traffic scenarios of Scenario Sets A, B and C with $B = 2C$, $B = 4C$ and $B = 8C$, respectively, and with $(th_P, Z) = (0.25, 3)$ used for validation of the fixed-point analytical model proposed for DRWL for the AWGN channel model.	120
6.4	The list of eighteen traffic scenarios of Scenario Set D with $(B, \Omega, th_P, Z) = (4C, 3, 0.25, 3)$ used for validation of the fixed-point analytical model proposed for DRWL for the AWGN channel model.	120
6.5	The list of eighteen traffic scenarios of Scenario Set E with $(B, \Omega, th_P, Z) = (4C, 3, 0.25, 3)$ used for validation of the fixed-point analytical model proposed for DRWL for the AWGN channel model.	121
6.6	TCP throughput and energy statistics obtained with ns-3 simulations and the fixed-point analytical model for Scenario Set A. . .	122
6.7	TCP throughput and energy statistics obtained with ns-3 simulations and the fixed-point analytical model for Scenario Set B. . . .	123
6.8	TCP throughput and energy statistics obtained with ns-3 simulations and the fixed-point analytical model for Scenario Set C. . .	123
6.9	TCP throughput and energy statistics obtained with ns-3 simulations and the fixed-point analytical model for Scenario Set D. . .	124
6.10	TCP throughput and energy statistics obtained with ns-3 simulations and the fixed-point analytical model for Scenario Set E. Results for ns-3 simulations are presented with the 99% confidence intervals.	124

List of Abbreviations and Acronyms

3GPP	3rd Generation Partnership Project
ABE	Available Bandwidth Estimation
ACK	Acknowledgment
AMC	Adaptive Modulation and Coding
AQM	Active Queue Management
ARQ	Automatic Repeat Request
AWGN	Additive White Gaussian Noise
BER	Bit Error Rate
BLER	Block Error Rate
BS	Base Station
BW	Bandwidth
CC	Chase Combining
CDF	Cumulative Distribution Function
CDMA	Code Division Multiple Access
CE	Congestion Experienced
CINR	Carrier-to-Interference-and-Noise Ratio
CML	Coded Modulation Library
CQI	Channel Quality Indicator
CSI	Channel State Information
CTC	Convolutional Turbo Codes

CW	Congestion Window
DL	Downlink
DRWL	Dual-Regime Wireless Link
DRWN	Dual-Regime Wireless Network
DTX	Discontinuous Transmission
DUPACK	Duplicate Acknowledgment
ECE	Explicit Congestion Echo
ECN	Explicit Congestion Notification
EE	Energy Efficiency
EESM	Exponential Effective SNR Mapping
eNB	Evolved Node B
EnQAWLA_wH	Energy Efficient Queue-Aware Link Adaptation with HARQ
ERD	Early Random Detection
FEC	Forward Error Correction
FER	FEC Block Error Rate
FIFO	First-In-First-Out
FS	Fixed Station
FTP	File Transfer Protocol
FTT	Fast Fourier Transform
GRED	Gentle RED
HARQ	Hybrid ARQ
iid	Independent and Identically Distributed
IoT	Internet of Things
IP	Internet Protocol
IR	Incremental Redundancy
ITU	International Telecommunication Union

ITU-A	ITU Vehicular-A
JOCP	Jointly Optimal Congestion Control and Power Control
JQLA	Joint Queue Length Aware
LA	Link Adaptation
LAN	Local Area Network
LLR	Log-Likelihood Ratio
LTE	Long Term Evolution
MCDM	Multi-Criteria Decision Making
MCS	Modulation and Coding Scheme
MD	Monotonically Decreasing
MI	Monotonically Increasing
MIMO	Multiple-Input-Multiple-Output
MMIB	Mean Mutual Information per Coded Bit
MMSE	Minimum Mean Square Error
MND	Monotonically Non-Decreasing
MRC	Maximal-Ratio Combining
MS	Mobile Station
NACK	Negative Acknowledgment
NC	Network Coding
OFDM	Orthogonal Frequency Division Multiplexing
OLA	Optimum Link Adaptation
OPEX	Operational Expenditure
PA	Power Amplifier
PAPR	Peak-to-Average-Power-Ratio
PDF	Probability Density Function
PER	Packet Error Rate

PHY	Physical Layer
PMF	Probability Mass Function
PTP	Point-To-Point
QAM	Quadrature-Amplitude-Modulation
QAWLA	Queue-Aware Link Adaptation
QoS	Quality of Service
RAN	Radio Access Network
RB	Resource Block
RED	Random Early Detection
RL	Reinforcement Learning
RTT	Round-Trip Time
RV	Random Variable
RW	Receive Window
RX	Receive
SE	Spectral Efficiency
SINR	Signal-to-Noise-plus-Interference Ratio
SISO	Single-Input-Single-Output
SM	Spatial Multiplexing
SNR	Signal-to-Noise-Ratio
SR	Selective Repeat
SRWN	Single-Regime Wireless Network
SS	Subscriber Station
SW	Stop-and-Wait
TAGLA	Traffic-Agnostic Link Adaptation
TAGLA_{wH}	Traffic-Agnostic Link Adaptation with HARQ
TCP	Transmission Control Protocol
TDD	Time Division Duplex
TX	Transmit

UDP	User Datagram Protocol
UE	User Equipment
WCS	Wireless Communication System
WiMAX	Worldwide Interoperability for Microwave Access
WLOG	Without Loss of Generality
WRED	Weighted Random Early Detection
ZF	Zero Forcing

Chapter 1

Introduction

1.1 Motivation and Objectives of the Thesis

With emerging high capacity wideband Wireless Communication Systems (WCSs) such as Long Term Evolution (LTE) and Worldwide Interoperability for Microwave Access (WiMAX), improving spectral and energy efficiency of such systems has become one of the major areas of study. Link Adaptation (LA) is the mechanism present in most WCSs responsible for controlling certain transmission parameters such as transmission power, modulation and coding level, etc., based on the current channel conditions with the ultimate goal of maximizing overall spectral and/or energy efficiency. When the parameters of higher layer traffic such as Transmission Control Protocol (TCP) are taken into consideration in the design of the LA schemes, the problem requires cross-layer handling. The objectives of this thesis are to devise a novel cross-layer queuing framework to characterize and model the interplay among TCP, Active Queue Management (AQM) and LA, and to propose novel implementation-friendly LA schemes with improved performance regarding TCP-level throughput and network-wide Energy Efficiency (EE).

1.2 Scope of the Thesis

Cross-layer analysis of TCP, AQM and LA can be described by the following abstract queuing problem. Consider a queuing system with M potential servers denoted by \mathcal{S}_j where $j \in \{0, 1, \dots, M-1\}$. We envision a decision entity which is to choose a particular server out of this server pool. The server \mathcal{S}_j is characterized by a number of features such as the packet service rate r_j , the loss probability of the packet in service p_j , the cost of serving a packet c_j , etc. The packets into the queuing system are generated by N different elastic sources whose sending rates are allowed to depend on the queue occupancy denoted by x , as well as the chosen server itself. Moreover, the arriving packets to the queue are probabilistically dropped according to a drop probability function $q(x)$. The queuing system can further be extended by allowing servers to retry servicing the lost packets. The queuing problem at hand is to choose the best server to optimize the performance for a given metric such as the overall throughput, the overall cost, etc. To motivate the queuing problem, first assume a pool of servers differentiated from each other according to the service rate only. In this case, the best server would typically be the one with the highest service rate. However, there might be cases in which some servers might have high service rates and high loss rates (or high costs) and other servers might have low service rates and low loss rates (or low costs). In this situation, the choice of the best server is not straightforward for a given performance metric. Moreover, the decision to choose the best server may also depend on other traffic parameter such as N and also the way by which these sources generate packets.

The abstract queuing system described in the previous paragraph plays a role in different disciplines including WCSs which is the main scope of this thesis. In the context of WCSs, \mathcal{S}_j corresponds to a Modulation and Coding Scheme (MCS) offered by the physical layer (PHY), and the aforementioned cost can be viewed as the energy consumed by the wireless transmitter. Furthermore, drop probability function $q(x)$ describes the employed AQM scheme. We address the LA problems of choosing the best possible MCS to maximize the total throughput of TCP flows or to minimize the total energy consumption of the wireless network. A typical

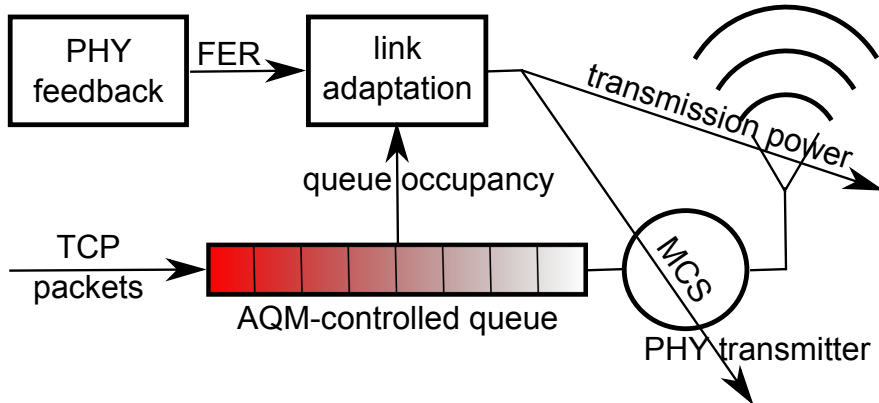


Figure 1.1: Illustration of the LA framework presented in this thesis.

LA process comprises the following two components: (i) estimation of the channel error statistics (ii) selection of an MCS based on a predetermined target range for error statistics. We study the second component for WCSs with and without Hybrid Automatic Repeat Request (HARQ). We let Packet Error Rate (PER) which is directly related to TCP throughput to be the error statistics of interest in the absence of HARQ or the probability of failure in the first transmission attempt otherwise. We also study the LA to jointly determine the target MCS and the transmission power within the context of EE. We outline algorithms to obtain link-level and network-wide solutions, whichever is applicable, to the presented LA schemes. We illustrate the LA framework of this thesis in Fig. 1.1. The channel error statistics in the form of Forward Error Correction (FEC) block Error Rate (FER) estimations for each MCS are assumed to be provided to “link adaptation” by “PHY feedback”. We carry out the performance analysis of the LA schemes for the Additive White Gaussian Noise (AWGN) and the ITU Vehicular-A multipath fading channels [1], for the latter of which the average FER performance over all realizations of the channel (via simulations) is taken into account rather than the individual ones.

Throughout this thesis, we use the IEEE 802.16 as the underlying PHY technology for the proposed cross-layer queuing framework, but the framework allows other technologies to be used if needed. Performance of the analyzed LA schemes as well as their proposed parameters, however, may change depending on the

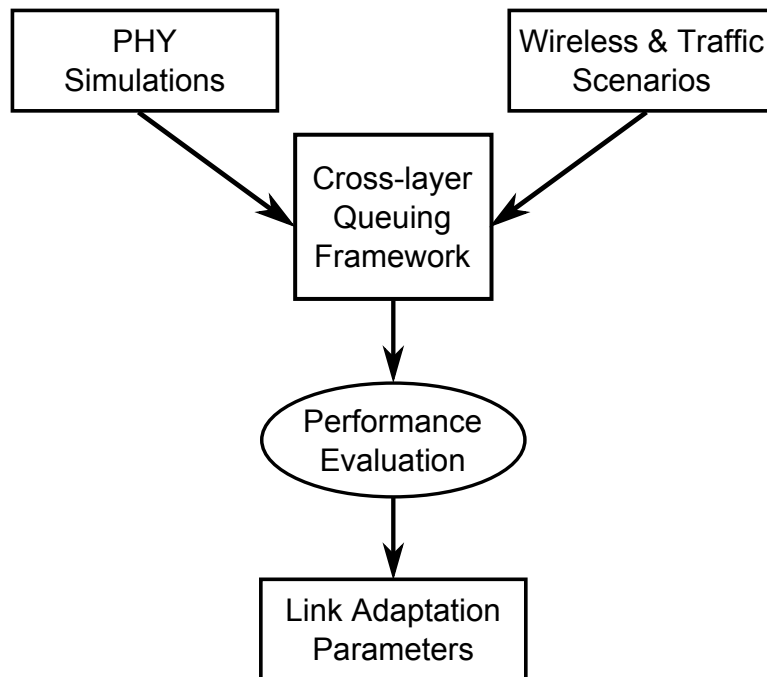


Figure 1.2: Methodology of this thesis.

underlying PHY technology. In Fig. 1.2, the methodology followed to design and analyze the LA schemes is depicted. In order to evaluate the performance and tune the parameters of the proposed LA schemes, PHY simulation results together with the wireless and TCP traffic scenarios are fed into the cross-layer queuing framework which is also validated with extensive ns-3 [2] and MATLAB® simulations.

1.3 Contribution of the Thesis

In this section, we highlight the contributions made by Chapter 3 through Chapter 6 along with the review of the related literature. Each chapter presents a novel analytical model used for the performance evaluation of the LA scheme studied therein. The novel queue-aware LA schemes referred to as QAWLA and En-QAWLAwH proposed in Chapter 5 and Chapter 6, respectively, are also among the main contributions of this thesis.

1.3.1 Traffic-Agnostic Link Adaptation (TAGLA)

A comparison of different approaches for improving TCP performance over wireless links is provided in [3]. The reference [4] uses the so-called “square-root” formula to analytically study the interaction between TCP and the amount of FEC to be used in wireless links. This study is then extended to the interaction of TCP and Automatic Repeat Request (ARQ) with Selective Repeat (SR), and in-order delivery of packets to the Internet Protocol (IP) layer, using the so-called “PFTK” formula [5]. Optimal design and analysis of hybrid FEC/ARQ schemes in TCP context is studied in [6] and [7] with Rayleigh fading. A recent work in [8] analyzes a wireless link with FEC and ARQ using fixed-point approximations and the PFTK formula in an $M/M/1/K$ setting. None of these references, however, focus on the interplay among TCP, AQM and LA for the purpose of proposing practical LA schemes. One of the goals of Chapter 3 is to introduce a novel queuing model for AQM-controlled wireless links with the specific goal of obtaining the steady-state queue occupancy distribution. The main contribution of Chapter 3 published in [9] is as follows:

- We introduce a novel workload-dependent $M/D/1$ queuing framework based on the $M(x)/G/1$ queuing model of [10] for an AQM-controlled wireless link with Bernoulli packet losses using the PFTK formula taking into account both the fast retransmit mechanism of TCP-Reno and the effect of TCP timeout on TCP packet sending rate to obtain the entire queue occupancy distribution. In most existing work such as [11] and [12], the focus has been on the mean queue occupancy as well as the average packet loss probability due to congestion. Moreover, fixed packet sizes are generally not taken into account. The following are the main features of the proposed model: (i) The proposed model provides a good match with simulations even in the vicinity of “empty queues” as opposed to other existing models. The empty queues scenario is particularly important when an MCS is used with high wireless loss rates and TCP sources throttle back relatively aggressively in a way that they cannot keep the queue full all the time. (ii) The analytical model presented in the reference [12] suffers when the

workload-dependent AQM packet drop probability is discontinuous with respect to the workload whereas the performance of our proposed method is insensitive to such behavior. (iii) The proposed method can further be used in the analysis of Quality of Service (QoS) differentiation mechanisms relying on per-class buffer management such as Weighted Random Early Detection (WRED) [13],[14].

- We present a novel cross-layer framework based on the proposed queuing model to obtain a range of target PERs that needs to be maintained by a PER-based Traffic-AGnostic LA (TAGLA) scheme for TCP throughput optimization. By being traffic-agnostic, optimality is shown to be sacrificed but the proposed range of target PERs allows one to obtain robust TCP performance for a wide range of traffic parameters including the number of TCP flows, their Round-Trip Times (RTTs), etc. In this description, a robust policy refers to one that does not deviate much from an optimal policy that requires a-priori information about the underlying traffic parameters.

1.3.2 Traffic-Agnostic Link Adaptation with HARQ (TAGLAwH)

In [15], the authors derive closed form analytical expressions for various performance metrics of different HARQ schemes, but they do not particularly study the TCP protocol. The reference [8] analyzes TCP performance of HARQ but assumes acknowledgment/negative acknowledgment (ACK/NACK) feedback for retransmissions to be instantaneous. In a more recent study [7], the authors analytically compare the performances of HARQ and ARQ schemes for TCP but they take neither packet re-ordering nor AQM into account. In Chapter 3, the $M(x)/G/1$ queuing model of [10] is adopted to relate the workload (queue occupancy level)-dependent loss and delay parameters of a wireless AQM router to aggregate TCP-level throughput with the ultimate aim of evaluating performance of an LA scheme called TAGLA with single transmission opportunity. TAGLA, indifferent to any TCP layer parameter, makes a selection among the offered

MCSs by its PHY based on their individual capacities and PER estimations. The main contribution of Chapter 4 published in [16] is as follows:

- We extend the queuing framework of Chapter 3 to accommodate the HARQ transmission technique and address the aforementioned deficiencies of the references [15], [8] and [7]. We introduce an approximate but simple resequencing delay model which makes this extension possible. We believe the proposed resequencing model would be useful to other researchers in need of a simple model with an acceptable accuracy.
- We obtain a range for the target rate of failure in the first transmission attempt that needs to be maintained by the TAGLA scheme with HARQ for average TCP throughput maximization.

1.3.3 Queue-Aware Link Adaptation (QAWLA)

In this chapter, we study a wireless bottleneck link carrying long-lived TCP-Reno traffic flows with AQM buffer management and Adaptive Modulation and Coding (AMC)-based LA. The interplay between these two components is the main topic of study of this chapter with the goal of potentially increasing the total TCP throughput. An aggressive MCS with high block error rates may lead to high PER which in turn throttles back the TCP sources, potentially leading to a queue with a high service rate but which is occasionally empty. PHY resources would be wasted in this situation when the queue is empty. On the other hand, a conservative MCS result in low PER leading to a situation with non-empty queues but with a lower service rate. Based on these observations, we propose a Queue-Aware Link Adaptation (QAWLA) scheme which employs an aggressive (conservative) MCS when the queue occupancy remains above (below) a certain queue threshold, leading to a Dual-Regime Wireless Link (DRWL). Queue-awareness has been extensively studied in the context of wireless scheduling in multi-user WCSs [17],[18],[19],[20]. EE is another subject of WCSs for which queue-awareness allows joint control of the transmission power and rate for given QoS constraints [21],[22],[23],[24]. Assuming an error-free Point-To-Point (PTP)

link operating at the channel capacity, the reference [25] devises an optimal power control scheme called Joint Queue Length Aware (JQLA) power control for a set of QoS constraints comprising packet drop probability (which occurs due to finite buffer length), maximum delay and the arrival rate. In a simulation-based study, the authors propose a distributed traffic-aware power control algorithm for multi-hop IEEE 802.11 wireless networks adapting transmission rates to satisfy the network-wide traffic demand [26]. For a fixed Signal-to-Noise-plus-Interference Ratio (SINR) level, however, a single MCS satisfying a pre-determined Bit Error Rate (BER) is chosen. By disseminating the so-called “virtual buffers” throughout the nodes of a hybrid wired and Code Division Multiple Access (CDMA) wireless cellular network with a distributed algorithm, joint transmission power and rate optimization is formulated as a network utility maximization problem which can be solved by the congestion control algorithms of TCP [27]. The so-called Jointly Optimal Congestion control and Power control (JOCP) algorithm outlined in the reference [28], on the other hand, iteratively updates the transmission power of each node in a multi-hop wireless network by sharing weighted queuing delay information in a distributed manner assuming TCP-Vegas to be the source of the generated traffic. Convergence of JOCP, however, is not guaranteed for TCP-Reno whose congestion control relies on packet losses rather than delays as with TCP-Vegas. Finally, the presented AMC scheme in the reference [29] for an interference-limited two-hop relay network chooses an MCS based on both the current SINR level and the number of available packets in the transmission queue of the relay node, whichever suggests the minimum, but does not take into account any higher layer traffic such as TCP. To the best of our knowledge, this is the first study employing queue-awareness in AMC decisions to specifically improve TCP-Reno throughput performance. The main contribution of Chapter 5 is as follows:

- We propose a fixed-point model of a single AQM-controlled wireless link with AMC decisions being based on the DRWL framework. Our modeling work is substantially different than [12] due to the special behavior at the boundary between the two regimes of interest. In [12], the queue service rate is fixed for all queue occupancies. However, in the current study, not

only the queue service rate but also the wireless packet error rate depends on the queue occupancy in a piece-wise continuous manner with a discontinuity at a single boundary point. Such discontinuities lead to scenarios where the boundary point may become the steady-state fluid limit and the conventional fixed-point model of [12] falls short of modeling discontinuous queue service rates and wireless packet loss rates. For such scenarios, we propose an extended fixed-point analytical model to model TCP throughput in AQM-controlled wireless links in the current study. The computational complexity of the proposed fixed-point analytical model is low enough to enable the exploration of the multi-dimensional problem space spanned by the number of TCP flows, the number of MCSs, and varying Signal-to-Noise-Ratio (SNR) levels, which would not be feasible with a study based solely on simulations. Existence and uniqueness conditions are presented for the solution of the fixed-point analytical model.

- Using the findings of the stochastic model, we obtain tangible results showing that robust TCP-level throughput improvement is attainable using QAWLA in a wide variety of scenarios. We show that relative to TAGLA, QAWLA is less sensitive to its choice of parameters and possible errors in channel assessment, which highlight its robustness.

1.3.4 Energy Efficient Queue-Aware Link Adaptation with HARQ (EnQAWLAwH)

Relying on sounding packets, the work in [30] solves the multi-dimensional (modulation order, coding rate, transmission power, number of RX/TX antennas and spatial streams) link adaptation problem for a given target throughput and packet loss rate for a Multiple-Input-Multiple-Output (MIMO)-Orthogonal Frequency Division Multiplexing (OFDM) system. The reference [31] proposes a joint power and rate adaptation algorithm for 802.11 wireless Local Area Networks (LANs), but does not make use of any transport layer information. In the references

[32] and [21], the authors study an EE scheduler adapting itself to both channel conditions and queued packets for a given delay constraint for time invariant and time-varying channels, respectively. Cross-layer design offers ample opportunities for the EE [33] provided that the associated complexity such as protocol/signaling overhead itself, does not lead to unintended inefficiency in terms of energy consumption [34]. A centralized joint power allocation and scheduling algorithm with a threshold-based rate selection for multi-hop wireless networks for given QoS constraints is presented in [35]. In a simulation-based study, the authors propose a QoS-aware green downlink scheduler which adaptively downgrades the MCS in order to lower transmission power [23]. In the reference [24], a Multi-Criteria Decision Making (MCDM)-based algorithm is proposed for the Energy Efficiency-Spectral Efficiency (EE-SE) optimization by adapting downlink data rate and transmission power for real-time traffic under certain delay constraints. Moreover, the work presented in [27] studies the interaction between congestion control and LA in wireless cellular CDMA networks and proposes algorithms reaching jointly optimal rate and power pairs for both interference-free and interference-limited scenarios, the former requiring an iterative bidding mechanism between the Base Station (BS) and the Mobile Stations (MSs). The author studies in [28] a distributed algorithm called JOCP which is jointly optimal for the congestion control of TCP-Vegas and power control in interference-limited multi-hop wireless networks. The main contribution of Chapter 6 is as follows:

- We extend the dual regime queuing framework of Chapter 5 to accommodate the HARQ transmission technique. For this purpose, we first modify the approximate resequencing delay model introduced in Chapter 4 to model retransmissions made at the regime boundary.
- We propose an Energy efficient and Queue-Aware Link Adaptation scheme with HARQ (EnQAWLAwH) trying to relinquish some portion of the link capacity that is not claimed by the contending TCP flows in return for a reduction in transmission power. In this respect, EnQAWLAwH belongs to the class of algorithms targeting the SE-EE tradeoff for which we express SE in terms of transport layer bits instead of PHY bits. In EnQAWLAwH,

retransmission statistics are collected so as to jointly choose a transmission power and a transmission rate (by means of the available MCSs) for the wireless link. Moreover, such decisions are allowed to depend on the queue occupancy. In this study, the focus is only on the case where the decisions are local and based on whether the queue is in a low or high occupancy regime dictated by a queue occupancy threshold. In other words, EnQAWLAWH requires no exchange of information among the nodes in the network, and thus does not yield additional protocol overhead which in turn makes EnQAWLAWH a scalable solution. EnQAWLAWH has a cross-layer design, yet it respects the modularity of the protocol stack.

- We present an algorithm to efficiently solve networks of dual-regime queues with arbitrary topology which in turn enables us to model a wide variety of wireless, traffic and network scenarios for the performance evaluation of the proposed EnQAWLAWH scheme.

In Fig. 1.3, the four aforementioned LA schemes studied in this thesis are depicted in a two-dimensional tabular form with the dimensions of HARQ availability and queue-awareness. QAWLA scheme exploits queue-awareness for robust TCP-level throughput improvement. To explain, a low target PER leads to a situation in which losses are mostly due to AQM drops but since the service rate of the queue would be relatively limited to achieve a low PER, reduced TCP-level throughput is inevitable. On the other hand, a high target PER increases the queue service rate but it becomes quite possible that the queue would occasionally be empty due to substantial wireless losses stemming from TCP reaction to such losses. Based on this observation, QAWLA scheme uses an aggressive (conservative) MCS when the queue occupancy is high (low) in order to achieve its objective. On the other hand, EnQAWLAWH scheme targets network-wide EE improvement using queue-awareness. Employing HARQ retransmissions, EnQAWLAWH reduces the wireless packet losses to a negligible level so that the empty queue situations become indicators of TCP flows being bottlenecked elsewhere in the network. In such cases, transmission energy can be saved by reducing the capacity of each wireless link to the level which matches the throughput demand of the TCP flows from that link. Based on this observation, EnQAWLAWH


	queue unaware		queue aware
without HARQ	TAGLA	robustness & performance	QAWLA
with HARQ	TAGLAWH	energy efficiency	EnQAWLAWH

Figure 1.3: Categorization of the LA schemes presented in this thesis.

scheme uses high (low) transmission power along with an MCS with high (low) spectral efficiency when the queue occupancy is high (low) in order to achieve its objective.

1.4 List of Publications

Publications arising from Chapter 3 and Chapter 4 of this thesis are respectively as follows:

O. Ozturk and N. Akar, “**Workload-dependent queuing model of an AQM-controlled wireless router with TCP traffic and its application to PER-based link adaptation,**” *EURASIP Journal on Wireless Communications and Networking*, vol. 67, Apr. 2014.

O. Ozturk and N. Akar, “**Analysis of an adaptive modulation and coding scheme with HARQ for TCP traffic,**” in *Wireless Telecommunications Symposium (WTS), 2015*, pp. 1–6, Apr. 2015.

1.5 Organization of the Thesis

The thesis is organized as follows. In Chapter 2, we provide the necessary background on the topics studied in this thesis. In Chapters 3, 4, 5 and 6, we study

TAGLA, TAGLA_{wH}, QAWLA, and EnQAWLA_{wH} link adaptation schemes, respectively, in the light of the analytical models developed for their performance evaluation. We conclude in the final chapter outlining future work. Each chapter is written in a self-contained manner, making the necessary introduction of the presumed notation after motivating the studied problem. Since the link adaptation scheme presented in each chapter either improves or extends those of the preceding ones, the reader is advised to read chapters one by one in the given order. Nevertheless, those who would be more interested in the novel queue-aware link adaptation schemes QAWLA and EnQAWLA_{wH}, which are the main contributions of this thesis, may start reading from Chapter 5 onwards.

Chapter 2

Background

In this chapter, background information on the key topics of this thesis, namely Transmission Control Protocol (TCP), Active Queue Management (AQM) and Link Adaptation (LA) is given.

2.1 Transmission Control Protocol (TCP)

TCP [36], along with User Datagram Protocol (UDP) [37], has been one of the most dominant transport protocols used in the Internet. TCP is used for a wide variety of applications such as Web browsing, file transfer, remote login, and more recently for video streaming [38]. TCP offers reliable and in-order packet delivery for the application layer. Born in a world of a basically-wired network for which congestion was assumed to be the sole source of packet losses, TCP is equipped by design with algorithms for congestion control [39], [40]. A specific implementation of TCP, namely TCP-Reno [41], has been the most studied variant of TCP [42]. The sender of a TCP-Reno connection declares a packet to be lost either upon a timeout expiry for its acknowledgment (ACK) packet to be sent by the TCP receiver or upon the reception of three duplicate acknowledgments

(DUPACKs) for a preceding packet. The latter case occurs when three out-of-order packets arrive at the receiver. Upon expiration of a timeout, the sender reduces its Congestion Window (CW) which represents the collection of packets that are allowed to be transmitted back-to-back without having to wait for their corresponding ACKs, down to the size of a single packet. DUPACKs are reacted to more gently than timeouts by most TCP variants considering the network to be on the verge of congestion. As an example, TCP-Reno triggers a fast retransmit mechanism to retransmit the missing packet reported by the DUPACKs and halves its CW. If an ACK is received in return, then the transmission continues where it is left off, otherwise the same procedure regarding the timeout condition is executed. After a timeout, TCP-Reno enters into a state called “slow start” at which the CW is incremented by one for each received ACK. In slow start, the CW doubles every Round-Trip Time (RTT) until a threshold is reached at which a transition to another state called “congestion avoidance” occurs. In the congestion avoidance state, the CW is approximately incremented at each RTT yielding a linear inflation until either another packet loss is experienced or the advertised TCP Receive Window (RW) limit is reached at the TCP receiver. The RW is essential for the sender in order not to overwhelm the receiver. A multitude of variants of TCP have emerged after the introduction of TCP-Reno to improve its performance in various ways. TCP-Vegas is such an example which promises to improve the TCP-Reno’s retransmission mechanism by proactively retransmitting packets based on their expected RTTs without having to wait for three DUPACKs [43]. By itself, TCP-Vegas is demonstrated to achieve higher throughput levels than TCP-Reno. However, TCP-Vegas performs worse than TCP-Reno if both variants co-exist in the same network since TCP-Vegas proactively reacts congestion and therefore abandons network resources earlier than its competitor [42]. TCP-Compound and TCP-CUBIC are two other variants of TCP designed for networks with large bandwidth-delay product that are currently in use in Windows and Linux operating systems, respectively, [44],[45],[46].

In wireless networks, packets experience losses stemming from both wireless transmission errors and congestion. TCP-Reno, on the other hand, does not make a distinction among the sources of packet losses. Therefore, throttling

TCP’s transmission rate by erroneously invoking congestion control mechanisms for wireless losses, have the potential to waste invaluable network resources [47]. One approach studied in the literature is to conceal the existence of the wireless domain by addressing the problem where it first appears. The so-called “Split Connection” scheme splits the TCP connection between a Mobile Station (MS) and a Fixed Station (FS) passing through a Base Station (BS) into two, one from FS to BS and the other from BS to MS. The purpose of this scheme is to use a specialized protocol between BS and MS so that the problems of the wireless network are shielded from the traditional wired network [48]. Split Connection does not respect for the semantics of the end-to-end TCP protocol and requires modifications at both the MS and BS protocol suites. The “Snoop Protocol” proposed in the reference [49] for a similar setting is a less invasive technique for which the BS caches the unacknowledged TCP packets and runs its own retransmission timer. Whenever a DUPACK is sent by MS or the local timeout expires, it intercepts the flow by transmitting the lost packets to the MS from its cache. Both Split Connection and Snoop Protocol mechanisms complicate the design of the BS and they do not scale well with the number of TCP connections. Moreover, these protocols are designed for cellular networks and are not appropriate in multi-hop wireless network settings.

Another approach is tailoring TCP to increase its robustness against wireless packet losses. One such variant of TCP, TCP-Veno (a hybrid of TCP-Vegas and TCP-Reno), monitors the congestion level of the network for the purpose of distinguishing random packet losses (i.e., caused by wireless transmission) from congestion losses [50]. A packet loss noticed in the absence of congestion is assumed to be random and reacted to, by reducing the CW more gently. TCP-Jersey, proposed in the reference [51], employs an Available Bandwidth Estimation (ABE) algorithm to estimate the available bandwidth to adjust its CW and expect to receive congestion warning from the intermediate routers to differentiate wireless packet losses from congestion losses. Existing Congestion Experienced (CE) and Explicit Congestion Echo (ECE) fields in the IP and TCP headers, respectively, are used to acquire congestion status from the Explicit Congestion Notification (ECN)-capable routers. The ABE algorithm of TCP-Jersey is improved by the

subsequent version TCP-New Jersey [52] and by TCP-New Jersey PLUS [53] later on. In a simulation-based study, TCP-New Jersey is found to be superior than both TCP-Veno and TCP-Reno regarding robustness and protocol overhead under high packet loss rates [54]. More recently, TCP/NC, first of its kind Network Coding (NC)-based TCP, has been proposed to employ Forward Error Correction (FEC) to compensate for the dropped packets in the network [55]. TCP/NC has a high decoding delay and complexity and the reference [56] replaces NC with LT Codes [57] to design TCP-Forward avoiding the above-mentioned drawbacks. LC Codes are the first practical realizations of Fountain Codes which are rateless erasure codes [58]. Principally, Fountain Codes can generate an infinite sequence of coded symbols from a finite-length of data, a feature that makes them uniquely suitable for TCP.

In this thesis, we concentrate on the performance of the most widely implemented and studied TCP variant, namely TCP-Reno [59], and use TCP-Reno and TCP interchangeably throughout the thesis unless otherwise stated. An analytical expression, known as the “PFTK” formula, gives the steady-state packet sending rate of a long-lived TCP-Reno flow (i.e., a flow with a large amount of data to send such as File Transfer Protocol (FTP) file transfers) as a function of its packet loss rate and RTT [5]. The PFTK formula takes into account both the fast retransmit mechanism of TCP-Reno and the effect of TCP timeout on the packet sending rate. For a related study on a simpler TCP packet sending rate expression which ignores certain features of TCP, the so-called “square-root” formula, see [60]. The reference [61] further integrates the square-root model with a generalized processor sharing model to analyze non-persistent TCP flows as well.

2.2 Active Queue Management (AQM)

The traditional technique of using buffer management based on tail-drop at wireline router links carrying TCP traffic leads to the so-called “full-queues” and “lock-out” problems described in [62]. The full-queues problem refers to the buffer being full most of the time, introducing large queuing delays which in turn

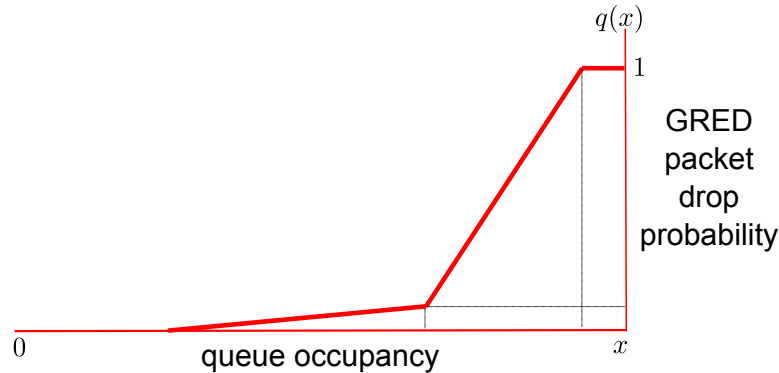


Figure 2.1: Packet drop probability function of the GRED AQM scheme used in this thesis.

impact adversely the TCP-level throughput. The lock-out problem refers to a situation in which a single or a few flows monopolize the queue space while starving others as a result of synchronization or other timing effects. To avoid the full-queues problem, AQM mechanisms drop packets before the queue becomes full [62]. Typically, the AQM drop decision is probabilistic on certain queue parameters to mitigate the lock-out problem [62]. For various AQM mechanisms proposed in the literature, we refer the reader to [62],[63],[64],[65]. One of the pioneering AQM schemes is Random Early Detection (RED) [66]. The packet drop rate of RED is linear with respect to the average queue occupancy in a certain regime of the queue defined by certain thresholds. Performance of RED, however, is known to exhibit considerable variation with respect to the particular choices for these thresholds [67]. As a remedy, the so-called Gentle RED (GRED) is proposed to make RED less sensitive to the choice of these parameters [68]. In Fig. 2.1, the packet drop probability function $q(x)$ of GRED is depicted, where x denotes the queue occupancy.

The reference [69] presents a comprehensive survey of AQM along with an elaborate classification and comparison of its proposed variants and its use in the wireless context. The reference [70] concludes that the standards-based WiMAX technology [71] introduced in the next section can indeed benefit from AQM in reducing its downlink latency. More recently, a parameterless policy called “CoDel” taking the local minimum queuing delay experienced by the packets as

the main metric for the detection of the full-queues problem has been proposed in [72].

Using fixed-point iterations, the PFTK formula can be used to approximate the absolute throughput of a TCP flow sharing an AQM router link with other TCP flows and also in a network of AQM routers with persistent and dynamic traffic scenarios [12]. However, the focus in [12] is the mean queue occupancy in router links, not the queue occupancy distribution. For related work on how to approximate the flow-level TCP throughput when the dynamic flows share a network of AQM routers using the $M/M/1/K$ queuing model, we also refer the reader to [73].

2.3 LTE and WiMAX

Unrelenting traffic demand of mobile users and applications facilitated by emerging advanced mobile devices (such as smart phones, tablets, laptops and Internet of Things (IoT) devices on the horizon) has led to the evolution of Wireless Communication Systems (WCSs) such as Long Term Evolution (LTE) and Worldwide Interoperability for Microwave Access (WiMAX) governed respectively by the 3rd Generation Partnership Project (3GPP) [74] and the WiMAX Forum [71]. WiMAX is based on the IEEE 802.16 standard [75], analogous to Wi-Fi and the IEEE 802.11 standard. Access network infrastructure of both LTE and WiMAX are cellular and possess similar components. LTE and WiMAX have a fixed central unit responsible for mobility and radio resource management called evolved Node B (eNB) and Base Station (BS), respectively, to provide service to a number of nomadic devices called User Equipment (UE) and Subscriber Station (SS), respectively. Communication direction from BS (SS) to SS (BS) is referred to as downlink (uplink) for WiMAX and also for LTE. Both standards rely on similar advanced physical layer (PHY) technologies two of which are discussed next.

Contrary to their single-carrier narrowband ancestors, LTE and WiMAX offer

wideband wireless access to their users with the multi-carrier Orthogonal Frequency Division Multiplexing (OFDM) modulation. OFDM aims to split the frequency-selective wideband channel into a collection of orthogonal flat-fading (i.e., non-frequency-selective) narrowband channels called sub-carriers. Since each sub-carrier experiences a memoryless (albeit arbitrary) channel characterized by only a complex scalar gain, frequency-domain equalization schemes such as Zero Forcing (ZF) or Minimum Mean Square Error (MMSE) (the latter taking the noise enhancement into account) with a single-tap filter, suffice. These filter taps, on the other hand, are estimated from a set of sounding symbols known to both transmitter and receiver, called pilots, inserted into the transmitted signal. Moreover, OFDM implementations exploit highly efficient decompositions of Fast Fourier Transform (FFT). Despite its aforementioned advantages, OFDM is not a constant envelope modulation and therefore suffers from high Peak-to-Average-Power-Ratio (PAPR). When no PAPR reduction techniques are applied, PAPR of OFDM is reported to exceed 11.7 dB with a probability of 10^{-3} which mandates a back-off with the same amount to the transmission power in order to avoid saturation in the Power Amplifier (PA) [76]. Efficiency of a typical PA, however, decreases with decreasing output power [77]. Another drawback of OFDM is its sensitivity to carrier frequency offsets and Doppler shifts. Since sub-carriers of OFDM are overlapping in the frequency domain, such frequency impairments distort the orthogonality of the sub-carriers [78]. OFDM is used in multipath fading channel simulations performed in this thesis.

Multiple-Input-Multiple-Output (MIMO) communication is another prominent feature of LTE and WiMAX WCSs. With MIMO, a linear capacity increase equivalent to $\min(A_T, A_R)$ is achievable, where A_T and A_R denote the number of transmit and receive antennas, respectively, provided that a rich scattering environment exists, establishing an independent channel between each transmit and receive antenna pair [79],[80]. Availability of a rich scattering environment depends on a number of factors such as spatial distribution of scatterers, antenna beamwidth and range of transmission, etc., [81]. MIMO keeps its promise without requiring an increase in bandwidth or in transmission power which makes it an indispensable tool for modern WCSs. In practice, high data rates with MIMO

is attained by the so-called Spatial Multiplexing (SM) scheme [82] whereas multiplexing gain can be traded-off for diversity gain with the Alamouti scheme [83],[84].

Throughout the numerical examples of this thesis, we use the downlink of the IEEE 802.16e *Wireless-MAN OFDMA PHY* air interface [75] and limit our scope to Single-Input-Single-Output (SISO) communication. For brevity, we use the IEEE 802.16e *Wireless-MAN OFDMA PHY* air interface and IEEE 802.16 interchangeably. We adopt a generic and non-standard specific term called Mobile Station (MS) instead of the term SS used in the IEEE 802.16 standards.

2.4 Link Adaptation (LA)

In wireless router links, non-congestion (or wireless) losses arise due to channel errors in addition to congestion losses caused by AQM drops. TCP suffers from wireless losses since it responds to all losses by triggering congestion avoidance algorithms which results in reduced performance on paths with lossy links [3]. Wireless losses are addressed by LA algorithms which adapts the transmission parameters of the WCS to changing channel conditions with the intention of increasing the overall spectral efficiency [85]. The key parameters to adapt are the modulation and coding levels also known as Adaptive Modulation and Coding (AMC), transmission power, spreading factors, etc., or a combination of above.

AMC refers to the class of algorithms in WCSs used to select one of the Modulation and Coding Schemes (MCSs) in a finite discrete set offered by the WCS air interfaces so as to satisfy certain Quality of Service (QoS) requirements without having to sacrifice spectral efficiency. In particular, MCSs are generally indexed for increasing spectral efficiency and they use atomic transmission units called FEC blocks for data transmission at the PHY. MCSs with relatively higher indices correspond to more aggressive MCSs with higher spectral efficiency but also with higher FEC block error rates. The basic goal of AMC is to choose the best possible MCS as a function of varying channel conditions on the basis

of Channel State Information (CSI) which is representative of the instantaneous condition of the wireless link [86],[87]. This optimization problem is involved in maximizing the spectral efficiency of the wireless link under certain block error rate constraints. When these constraints are driven by performance requirements of higher layer applications like multimedia [88], Web browsing, bulk-data transfer [89], etc., the AMC requires cross-layer handling. Impact of packet loss and delay incurred by queuing at the data link layer is another research topic for cross-layer analysis [90]. Applications relying on TCP are generally delay insensitive but loss intolerant. TCP itself, however, is both loss-and delay-tolerant allowing optimization of the loss and delay experienced at the data link layer to maximize its throughput as studied in [8].

AMC generally takes the Signal-to-Noise-Ratio (SNR) or Signal-to-Noise-plus-Interference Ratio (SINR) that is available from the PHY as CSI [85]. Mapping SNR values to MCSs, however, presents a challenge in multipath fading channels for which the performance of a given MCS may exhibit significant variation across different channel models. It is shown in the references [91] and [92] that the average throughput can be significantly increased if the MCS selection is based on an accurate prediction of Packet Error Rate (PER) to be expected for the current channel conditions. In OFDM-based WCSs, each sub-carrier of a FEC block may propagate through a different flat-fading channel which is perceived by the receiver as a varying level of SNR for each sub-carrier. Let N be the number of sub-carriers used to transmit a FEC block at a particular instant of transmission. The SNR level of sub-carrier $i \in \{0, 1, \dots, N - 1\}$ measured at the receiver can then be denoted by γ_i . In this case, one could theoretically use an N -dimensional massive MCS look-up table with colossal amount of entries to select a proper MCS, which is obviously impractical to generate and store [93]. A remarkably simple and accurate solution to this problem, called Exponential Effective SNR Mapping (EESM) is proposed by the reference [94]. EESM converts the vector of sub-carrier SNRs $\bar{\gamma}$ into a single flat-fading equivalent SNR called γ_{eff} as shown below, with which the FEC block used in the transmission would have the same FEC block Error Rate (FER) in the Additive White Gaussian Noise (AWGN)

channel:

$$\gamma_{eff} = \beta \ln \left(\frac{1}{N} \sum_{i=0}^{N-1} \exp \left(-\frac{\gamma_i}{\beta} \right) \right), \quad (2.1)$$

where β is an MCS specific parameter to be determined empirically. Related values of β are provided for WiMAX in the studies [95],[96] and for LTE in [93], and in [97]. We note that γ_{eff} is different for each MCS because of its dependency on β . Therefore, an EESM-based AMC has to check all MCSs for the corresponding AWGN FERs each time $\bar{\gamma}$ is updated. Assuming Rayleigh distributed sub-carrier channel gains, the expression inside the natural logarithm of equation (2.1) is modeled with the Beta distribution in order to facilitate tractable analysis of EESM-based AMC [93]. EESM is also considered as an efficient way of abstracting the PHY in system-level simulations [98],[93]. Alternative methods for FER estimation in frequency-selective channels also exist, such as “PER-indicator” relating the variance of the channel transfer function to the shifts in the FER vs. SNR curves of the AWGN channel [91], and Mean Mutual Information per coded Bit (MMIB) mapping $\bar{\gamma}$ to the mean mutual information between the Log-Likelihood Ratios (LLRs) and the bits of the Quadrature-Amplitude-Modulation (QAM) symbols which is then used to look up pre-computed FER vs. MMIB curves for the AWGN channel [99]. Accuracy of EESM is shown to be higher than PER-indicator but lower than MMIB both by a fraction of dB [100],[99].

LTE mandates feedback from the UE in the form of a 4-bit Channel Quality Indicator (CQI) corresponding to the most spectrally efficient MCS out of fifteen different MCSs whose FER, or synonymously BLock Error Rate (BLER), is expected to stay below 0.1 for downlink transmission [101],[102]. To this end, after characterizing the AWGN performance of the UE for each MCS, only the MCS switching thresholds on γ_{eff} can be stored in a look-up table and used whenever necessary for the EESM method [103]. In LTE, necessary mechanisms are established to provide a CQI feedback not only for the entire bandwidth but also at the subband-level (a contiguous subset of sub-carriers) for subbands favoring the UE so as to enable frequency-domain scheduling at the eNB [104]. In a similar manner, WiMAX defines the effective-Carrier-to-Interference-and-Noise Ratio (CINR) report from the SS which is encoded with eleven MCS levels. An

optional “frequency selectivity characterization” feedback mechanism is also offered to the SSs capable of experimentally deriving a quadratic approximation of their effective-CINR vs. β curves [75],[105]. It is noted in the reference [106] that an increase in transmission power does not translate to an increase with the same amount in the effective-CINR. Therefore, it proposed to characterize the effective-CINR of SS at the BS for the purpose of joint MCS selection and power control.

Although methods to take measurements for channel quality feedback are implementation-specific, i.e., left to vendors, EESM has become a viable and widely accepted solution for both standards. Nevertheless, while reaching a final decision, AMC may take the QoS constraints into account as well. For example, WiMAX allows to define the target PER for the service flows. Moreover, delays and errors in channel quality feedback of practical WCSs pose a threat to the performance of AMC in time-varying channels [107],[108],[109]. As a remedy, a machine learning-based scheme called Reinforcement Learning-based AMC (RL-AMC) is proposed in the reference [103] to increase the robustness of AMC based on the outcomes of past AMC decisions.

AMC may also be equipped with Automatic Repeat Request (ARQ) and Hybrid ARQ (HARQ) techniques for which the errored packets at the receiver are retransmitted by the transmitter until either they are successfully decoded or a retransmission limit is reached. Different from ARQ, HARQ combines information from all (re)transmissions to enhance FEC block decoding performance expect for Type-I HARQ. Type-I HARQ scheme (re)transmits the same replica of the encoded FEC block at each (re)transmission and the receiver discards the failing blocks at the decoder [110]. In a more advanced scheme called Type-II HARQ, on the other hand, failing blocks at the decoder are saved for later use. Type-II HARQ with Chase Combining (HARQ-CC) needs (re)transmission of identical blocks similar to Type-I HARQ but decodes them with Maximal-Ratio Combining (MRC) making use of the blocks saved from the previous (re)transmissions [111],[112],[113]. Type-II HARQ with Incremental Redundancy (HARQ-IR) generates a new set of parity bits for each retransmission after the initially transmitted FEC block effectively decreasing its code rate [114],[115]. A subset of

HARQ-IR schemes whose every (re)transmitted FEC block is also self-decodable is referred to as Type-III HARQ [110]. The two main protocols used to manage retransmissions are Selective Repeat (SR) and Stop-and-Wait (SW). As the names suggest, SR retransmits only the lost packets whereas SW waits for the current packet to succeed before dealing with the next packet in turn. SR retransmissions require a more complicated buffering mechanism at the receiver in order to preserve the original packet order. SW protocol, on the other hand, underutilizes the transmitter due to the time gaps left between the (re)transmissions and the associated ACKs which can be overcome by running parallel instances of the protocol as preferred in LTE and WiMAX for HARQ. SW finds a single-bit sufficient to signal the ACK/NACK status of each HARQ packet whereas SR requires to give feedback on the sequence number for each failing packet which is random in nature [116]. Clearly, the higher the probability of retransmissions gets, the more resource efficient SW becomes compared to SR. Finally, SW disregards the packet order just like SR, if the packets of a particular flow are to be multiplexed between the concurrent SW processes. **In this thesis, we assume SR retransmission protocol while studying the LA schemes with HARQ-CC for the sake of convenience in devising the analytical models. We do not attempt to provide a model for the ARQ protocol.**

Both ARQ and HARQ prove to be powerful techniques to combat multipath fading in wireless channels at the expense of increased delay and jitter caused by random retransmissions. Out-of-order packet delivery which is a natural consequence of these techniques can be detrimental to TCP throughput if left uncompensated at the wireless receiver [117]. As discussed in Section 2.1, out-of-order packets force TCP receivers to send DUPACKs which in turn throttles back the transmitter's packet injection rate to the network. It is reported in the reference [117] that TCP throughput of a single flow may drop by as much as 90% provided that 10% of the packets are re-ordered in three locations. There is therefore a need to restore the original packet order at the wireless receiver by means of a resequencing mechanism [118]. The drawback of resequencing, however, is increased RTTs which might adversely affect TCP throughput. We note that with HARQ, much higher rates of packet loss can be targeted for the first

transmission attempt compared to the single transmission case, which renders an adaptation algorithm based on error rate statistics feasible even for channels with high variability [103],[119].

Adapting transmission power is another tool for LA in wireless networks where interference mitigation is required for users sharing the same or nearby spectrum. Developing transmission power control algorithms for the purpose of maximizing data rates of interference-limited networks is an open research area which we leave out of the scope of this thesis [120],[121],[122],[123]. We rather turn our attention to the analysis of the LA schemes using power control within the context of Energy Efficiency (EE) of interference-free wireless networks. In the following section, we present the related work in the area of EE in general.

2.5 Green Communications

Proliferation of WCSs boosted by ever-increasing amount of carried traffic accompanied by increasing number of subscribers, have raised concerns about the EE of such systems. With its foreseen environmental and economical impact on a global scale, lowering carbon footprint and OPerational EXpenditure (OPEX) of Radio Access Networks (RANs) is essential for sustainable and green wireless communications [124]. Therefore, it is imperative to optimize WCSs not only for Spectral Efficiency (SE) but also for EE.

Energy in RANs is dominantly consumed by the PA followed by the air conditioning equipment, signal processing circuitry and power supply unit [125] where the signal processing may take the lead for short range communications [126]. Approaches to reduce energy consumption of the PA can be given under three broad categories: (i) improving efficiency and linearity of PAs at the component-level, (ii) designing PAPR reduction [76] and linearization techniques at the signal-level, and (iii) designing efficient network topologies and algorithms at the network and MAC layers [77]. In this thesis, we propose a cross-layer link adaptation scheme jointly controlling the transmission power and the transmission rate, which can

be viewed to belong to the last category of approaches to which an extensive body of literature is devoted.

With the so-called Discontinuous Transmission (DTX) technique [127], LTE downlink transmission is adaptively switched off to prevent waste of energy invested in transmission of reference signals in unused Resource Blocks (RBs). For lightly loaded cellular networks, a significant percentage of energy is shown to be saved by DTX which has also been standardized in LTE [74]. Trading bandwidth (BW) for EE [128],[129] by means of allocating unused RBs to the subscriber in schedule and reducing the associated modulation order and transmission power to maintain the original transmission rate is also studied in the literature. The reference [130] takes a game-theoretic approach for the BW-EE tradeoff focusing on the optimization of the circuit power. The work in [131] carries out an information-theoretic analysis of the BW-EE tradeoff for a one-dimensional slow fading multi-hop relay network with equidistantly-spaced nodes and coins the notion of “multi-hop diversity”. In a similar setting, the reference [132] relaxes the equidistant node assumption made in the reference [131] taking the circuit power into account as well.

Another potential tradeoff is SE-EE [133] which exhibits a non-monotonic behavior for practical systems, contrary to what is suggested by the Shannon’s channel capacity formula. In practice, the PA efficiency increases with increasing output power and the circuit power increases with increasing bit rate. The references [134] and [135] explore the SE-EE tradeoff for ARQ and HARQ systems, respectively. The latter finds the optimum power assignments for each (re)transmission round for a given outage probability and maximum number of retransmissions and reports results rendering equal-power allocation scheme being far from optimal. In the reference [23], the entire optimal EE-throughput curve is characterized, employing a multi-criteria optimization approach for an interference-free multi-hop wireless network. We refer the reader to the following non-exhaustive list of surveys [136],[137],[138],[139],[140] on the EE of WCSs.

Chapter 3

Traffic-Agnostic Link Adaptation (TAGLA)

This chapter is organized as follows. In Section 3.1, problem description of the Traffic-AGnostic Link Adaptation (TAGLA) scheme is given. In Section 3.2, the workload-dependent queuing model for an Active Queue Management (AQM)-controlled wireless link with Bernoulli wireless packet losses is presented. In Section 3.3, the model is validated in both wireline and wireless scenarios using simulations. Section 3.4 addresses the framework we introduce using the proposed queuing model to obtain the target Packet Error Rate (PER) for TCP throughput optimization for a wide range of scenarios.

3.1 Problem Description

In this chapter, we study a wireless link which can be viewed as the downlink of a cellular wireless network comprising a Base Station (BS) serving a number of Mobile Stations (MSs) or a wireless link between two routers. For the downlink scenario, data flows from the network to MSs which send their ACK packets in the reverse (uplink) direction and the uplink data traffic is not considered. Such

wireless links are categorized as infrastructure-type in [69] and they are identified as potential bottleneck links due to possible bandwidth mismatch between the wireless and wired domains. In accordance with this observation, we assume in this study that all flows are either bottlenecked at this particular link or the bottleneck bandwidth of the flows are fixed and known in advance. We show that TCP throughput optimization is dependent not only on PER but also on traffic related parameters such as the number of TCP flows and their Round-Trip Time (RTT) values. However, estimating the number of active TCP connections and their RTT values is computationally difficult to implement. In this respect, we perform a cross-layer study of a PER-based link adaptation scheme called Traffic-AGnostic Link Adaptation (TAGLA) in order to discover its potential from the perspective of TCP layer.

3.2 Analytical Model

We assume that the wireless link employs AQM and is offered with a fixed number N of long-lived TCP-Reno flows in one direction, all using a fixed packet size L . TCP ACK packets are transmitted in the other direction with priority given to ACK traffic so that delay and losses for ACK traffic can safely be neglected. Propagation delays which are fixed part of the RTT of individual flows are allowed to be arbitrary. A Modulation and Coding Scheme (MCS) is used to serve the packets waiting in the queue and errored packets are not retransmitted, i.e., ARQ or Hybrid ARQ (HARQ) mechanisms are not in action. Based on these fundamental assumptions we elaborate on the proposed queuing framework next.

3.2.1 Workload-Dependent $M(x)/G/1$ Queue

The following description of workload-dependent $M(x)/G/1$ queues and the accompanying notation is based on [10]. We consider a Markovian workload process in which the server drains the queue according to a workload-dependent service rate function $r(x)$ (in units of bps) where x denotes the current workload (in units

of bits) in the queue. On the other hand, the packet arrivals to the queue are governed by a Poisson process with a workload-dependent intensity function $\lambda(x)$. We assume $r(0) = 0$, $r(x)$ is strictly positive, left-continuous, and has a strictly positive right limit on $(0, \infty)$. Each arrival increases the workload by the job size (in units of bits) whose Cumulative Distribution Function (CDF) is denoted by $B(\cdot)$ with mean job size β . Under the condition $\limsup_{x \rightarrow \infty} \beta \frac{\lambda(x)}{r(x)} < 1$, the workload process is ergodic and possesses a stationary Probability Density Function (PDF) denoted by $v(x)$, $x > 0$. The workload process may also have a probability mass (atom) at zero denoted by $V(0)$. It is shown in [10] the steady-state workload density $v(\cdot)$ satisfies the following integro-differential equation for $x > 0$:

$$r(x)v(x) = \lambda(0)V(0)(1 - B(x)) + \int_{y=0^+}^x (1 - B(x - y))\lambda(y)v(y) dy, \quad (3.1)$$

where the function $\tilde{R}(x)$ defined as $\int_0^x \frac{\lambda(y)}{r(y)} dy$ and in case $\tilde{R}(x) < \infty$, $0 < x < \infty$, then (3.1) has a non-zero atom $V(0)$ at $x = 0$. A closed form solution to (3.1) for the workload-dependent $M/M/1$ queue is given in [10]. For persistent TCP flows, packet sizes are generally fixed rather than being variable for a given flow. Therefore, the specific case of the workload-dependent $M/D/1$ queue and a numerical solution for finding the stationary density $v(x)$ is crucial for TCP modeling which is described next. For this purpose, we fix the deterministic packet length to L bits. The buffer occupancy is then discretized with a discretization interval Δ such that $l = L/\Delta \gg 1$ is an integer. We then define $v_i = v(i\Delta)$ for $i > 0$ and discretize the integro-differential equation (3.1) to obtain

$$v_i = \begin{cases} \frac{\lambda_0 V(0) + \sum_{j=1}^{i-1} \lambda_j v_j \Delta}{r_i - \lambda_i \Delta}, & i < l. \\ \frac{\sum_{j=i-l+1}^{i-1} \lambda_j v_j \Delta}{r_i - \lambda_i \Delta}, & \text{otherwise.} \end{cases} \quad (3.2)$$

Note that the identity (3.2) enables us to calculate v_i as a weighted sum of v_j 's for $j < i$ which lends itself to an iterative procedure. We propose to set $V(0) = 1$ and iteratively calculate v_i for $1 \leq i \leq K$ as in (3.2) for some large choice of K . Note that K should be chosen such that $\sum_{K+1}^{\infty} v_i \Delta$ should be small enough to yield an acceptable approximation error. Finally, we first define $V = V(0) + \sum_{i=1}^K v_i \Delta$ and then normalize as follows:

$$V(0) := \frac{V(0)}{V}, v_i := \frac{v_i}{V}, \quad 1 \leq i \leq K. \quad (3.3)$$

3.2.2 Equation-Based TCP Model

In line with the majority of the existing work on TCP modeling, we propose to use the so-called ‘‘PFTK’’ TCP model of [5] to relate the packet sending rate of a TCP flow to the packet loss rate seen by the flow. For details, we refer the reader to [5]. Let p , λ , and T_0 denote the packet loss rate, packet send rate, and the retransmission timeout parameter of a TCP source, respectively. In our model, we use the following relationship used in the implementation of TCP in [2]:

$$T_0 = \max(T_{0,\min}, RTT + 4\sigma_{RTT}), \quad (3.4)$$

where RTT and σ_{RTT} are the smoothed estimates for RTT and its standard deviation, respectively, and $T_{0,\min}$ is a minimum limit imposed on the timeout parameter. Let W_u denote the random variable associated with the unconstrained window size of the TCP source. Also let $W_{\max} = W/L$ and b denote the maximum window size in units of packets and the number of packets to wait before sending a cumulative ACK packet by the TCP receiver, respectively, where W is the receiver’s buffer size. The reference [5] proposes the following equation for the TCP send rate λ if the TCP flow is exposed to a packet loss rate of p :

$$\lambda = \begin{cases} \frac{\frac{1-p}{p} + E[W_u] + \tilde{Q}(E[W_u])\frac{1}{1-p}}{RTT(\frac{b}{2}E[W_u] + 1) + \tilde{Q}(E[W_u])T_0\frac{f(p)}{1-p}}, & E[W_u] < W_{\max} \\ \frac{\frac{1-p}{p} + W_{\max} + \tilde{Q}(W_{\max})\frac{1}{1-p}}{RTT(\frac{b}{8}W_{\max} + \frac{1-p}{pW_{\max}} + 2) + \tilde{Q}(W_{\max})T_0\frac{f(p)}{1-p}}, & \text{otherwise} \end{cases} \quad (3.5)$$

where

$$f(p) = 1 + p + 2p^2 + 4p^3 + 8p^4 + 16p^5 + 32p^6, \quad (3.6)$$

$$\tilde{Q}(w) = \min(1, \frac{(1 - (1-p)^3)(1 + (1-p)^3)(1 - (1-p)^{(w-3)})}{1 - (1-p)^w}), \quad (3.7)$$

and

$$E[W_u] = \frac{2+b}{3b} + \sqrt{\frac{8(1-p)}{3bp} + \left(\frac{2+b}{3b}\right)^2}. \quad (3.8)$$

Throughout our numerical studies, we fix $T_{0,\min} = 0.2$ s as in [141], $b = 2$, $W = 64$ Kbytes as in [2] and $L = 1500$ bytes (unless otherwise stated). With these, the equation (3.5) provides a closed-form expression for the TCP send rate λ in terms of p , RTT and σ_{RTT} .

3.2.3 Active Queue Management

Active Queue Management (AQM) refers to a set of buffer management disciplines that are used in routers by which packets are dropped long before the queue reaches its full capacity [65]. AQM disciplines maintain a shorter average queue length than their drop-tail counterparts which drop packets only when the queue capacity is full. Moreover, typical AQM schemes probabilistically drop packets to mitigate synchronization of TCP sources sharing the link. One of the pioneering AQM schemes is Random Early Detection (RED) [66] for which an arriving packet is probabilistically dropped as a function of the average queue occupancy that is obtained by applying an auto-regressive filter to the queue occupancy time series data. Stochastic modeling of the auto-regressive filtering operation used in such RED-like schemes is generally known to be difficult and costly [142],[143]. We therefore propose to use Early Random Detection (ERD) [63] for which an arriving packet is dropped with probability $p(x)$ when the instantaneous queue length takes the value x . The gentle variant of the ERD discipline we study in this chapter refers to the particular choice of $p(x)$ as follows.

$$p(x) = \begin{cases} 0, & 0 \leq x < th_{\min} \\ \frac{x-th_{\min}}{th_{\max}-th_{\min}} p_{\max}, & th_{\min} \leq x < th_{\max} \\ p_{\max} + \frac{x-th_{\max}}{th_{\max}} (1 - p_{\max}), & th_{\max} \leq x < 2th_{\max} \\ 1, & \text{otherwise.} \end{cases} \quad (3.9)$$

In this study, th_{\min} and th_{\max} are set to $30L$ and $90L$, respectively, in units of bits, and p_{\max} is set to 0.1 as in [12].

3.2.4 Proposed Model

We envision a wireless router link that is offered with persistent TCP flows with the following assumptions:

- N persistent TCP flows share the wireless link using First-In-First-Out (FIFO) queuing.

- All flows use the same packet size L .
- Incoming packets from the TCP flows are dropped according to the specific ERD AQM scheme given in (3.9) with the drop decision depending solely on the instantaneous queue occupancy x .
- The link serves the waiting packets in the queue with a fixed transmission rate r_m dictated by the underlying MCS. We assume M different physical layer (PHY) MCSs denoted by MCS_m , $m \in \{0, 1, \dots, M-1\}$, that are supported by the link's air interface. For this study, we will be given a fixed MCS_m and SNR level denoted by SNR_s , $s \in \{0, 1, \dots, S-1\}$, and we will assume that transmitted packets are errored at the receiver with a probability denoted by $PER_{m,s}$. Lost packets are not retransmitted and loss events are assumed to be independent and identically distributed (iid) following the Bernoulli wireless loss model.
- Flow i , $i \in \{0, 1, \dots, N-1\}$, is exposed to
 - an average packet loss probability $\overline{p_i}$ accounting for losses generated by both the ERD scheme and wireless transmission.
 - an instantaneous workload-dependent queuing delay $D(x) = x/r_m$ at the router when the instantaneous queue occupancy takes the value x . Without loss of generality, $D_T = L/r_m$ and D_F account for the transmission and one-way framing delays, respectively, the latter including other processing delays of any wireless communication system. D_F is multiplied by a factor of two in order to account for both forward and reverse (TCP ACK messages) path delays.
- Queuing and transmission delays as well as the error rates of the TCP ACK packets are assumed to be negligibly small and will be ignored by the analytical model assuming that TCP ACK prioritization is deployed [144] and enhanced wireless protection is established in the reverse path of the flows [145].
- In addition to the delay encountered at the router, each flow has an additional fixed RTT denoted by $RTT_{0,i}$, $i \in \{0, 1, \dots, N-1\}$, taking into

account the propagation delays of all links on the path of the flow.

- We assume all flows are either bottlenecked at the particular wireless link of interest or their bottleneck bandwidths at other links are known in advance and they remain unaffected by the dynamics of the wireless link. Packet error rates on other links are assumed to be negligible. We therefore do not attempt to model networks of AQM router links but rather focus on a single AQM link.
- The packet send process for each flow is Poisson with intensity λ_i which will be shown to depend on the instantaneous queue occupancy x in our proposed model. We note that the Poisson assumption has successfully been used for TCP modeling in previous studies [8].
- All TCP flows use the same minimum timeout parameter $T_{0,\min}$.

The central idea of this study is to use the PFTK TCP model given in (3.5) to write λ_i as a function of the single independent parameter x so that the stationary queue density can be obtained by solving the workload-dependent $M/D/1$ queue described in Section 3.2.1. For this purpose, let the workload-dependent RTT of flow i be denoted by $RTT_i(x)$ which can be expressed as the sum of the following components:

$$RTT_i(x) = RTT_{0,i} + 2D_F + L/r_m + x/r_m. \quad (3.10)$$

Furthermore, let $T_{0,i}(x)$ denote the workload-dependent timeout parameter for flow i which can be expressed via (3.4) as

$$T_{0,i}(x) = \max(T_{0,\min}, RTT_i(x) + 4\sigma_{RTT,i}), \quad (3.11)$$

where $\sigma_{RTT,i}$ stands for the standard deviation of the router queuing delay for flow i . The overall rate of packets that are admitted into the queue denoted by $\lambda(x)$ can then be written as

$$\lambda(x) = \sum_{i=0}^{N-1} \kappa_i(x), \quad (3.12)$$

where

$$\kappa_i(x) = (1 - p(x))\lambda_i(x), \quad (3.13)$$

is the rate of packets belonging to individual flow i that is admitted into the queue. In our proposed model, $\lambda_i(x)$ is the send rate of flow i when the queue occupancy takes the value x and we propose to use the PFTK TCP model (3.5) to write $\lambda_i(x)$ with RTT and T_0 being replaced with their per-flow based workload-dependent counterparts $RTT_i(x)$ and $T_{0,i}(x)$, respectively, and p being replaced with its per-flow counterpart \bar{p}_i which is the average packet loss probability for flow i . We put $\lambda_{i,\max}$ as an upper bound on $\lambda_i(x)$ representing the maximum send rate imposed on flow i by the links it traverses other than the one under analysis. $\lambda_{i,\max}$ is assumed to be known and set to ∞ throughout this chapter unless otherwise stated. We note that the delay terms in (3.5) are taken as a function of the instantaneous queue occupancy x whereas the loss probability term is obtained by averaging out over all possible values of x . We also studied alternative formulations for which the loss probability term be allowed to depend on x which produced much less favorable results and are therefore not given in this study. We plug (3.12) into (3.1) and employ $B(x) = 1$ for $x \geq L$ and zero otherwise. Moreover, for a given MCS_m , we set $r(x) = r_m$ which then leads us to the framework of the workload-dependent $M/D/1$ queuing with fixed service speed. Since $p(x) = 1$ and thus $\lambda(x) = 0$ for $x \geq 2th_{\max}$ bits, the condition on $\tilde{R}(x)$ for a stationary solution $v(x)$ with an atom at zero can be shown to be satisfied for this particular model. Since the stationary density $v(x) = 0$ for $x > x_{\max} = (2th_{\max} + L)$, we set $K = x_{\max}/\Delta$ in our numerical examples where $\Delta = 1$ bit unless otherwise stated.

Let $\bar{\lambda}_i$ and $\bar{\kappa}_i$ denote the average packet arrival and acceptance rates, respectively, into the queue from flow i . We can then write by queue-averaging arguments the following two identities:

$$\bar{\lambda}_i = V(0)\lambda_i(0) + \int_{0+}^{x_{\max}} \lambda_i(x)v(x) dx, \quad (3.14)$$

$$\bar{\kappa}_i = V(0)\kappa_i(0) + \int_{0+}^{x_{\max}} \kappa_i(x)v(x) dx. \quad (3.15)$$

Assuming AQM and wireless packet losses to be independent from each other, the average packet loss probability for flow i stemming from both ERD buffer management and wireless losses, denoted by \bar{p}_i , can be written as follows:

$$\bar{p}_i = 1 - (1 - PER_{m,s})(1 - \bar{q}_i), \quad (3.16)$$

where \bar{q}_i , average packet loss probability for flow i stemming only from ERD, is obtained via queue averaging:

$$\bar{q}_i = \frac{1}{\bar{\lambda}_i} \left(\int_{0^+}^{x_{\max}} p(x) \lambda_i(x) v(x) dx \right). \quad (3.17)$$

Furthermore, let \bar{D}_i denote the average queuing delay in the router seen by flow i . Then, we can write

$$\bar{D}_i = \frac{1}{\bar{\kappa}_i} \left(\int_{0^+}^{x_{\max}} \frac{x}{r_m} \kappa_i(x) v(x) dx \right). \quad (3.18)$$

Consequently,

$$\sigma_{RTT,i}^2 = \frac{1}{\bar{\kappa}_i} \left(\int_{0^+}^{x_{\max}} \left(\frac{x}{r_m} - \bar{D}_i \right)^2 \kappa_i(x) v(x) dx + \bar{D}_i^2 \kappa_i(0) V(0) \right). \quad (3.19)$$

If we know the workload-dependent intensity of packet arrivals $\lambda(x)$, then we can find the stationary density $v(x)$ and the atom at zero $V(0)$ with the algorithm outlined before. However, $\lambda(x)$ depends on $RTT_i(x)$ and $T_{0,i}(x)$ the latter depending on $\sigma_{RTT,i}$ for all i . Moreover, $\lambda(x)$ depends on \bar{p}_i . Recognizing that $\sigma_{RTT,i}$ and \bar{p}_i can be obtained provided $v(x)$ and $V(0)$ are available, we propose a fixed-point algorithm for obtaining the stationary density of the queue occupancy. For this purpose, we define $\sigma_{RTT,i}^{(k)}$ and $\bar{p}_i^{(k)}$ to denote the estimates for the corresponding quantities at iteration k . At iteration $k+1$, $\lambda(x)$ is obtained using $\sigma_{RTT,i}^{(k)}$ and $\bar{p}_i^{(k)}$. Via the solution of the workload-dependent $M/D/1$ queue with intensity function $\lambda(x)$, we obtain $v(x)$ and $V(0)$. The new values of $\sigma_{RTT,i}$ and \bar{p}_i are obtained at this iteration using the identities (3.19) and (3.16), respectively, but exponentially smoothed with smoothing parameters α_1 and α_2 , respectively, to obtain $\sigma_{RTT,i}^{(k+1)}$ and $\bar{p}_i^{(k+1)}$. Iterations continue until the following two conditions are simultaneously satisfied:

$$|\sigma_{RTT,i}^{(k+1)} - \sigma_{RTT,i}^{(k)}| / \sigma_{RTT,i}^{(k)} < \epsilon_1, |\bar{p}_i^{(k+1)} - \bar{p}_i^{(k)}| / \bar{p}_i^{(k)} < \epsilon_2, \quad (3.20)$$

for some normalized tolerance parameters ϵ_1 and ϵ_2 . For numerical experimentation with the fixed-point algorithm, we fix $\epsilon_1 = \epsilon_2 = 0.01$, $\alpha_1 = 0.7$, and $\alpha_2 = 0.9$. We finalize this section by expressing the aggregate TCP throughput, the key parameter to be studied in our numerical examples, as $(1 - PER_{m,s})L \sum_{i=0}^{N-1} \bar{\kappa}_i$.

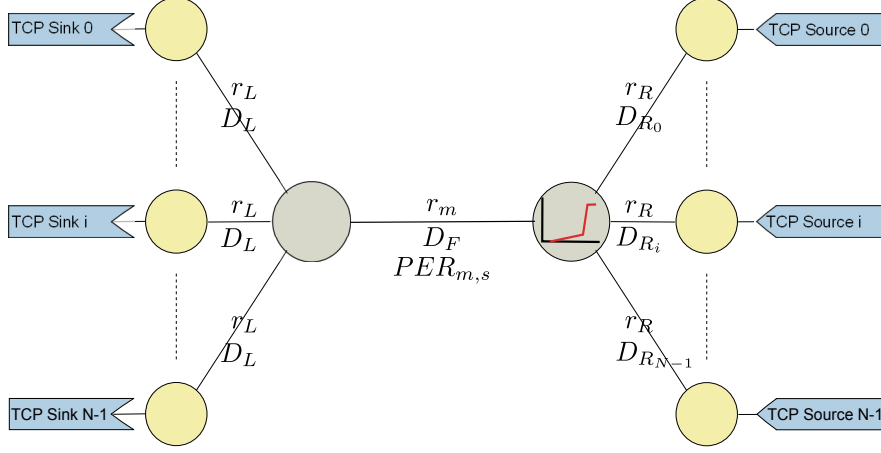


Figure 3.1: ns-3 simulation topology.

3.3 Model Validation

The so-called *proposed* analysis method of this chapter is validated using the ns-3 network simulator [2] for both wireline and wireless scenarios. We prefer to use a dumb-bell topology, which is a common topology to study TCP congestion algorithms in bottleneck links, involving N TCP-Reno flows in our simulations as shown in Fig. 3.1 [146],[147]. The ingress link for flow i , $0 \leq i < N$, has capacity r_R and one-way propagation delay D_{R_i} whereas the egress link for the same flow has capacity r_L and one-way propagation delay D_L . The central link in the middle is the wireless bottleneck link with one-way propagation delay D_F using an MCS_m yielding a capacity r_m and a wireless loss rate $PER_{m,s}$ at SNR level SNR_s . TCP flow statistics are obtained using the *FlowMonitor* which is a monitoring framework developed for ns-3 [148]. The *RateErrorModel* class of ns-3 is used whenever a non-zero $PER_{m,s}$ is to be simulated.

In ns-3, it is more appropriate to probe queue occupancy in units of packets as opposed to the unfinished work density $v(x)$ obtained through the workload-dependent $M/G/1$ queuing model. Therefore, for the sake of comparing our results to those obtained by ns-3, we approximate the steady-state queue occupancy Probability Mass Function (PMF) in units of packets denoted by u_k as

follows:

$$u_k = \begin{cases} \sum_{i=1}^{\lceil x_{\max}/L \rceil} \left(\int_{y=((i-1)L)^+}^{iL} v(x) dx \right) \delta(k-i), & k > 0 \\ V(0), & k = 0 \end{cases} \quad (3.21)$$

where $\delta(\cdot)$ denotes the Dirac-delta function. Simulations are terminated after five minutes but the first thirty seconds corresponding to transients are ignored. Each simulation is repeated ten times unless otherwise is stated and the average results are reported together with the associated confidence intervals computed for 95% confidence level.

We compare the *proposed* analysis method with the one presented in [12] which is referred to as the *fixed-point* method for the wireline scenario for which we set $PER_{m,s} = 0$. The method *fixed-point* pursues a similar approach to *proposed* in relating the TCP packet sending rate to the queue occupancy by the PFTK formula but it uses a fluid model to obtain only the average queue occupancy, not its distribution. Moreover, *fixed-point* does not take wireless losses into account. We set $(r_L, r_m, r_R) = (1000, 10, 1000)$ Mbps ensuring that the central link is the bottleneck link.

In Fig. 3.2, the PMF u_k is obtained using *proposed*, *fixed-point*, and ns-3 simulations for Scenario A which refers to $(D_L, D_F, D_{R_i}) = (5, 0, 5)$ ms and depicted for three different values of N . In Fig. 3.3, the PMF u_k is depicted for Scenario B which refers to $(D_L, D_F, D_{R_i}) = (15, 0, 5 + 5 \lfloor i/(N/10) \rfloor)$ ms again for three values of N . It is clear that the method *proposed* matches the PMF obtained by ns-3 simulations in both shape and magnitude especially for smaller number of flows. The deviation from the simulation results for larger number of flows is probably due to the fact that the instantaneous queuing delay is used in our workload-dependent queuing model although in actual TCP implementations, this information would be slightly delayed. Consequently, *proposed* improves upon *fixed-point* as far as the queue occupancy PMF is concerned.

For Scenario B, we now set $N = 10$ and $r_L = 0.9$ Mbps (corresponding to $\lambda_{i,\max} = r_L/L$ of *proposed*), for which the numerical results are given in Fig. 3.4. We also increase the number of ns-3 simulations to 120 to obtain more reasonable confidence intervals. In this case, *fixed-point* ends up with an always-empty queue

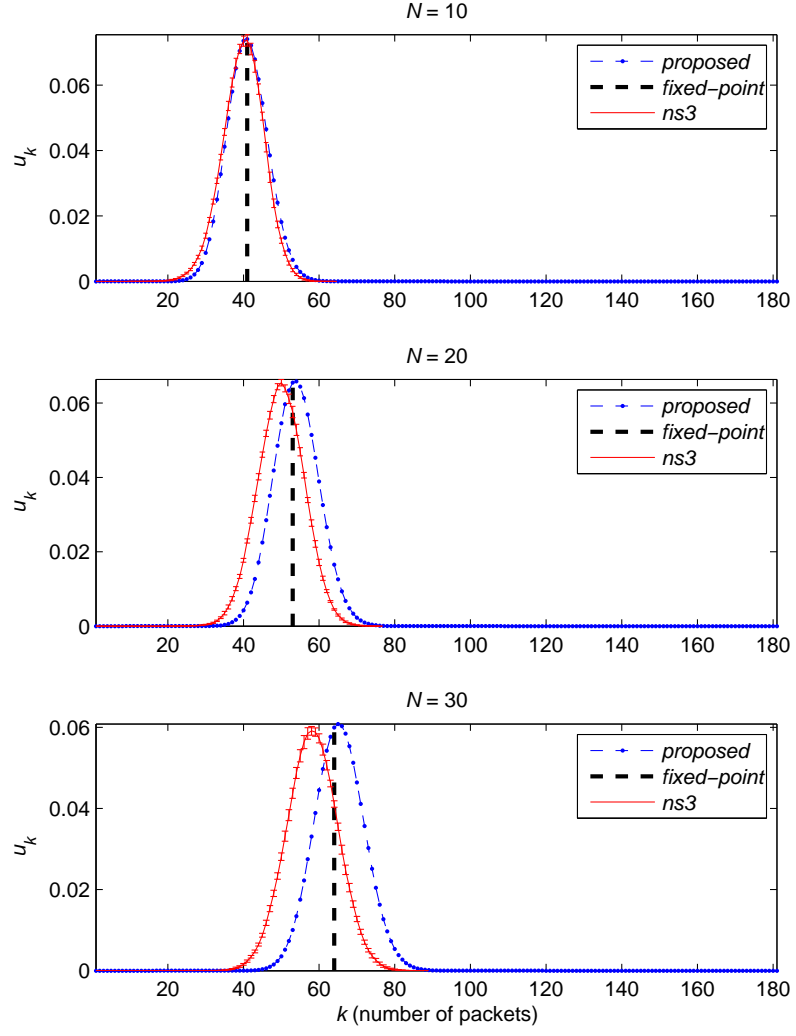


Figure 3.2: Queue occupancy PMF u_k for three values of N for Scenario A: $(D_L, D_F, D_{R_i}) = (5, 0, 5)$ ms.

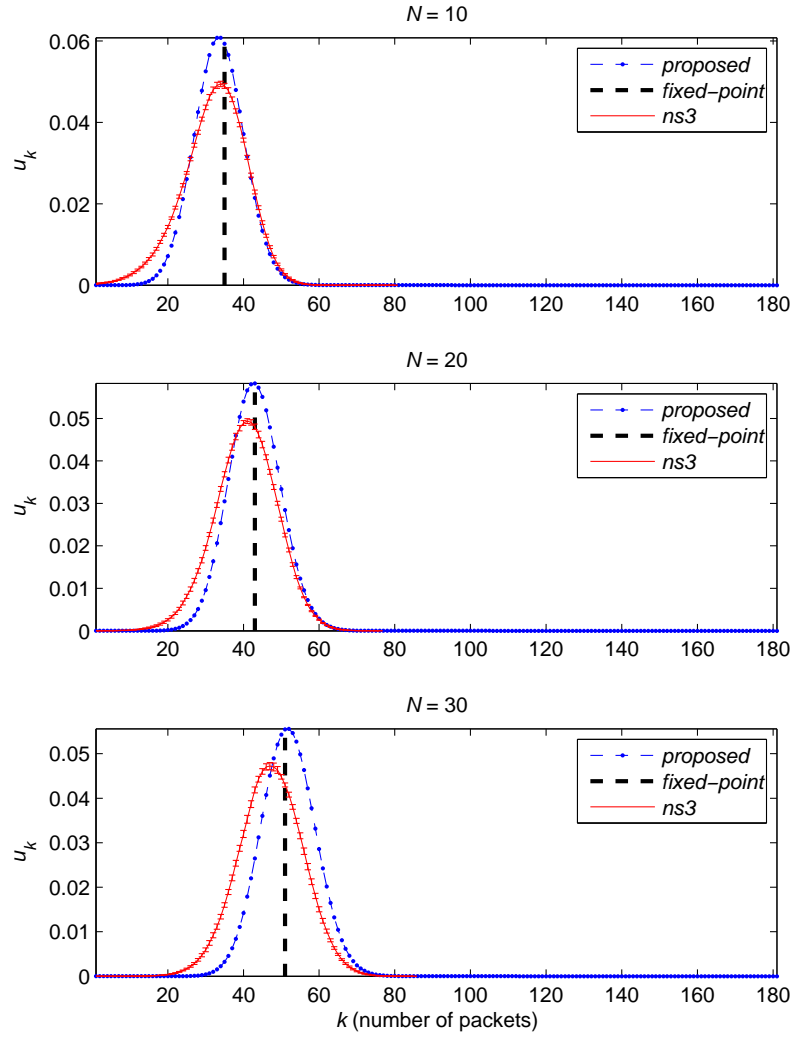


Figure 3.3: Queue occupancy PMF u_k for three values of N for Scenario B: $(D_L, D_F, D_{R_i}) = (15, 0, 5 + 5\lfloor i/(N/10) \rfloor)$ ms.

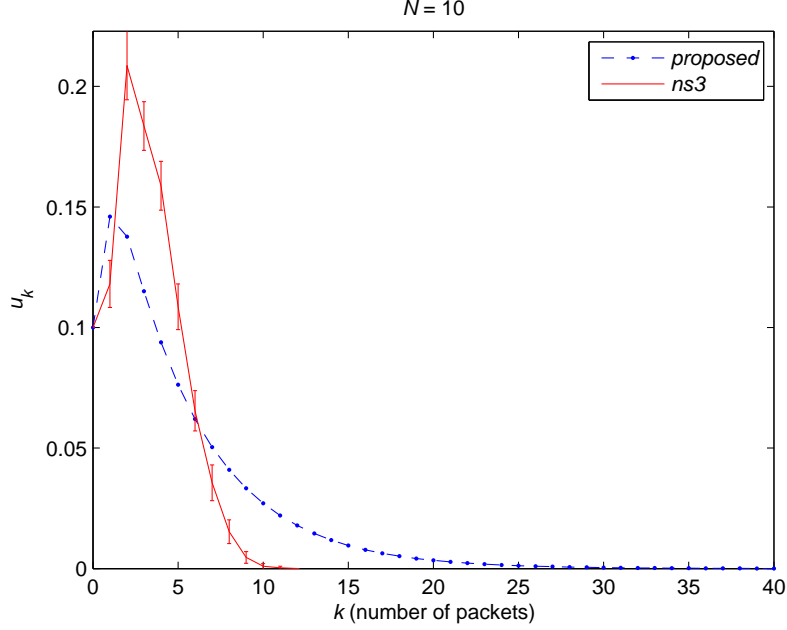


Figure 3.4: Queue occupancy PMF u_k for Scenario B with $N = 10$ and $r_L = 0.9$ Mbps.

whereas the *proposed* captures the actual PMF acceptably well. In particular, the probability mass at zero $V(0)$ is found to be 0.1000188, 1, and 0.0999987, using *proposed*, *fixed-point*, and simulations, respectively. In a network of queues, it is likely that most of the links will be operating at an empty queue regime. We believe that PMF capturing capability of *proposed* in the empty-queue regime will be crucial in the analysis of such systems.

For the final validation example in the wireless context, we study Scenario C which refers to $(D_L, D_F, D_{R_i}) = (5, 5, 10)$ ms employing non-zero $PER_{m,s}$. Queue occupancy PMF results using *proposed* and simulations are provided in Figs. 3.5, 3.6 and 3.7, for $PER_{m,s}$ being equal to 0.1, 0.01, and 0.001, respectively, each for three values of N , i.e., $N = 1, 4, 16$. For $N = 4$ and $PER_{m,s} = 0.01$ in Fig. 3.6, number of simulations is again set to 120 in order to increase the reliability of simulations. The simulation PMF appears to be captured well by the proposed analysis method for a wide range of packet error rates. For $N = 1$ and $PER_{m,s} = 0.001$, ns-3 simulations show a peak which is caused by alternating on

and off times during which the queue is on and off, respectively, and the Poisson assumption does not hold as well as the other cases. However, the general shape of the PMF is still captured for this challenging scenario.

3.4 Cross Layer Framework

The PHY *Wireless-MAN OFDMA PHY* specifies a cellular system comprising a Base Station (BS) and a number of Mobile Stations (MSs) [75]. In this section, we perform cross-layer analysis of the IEEE 802.16 *Wireless-MAN OFDMA PHY* air interface which can also alternatively be used for a Point-To-Point (PTP) wireless link [149],[150]. We study this wireless link carrying long-lived TCP traffic flows for different values of N , $RTT_{0,i}$, and SNR_s , and for two different wireless channel models. This analysis suits well to the OFDM-based air interfaces which became viable for PTP wireless links [151],[152] while also being applicable to the downlink of a cellular system with FIFO queuing.

We run the PHY simulations with Coded Modulation Library (CML) to obtain the $PER_{m,s}$ values for given MCS_m and SNR_s [153]. For this purpose, we choose the MCSs that use Convolutional Turbo Codes (CTC). There exist 32 MCSs for CTC out of which $M = 8$ are enumerated in Table 3.1 for use in the current study which differ according to their modulation order V_m (i.e., the number of points in the constellation diagram), code rate R_m , and Forward Error Correction (FEC) block length k_m . Assuming FEC block error events of a packet to be iid Bernoulli distributed, $PER_{m,s}$ can be derived from the FEC block Error Rate (FER) $FER_{m,s}$ as follows:

$$PER_{m,s} = 1 - (1 - FER_{m,s})^{\lceil L/k_m \rceil}. \quad (3.22)$$

On the other hand, the $FER_{m,s}$ values in (3.22) can be obtained using CML. For the sake of completeness, we present all $FER_{m,s}$ vs. SNR_s curves in Figs. 3.8 and 3.9 for the Additive White Gaussian Noise (AWGN) and ITU Vehicular-A channels, respectively, the latter corresponding to an MS with velocity 90 km/hr.,

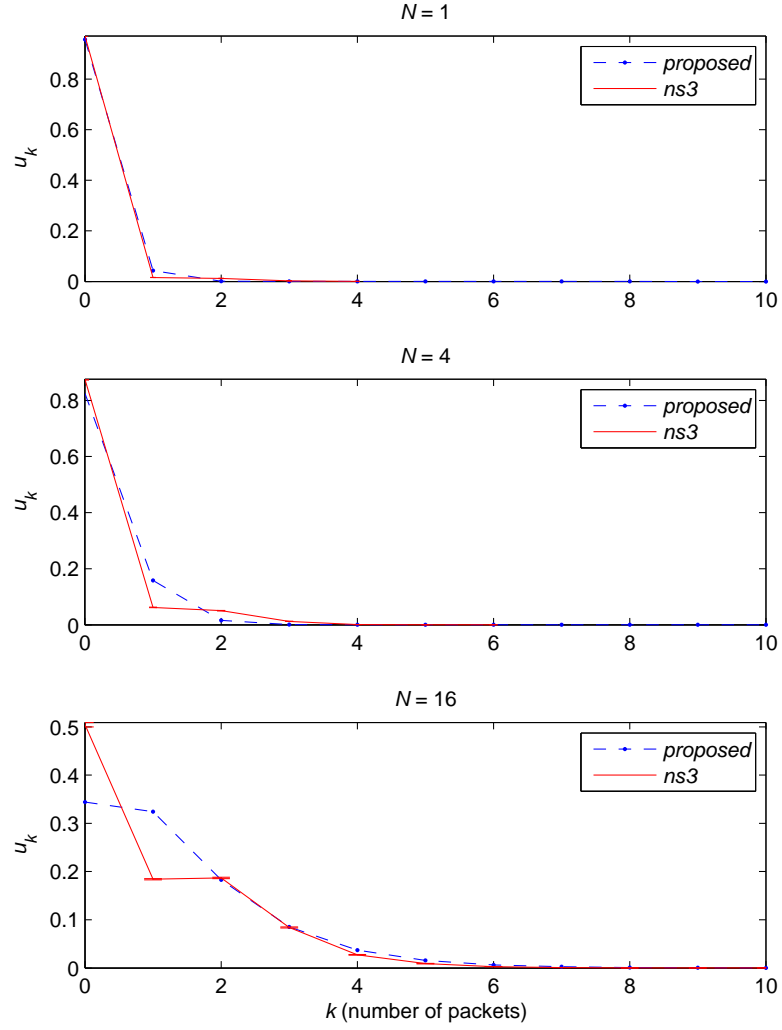


Figure 3.5: Queue occupancy PMF u_k for Scenario C: $(D_L, D_F, D_{R_i}) = (5, 5, 10)$ ms with $PER_{m,s} = 0.1$ for three different N values.

Table 3.1: Modulation and coding schemes of IEEE 802.16 used in this study.

m	0	1	2	3	4	5	6	7
V_m	4	4	16	16	64	64	64	64
R_m	1/2	3/4	1/2	3/4	1/2	2/3	3/4	5/6
$k_m(\text{bytes})$	60	54	60	54	54	48	54	60

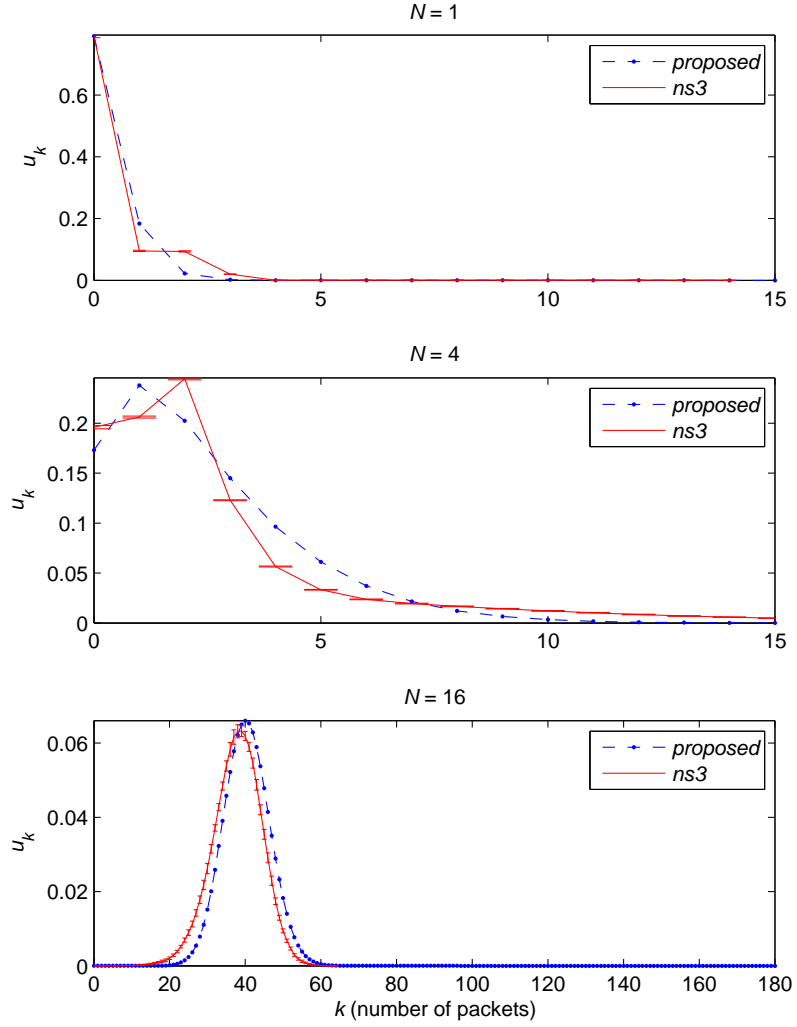


Figure 3.6: Queue occupancy PMF u_k for Scenario C: $(D_L, D_F, D_{R_i}) = (5, 5, 10)$ ms with $PER_{m,s} = 0.01$ for three different N values.

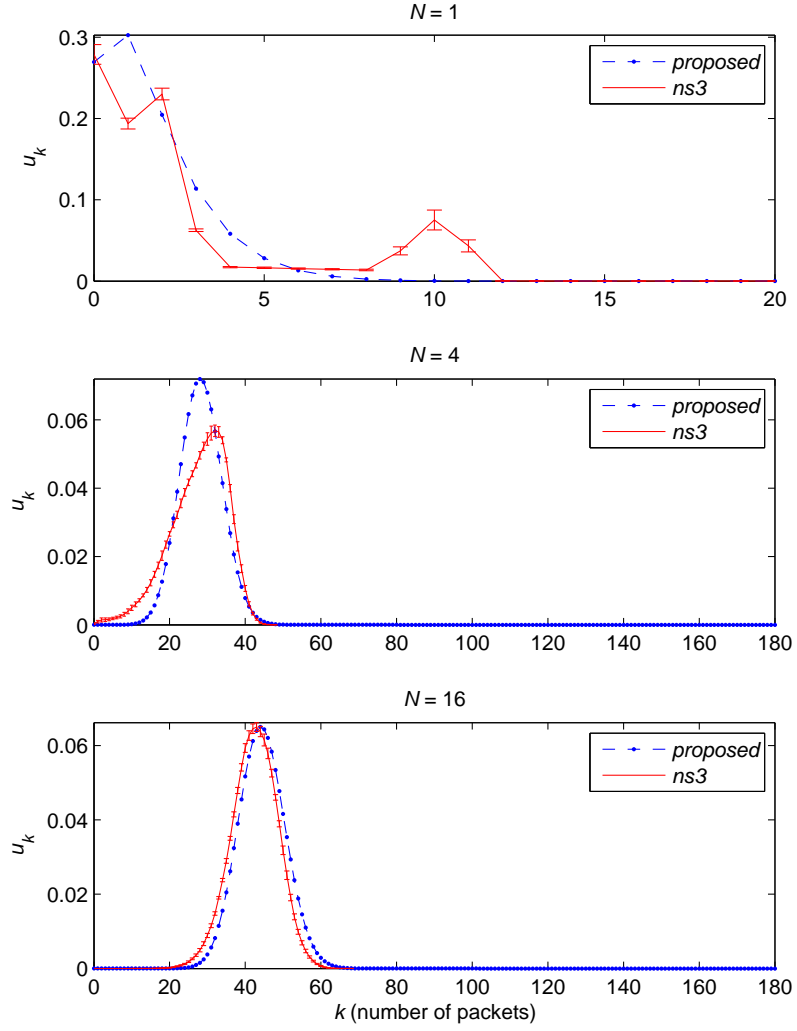


Figure 3.7: Queue occupancy PMF u_k for Scenario C: $(D_L, D_F, D_{R_i}) = (5, 5, 10)$ ms with $PER_{m,s} = 0.001$ for three different N values.

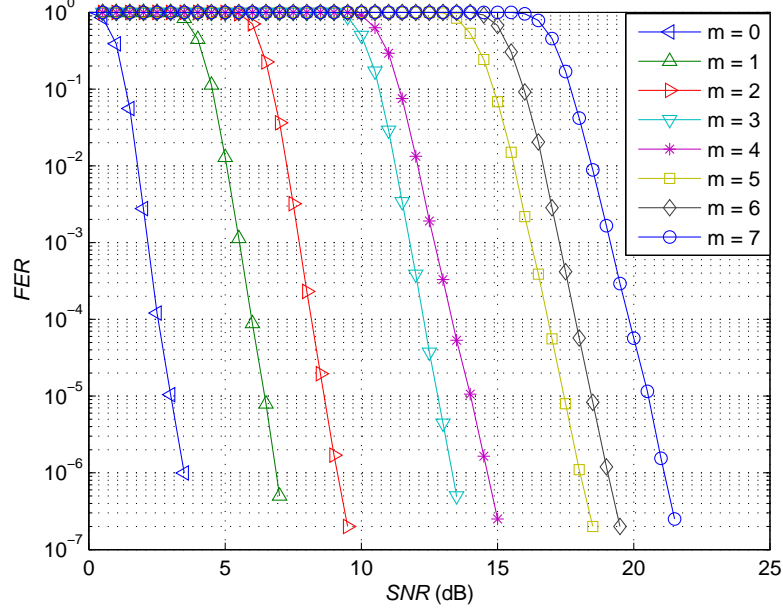


Figure 3.8: Simulated FER $FER_{m,s}$ for the AWGN channel.

which is referred to as the ITU-A channel for the rest of the chapter [1]. SNR ranges of $[0 \text{ dB}, 22 \text{ dB}]$ and $[0 \text{ dB}, 40 \text{ dB}]$ are sampled with a resolution of 0.5 dB and 2 dB to obtain the corresponding SNR_s values for the AWGN and ITU-A channels respectively. At least 10^7 FEC blocks are decoded to reach the presented FER values unless 400 FEC block error events are encountered. Once the $PER_{m,s}$ values are obtained, they are fed into the workload-dependent $M/D/1$ queuing model to estimate the aggregate TCP throughput for a given MCS_m and SNR_s .

For the sake of fairness in throughput comparisons between different MCSs, L in (3.22) is set to the least common multiple of the k_m values for $m \in \{0, 1, \dots, M-1\}$, which equals 2160 bytes to avoid padding for any MCS_m . Discretization interval Δ of the queue is set to 9.6 bits for this section which amounts to the packet size L divided by 1800. Time Division Duplex (TDD) mode as specified by WiMAX [154] dictates 35 downlink (DL) OFDM symbols each having 768 data sub-carriers for a channel bandwidth of 10 MHz [75] within a TDD frame duration of 5 ms, resulting in an average PHY rate of $r = 5.376 \cdot 10^6$

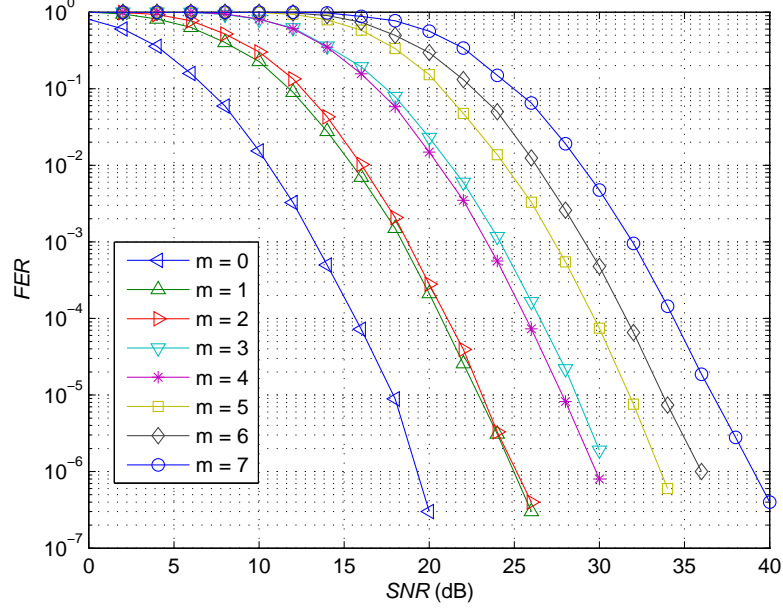


Figure 3.9: Simulated FER $FER_{m,s}$ for the ITU-A channel.

sub-carriers/s. Based on these parameters, the raw bit rate r_m of the IEEE 802.16 *Wireless-MAN OFDMA PHY* air interface can be calculated in bps as follows:

$$r_m = r \log_2(V_m) R_m. \quad (3.23)$$

In order to account for transmission, framing and processing delays of the system, $D_T + 2D_F$ is set to 5 ms. For the remaining set of parameters, we study scenarios both for the AWGN and ITU-A channels spanning a wide range of N , $RTT_{0,i}$, and SNR_s values where $s \in \{s_{\min}, \dots, S-1\}$ and s_{\min} is such that $PER_{0,s_{\min}} < 0.1$ for each channel type. In particular, we study two groups of scenarios having fixed and uniformly spaced $RTT_{0,i}$ denoted by $SF_{N,F}$ and $SU_{N,F}$, respectively, where $N \in \{1, 4, 16\}$ and $F \in \{1, 5, 10, 20, 40, 80, 120, 160\}$ ms. In scenario $SF_{N,F}$, there are N long-lived TCP flows and all flows have the same $RTT_{0,i}$ of F ms. On the other hand, in scenario $SU_{N,F}$, there are again N flows but each with a different $RTT_{0,i}$. For $N = 4$, flow i , $0 \leq i \leq 3$, has its $RTT_{0,i}$ set to $2(i+1)F/5$ leading to an average fixed RTT of F ms. For example, in $SU_{4,10}$, flows have individual fixed RTT values of 4, 8, 12 and 16 ms, with an average of 10 ms. For $N = 16$, each $RTT_{0,i}$ value for the $N = 4$ case is further mapped to four different fixed

RTTs in a similar fashion to obtain the same average fixed RTT of F ms. For example, in $SU_{16,10}$, flows have individual fixed RTT values of 1.6, 3.2, 4.8, 6.4, 3.2, 6.4, 9.6, 12.8, 4.8, 9.6, 14.4, 19.2, 6.4, 12.8, 19.2 and 25.6 ms, again with an average of 10 ms. Note that scenarios represented by $SF_{1,F}$ and $SU_{1,F}$ are identical, thus leading to an overall of forty unique scenarios.

In the first example, we study the particular scenarios $SF_{N,160}$ for different values of N by solving the proposed queuing model and calculating the aggregate TCP throughput for each MCS_m , N and SNR_s for the AWGN channel. We present the optimal MCS index, denoted by m^* , leading to the highest aggregate TCP throughput in Fig. 3.10 as a function of the channel SNR for all values of N . We observe that as N increases, the benefit of increasing the spectral efficiency by choosing a higher order MCS outweighs the penalty of increasing wireless loss rate at certain SNR values. It is therefore clear that the optimal decision on MCS relies on a-priori knowledge on the number of TCP flows sharing the link. Obtaining the optimum MCS in an on-line setting, however, requires the estimation of N and $RTT_{0,i}$ which is generally known to be difficult. As a remedy, we propose the so-called Traffic-AGnostic Link Adaptation (*TAGLA*) scheme which does not require the estimation of traffic parameters but takes into consideration only the spectral efficiency and FER values of the MCSs that its PHY has to offer. In particular, *TAGLA* chooses the MCS with the highest spectral efficiency whose resulting $PER_{m,s} \leq th_{PER}$ for a threshold parameter th_{PER} . In case of plurality of such MCSs with the same spectral efficiency, *TAGLA* chooses the one with the lowest PER. At the limiting cases $th_{PER} = 0$ and $th_{PER} = 1$, *TAGLA* resorts to MCS_0 and MCS_7 , respectively, regardless of the SNR_s value. The *TAGLA* scheme only requires a mapping between the target PER values and the FER estimations to be continuously fed back by the PHY. Choice of the target PER parameter th_{PER} is then crucial for the performance of the *TAGLA* scheme which we now study.

Averaging the results of the proposed model over all possible SNR values we study, the average aggregate TCP throughput as a function of these forty scenarios is depicted in Figs. 3.11 and 3.12 for various values of the th_{PER} parameter and for both channel models. The optimum aggregate TCP throughput obtained

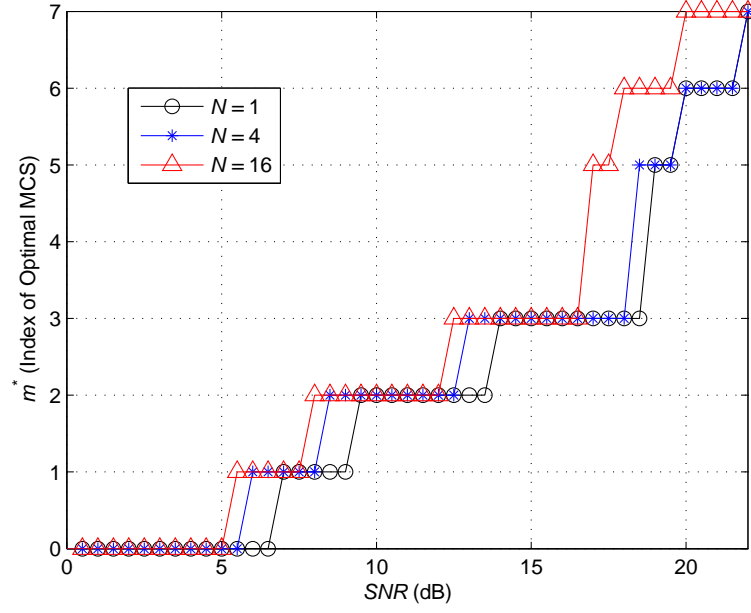


Figure 3.10: Optimum MCS selection for the AWGN channel as a function of SNR level SNR_s for scenarios $SF_{1,160}$, $SF_{4,160}$ and $SF_{16,160}$ corresponding to $RTT_{0,i} = 160$ ms and $N = 1$, $N = 4$, $N = 16$, respectively.

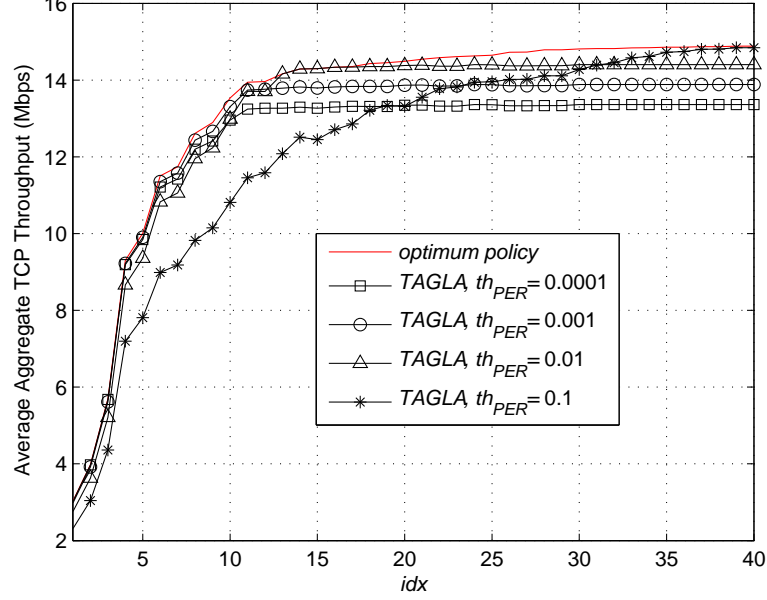


Figure 3.11: Average aggregate TCP throughput achieved by the *optimum policy* and *TAGLA* averaged over SNR_s for each scenario of Table 3.2 for the AWGN channel.

by choosing the best possible MCS given SNR_s , N , and $RTT_{0,i}$, is also averaged in the same way and presented as a benchmark.

The scenarios are indexed with a parameter called idx as shown in Tables 3.2 and 3.3, for increasing throughput of the so-called *optimum policy* in the AWGN and ITU-A channels, respectively. Low values of idx , corresponding to relatively low values for N and large values for $RTT_{0,i}$, are representative of situations in which the TCP flows cannot keep the queue always full. In such cases, the throughput is lower and the penalty of using larger values of th_{PER} is apparent. Conversely, large values for idx are indicative of a situation in which TCP can keep the queue full all the time despite wireless losses and the optimum policy is to use the MCS with the best spectral efficiency but with larger wireless loss rates. This observation remains intact for both channel models.

In order to assess the sensitivity of throughput to th_{PER} in different scenario settings, we form two groups among the scenarios studied so-far, namely G_{low}

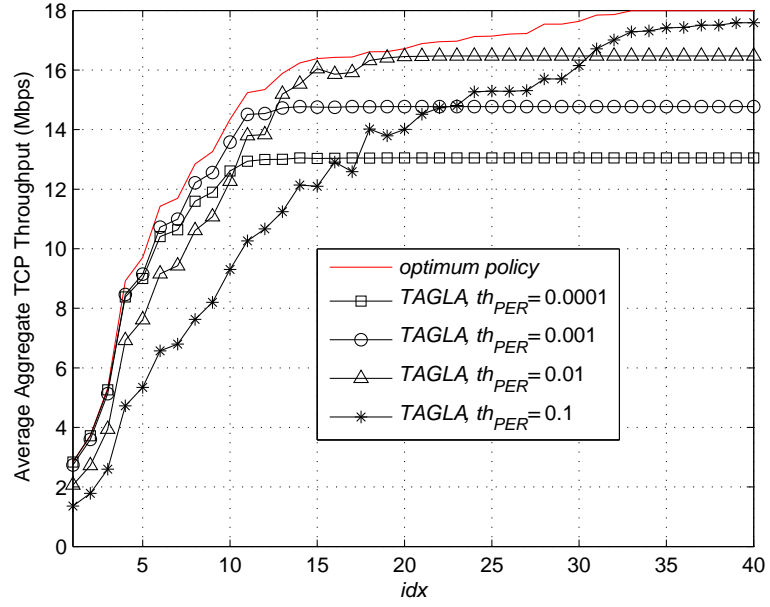


Figure 3.12: Average aggregate TCP throughput achieved by the *optimum policy* and *TAGLA* averaged over SNR_s for each scenario of Table 3.3 for the ITU-A channel.

Table 3.2: Scenarios $SF_{N,F}$ and $SU_{N,F}$ indexed by increasing throughput of *optimum policy* for the AWGN channel.

idx	scenario	idx	scenario
1	$SF_{1,160}$	21	$SU_{16,160}$
2	$SF_{1,120}$	22	$SF_{4,10}$
3	$SF_{1,80}$	23	$SU_{4,10}$
4	$SF_{1,40}$	24	$SF_{16,80}$
5	$SF_{4,160}$	25	$SU_{16,120}$
6	$SU_{4,160}$	26	$SF_{4,5}$
7	$SF_{4,120}$	27	$SU_{4,5}$
8	$SF_{1,20}$	28	$SF_{4,1}$
9	$SU_{4,120}$	29	$SU_{4,1}$
10	$SF_{4,80}$	30	$SU_{16,80}$
11	$SF_{1,10}$	31	$SF_{16,40}$
12	$SU_{4,80}$	32	$SU_{16,40}$
13	$SF_{1,5}$	33	$SF_{16,20}$
14	$SF_{4,40}$	34	$SU_{16,20}$
15	$SF_{1,1}$	35	$SF_{16,10}$
16	$SU_{4,40}$	36	$SU_{16,10}$
17	$SF_{16,160}$	37	$SF_{16,5}$
18	$SF_{4,20}$	38	$SU_{16,5}$
19	$SU_{4,20}$	39	$SF_{16,1}$
20	$SF_{16,120}$	40	$SU_{16,1}$

Table 3.3: Scenarios $SF_{N,F}$ and $SU_{N,F}$ indexed by increasing throughput of *optimum policy* for the ITU-A channel.

idx	scenario	idx	scenario
1	$SF_{1,160}$	21	$SU_{16,160}$
2	$SF_{1,120}$	22	$SF_{4,10}$
3	$SF_{1,80}$	23	$SU_{4,10}$
4	$SF_{1,40}$	24	$SU_{16,120}$
5	$SF_{4,160}$	25	$SF_{16,80}$
6	$SU_{4,160}$	26	$SF_{4,5}$
7	$SF_{4,120}$	27	$SU_{4,5}$
8	$SF_{1,20}$	28	$SF_{4,1}$
9	$SU_{4,120}$	29	$SU_{4,1}$
10	$SF_{4,80}$	30	$SU_{16,80}$
11	$SF_{1,10}$	31	$SF_{16,40}$
12	$SU_{4,80}$	32	$SU_{16,40}$
13	$SF_{1,5}$	33	$SF_{16,20}$
14	$SF_{4,40}$	34	$SU_{16,20}$
15	$SF_{1,1}$	35	$SF_{16,10}$
16	$SF_{16,160}$	36	$SU_{16,10}$
17	$SU_{4,40}$	37	$SF_{16,5}$
18	$SF_{16,120}$	38	$SU_{16,5}$
19	$SF_{4,20}$	39	$SF_{16,1}$
20	$SU_{4,20}$	40	$SU_{16,1}$

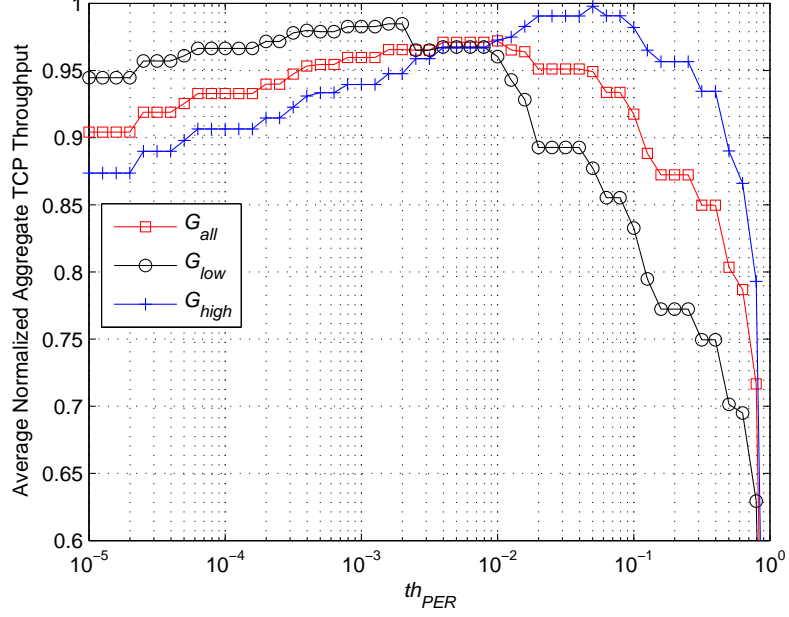


Figure 3.13: Average normalized aggregate TCP throughput achieved by *TAGLA* averaged over SNR_s for scenarios G_{all} , G_{low} , and G_{high} for the AWGN channel.

and G_{high} , by partitioning the range of idx into subsets $[1, \dots, 15]$ and $[26, \dots, 40]$, respectively. We also let G_{all} represent the group of all scenarios with $idx \in [1, \dots, 40]$. First, we normalize the throughput of *TAGLA* with that of *optimum policy* for each SNR_s and idx to avoid a bias favoring MCSs with high spectral efficiency. Then, we average the normalized throughput values over SNR_s and idx within the ranges of each group to obtain the average normalized aggregate TCP throughput shown in Figs. 3.13 and 3.14 for the AWGN and ITU-A channels, respectively.

The choice of $th_{PER} = 5 \times 10^{-3}$ turns out to be a robust operating point for the three groups resulting in at most 4% and 12% performance penalties with respect to the *optimum policy* for the AWGN and ITU-A channels, respectively. Targeting higher (lower) wireless loss rates has a negative impact on the TCP throughput especially for G_{low} (G_{high}). The reduction in TCP throughput around the proposed th_{PER} value is more pronounced for the ITU-A channel which can be accounted for its relatively flat FER vs. SNR curves shown in Fig. 3.9. For a

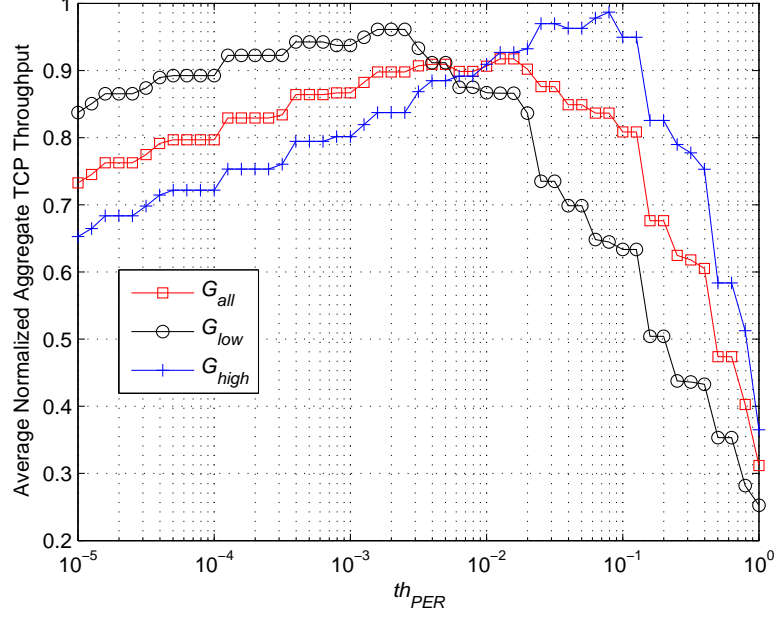


Figure 3.14: Average normalized aggregate TCP throughput achieved by *TAGLA* averaged over SNR_s for scenarios G_{all} , G_{low} , and G_{high} for the ITU-A channel.

given SNR, FER values of the ITU-A channel are relatively closer to each other on the average. For this reason, the performance of *TAGLA* is more sensitive to the choice of th_{PER} for this multipath fading channel model. The *TAGLA* scheme appears to have a potential for improvement provided that the threshold parameter th_{PER} could be adaptively changed based on an estimation of the underlying traffic parameters.

Chapter 4

Traffic-Agnostic Link Adaptation with HARQ (TAGLA_wH)

This chapter is organized as follows. In Section 4.1, problem description of the Traffic-AGnostic Link Adaptation with Hybrid ARQ (HARQ) (TAGLA_wH) is given. In Section 4.2, we present the workload-dependent queuing model along with an approximate resequencing delay model for HARQ. In Section 4.3, first the proposed resequencing delay model is validated and then the numerical results for the performance of the TAGLA_wH scheme are presented.

4.1 Problem Description

In this chapter, we generalize the framework presented in Chapter 3 to accommodate the HARQ retransmission technique. From a modeling perspective, one needs to address the following issues raised by the use of HARQ: (i) the workload increase caused by retransmissions, (ii) enhanced physical layer (PHY) decoding performance reflected to the resulting Packet Error Rate (PER), (iii) retransmission delays and (iv) out-of-order packet arrivals at the TCP receiver. We address the effect of out-of-order packet arrivals by claiming resequencing to be an integral

part of any HARQ-TCP system changing the original packet order. Drawback of resequencing, however, is an additional delay added to the Round-Trip Times (RTTs) of the TCP flows. In the current chapter, we address these issues on the basis of the queuing model of Chapter 3. Since the workload-dependent queuing framework of Chapter 3 is extensively validated for a wide variety of traffic scenarios, in terms of both packet delay and loss values, this effort is not replicated in this chapter. On the other hand, the proposed approximate model for the resequencing delay is validated with MATLAB[®] simulations and is shown to lead to an acceptable level of accuracy. The presented analytical method is then used to evaluate the performance of a Traffic AGnostic Link Adaptation scheme with HARQ (TAGLAWH) tracking the probability of failure in the first transmission attempt.

4.2 Analytical Model

In this study, we analyze a wireless link which is the bottleneck link (i.e., packet losses and bandwidth limitations at other links are negligible) for a fixed number, say N , of contending TCP flows. The link is offered with M Modulation and Coding Schemes (MCSs) denoted by MCS_m , where $m \in [0, M - 1]$, operating at an SNR level SNR_s , where $s \in [0, S - 1]$, among S possible SNR levels. The PHY of the system transmits each packet at a raw bit rate of r_m bps by means of Forward Error Correction (FEC) blocks of k_m bytes. Upon failure of decoding a FEC block at the receiver, the block is retransmitted up to Z times adhering to the Selective Repeat policy using Type-II HARQ with Chase Combining (HARQ-CC). The TCP flows have arbitrary but fixed RTTs denoted by $RTT_{0,i}$ for flow i , $i \in [0, N - 1]$. Packets have a common and deterministic packet length of L bytes and are subject to Active Queue Management (AQM) at the ingress of the wireless transmitter's First-In-First-Out (FIFO) queue. The packets experience a two-way framing delay $2D_F$ and a mean resequencing delay $X_{m,s}$ accounting for the delay caused by both the random retransmissions and the resequencing process at the receiver. TCP ACK packets transmitted at the reverse path are assumed to be prioritized so that associated delay and losses can be neglected.

4.2.1 $M(x)/G/1$ Queuing Model

We adopt the description and the accompanying notation for workload-dependent $M(x)/G/1$ queues from [10]. In this study, we model the wireless link as an $M/D/1$ queue with Poisson TCP packet arrivals with a workload-dependent intensity function $\lambda(x)$, and a deterministic workload-dependent service rate $r(x)$ (in units of bps) where x is the instantaneous workload (in units of bits) of the queue. Packets contribute to the workload of the queue by a job size (in units of bits) whose Cumulative Distribution Function (CDF) is denoted by $B(\cdot)$. It is shown in [10] that the steady-state workload density $v(\cdot)$ satisfies the following integro-differential equation for $x > 0$:

$$\begin{aligned} r(x)v(x) &= \lambda(0)V(0)(1 - B(x)) \\ &+ \int_{y=0^+}^x (1 - B(x - y))\lambda(y)v(y) dy, \end{aligned} \quad (4.1)$$

with a non-zero atom $V(0)$ at $x = 0$, for finite length buffer space as shown in Chapter 3.

In order to find $\lambda(x)$ in (4.1), we use the so-called ‘‘PFTK’’ TCP model of [5] which relates the packet loss rate and RTT seen by a flow to its TCP packet sending rate. Let p , λ , and T_0 denote the packet loss rate, packet send rate, and the TCP retransmission timeout parameter of a TCP source, respectively. In our model, we use the following relationship used in the implementation of TCP in [2]:

$$T_0 = \max(T_{0,\min}, RTT + 4\sigma_{RTT}), \quad (4.2)$$

where RTT and σ_{RTT} are the estimates for the mean and standard deviation of RTT, respectively, and $T_{0,\min}$ is the minimum value the timeout parameter can take. Let W_u and $W_{\max} = W/L$ denote the random variables associated with the unconstrained window size and the maximum window size (in units of packets) of the TCP source where W is the TCP receiver’s buffer size. Also let b denote the number of packets referred to, by a single cumulative ACK packet sent by the TCP receiver. The reference [5] proposes the following equation to relate the

TCP packet send rate λ to p and RTT seen by a flow:

$$\lambda = \begin{cases} \frac{\frac{1-p}{p} + E[W_u] + \tilde{Q}(E[W_u])\frac{1}{1-p}}{RTT(\frac{b}{2}E[W_u] + 1) + \tilde{Q}(E[W_u])T_0\frac{f(p)}{1-p}}, & E[W_u] < W_{\max} \\ \frac{\frac{1-p}{p} + W_{\max} + \tilde{Q}(W_{\max})\frac{1}{1-p}}{RTT(\frac{b}{8}W_{\max} + \frac{1-p}{pW_{\max}} + 2) + \tilde{Q}(W_{\max})T_0\frac{f(p)}{1-p}}, & \text{otherwise,} \end{cases} \quad (4.3)$$

where

$$f(p) = 1 + p + 2p^2 + 4p^3 + 8p^4 + 16p^5 + 32p^6, \quad (4.4)$$

$$\tilde{Q}(w) = \min(1, \frac{(1 - (1-p)^3)(1 + (1-p)^3)(1 - (1-p)^{(w-3)})}{1 - (1-p)^w}), \quad (4.5)$$

and

$$E[W_u] = \frac{2+b}{3b} + \sqrt{\frac{8(1-p)}{3bp} + \left(\frac{2+b}{3b}\right)^2}. \quad (4.6)$$

Throughout our numerical studies, we fix $T_{0,\min} = 0.2$ s as in [141], $b = 2$, $W = 64$ Kbytes as in [2] and $L = 1500$ bytes. With these, (4.3) provides a closed-form expression for the TCP send rate λ in terms of p , RTT and σ_{RTT} .

Loss component p in (4.3) is assumed to be comprised of the wireless packet errors and the intentional packet drops of the AQM policy which are statistically independent from each other. We assume Gentle variant of RED, GRED [68], to be the selected AQM scheme for regulating TCP traffic whose drop policy is as follows:

$$p(x) = \begin{cases} 0, & 0 \leq x < th_{\min} \\ \frac{x-th_{\min}}{th_{\max}-th_{\min}}p_{\max}, & th_{\min} \leq x < th_{\max} \\ p_{\max} + \frac{x-th_{\max}}{th_{\max}}(1-p_{\max}), & th_{\max} \leq x < 2th_{\max} \\ 1, & \text{otherwise.} \end{cases} \quad (4.7)$$

In this study, th_{\min} and th_{\max} are set to $30L$ and $90L$, respectively, in units of bits, and p_{\max} is set to 0.1 as in Chapter 3. Let $FER_{m,s,z}$ denote the FEC block Error Rate (FER) at the z^{th} retransmission where $z \in [0, Z]$. Then overall wireless packet loss probability $PER_{m,s}$ can be found as

$$PER_{m,s} = 1 - (1 - \prod_{z=0}^Z FER_{m,s,z})^{F_m}, \quad (4.8)$$

where $F_m = \lceil L/k_m \rceil$ stands for the minimum number of FEC blocks required to transmit a single packet, yielding an effective packet length of $L_m = F_mk_m$ bytes.

The RTT term of each flow also consists of multiple components as follows:

$$RTT_i(x) = RTT_{0,i} + 2D_F + L_m/r_m + x/r_m + X_{m,s}, \quad (4.9)$$

where L_m/r_m and x/r_m are the transmission and the queuing delays, respectively. We let V_m and R_m be the modulation order and the code rate of MCS_m and further decompose $r(x) = r_m$ as in (4.10) where r is the symbol rate of the PHY.

$$r_m = r \log_2(V_m) R_m. \quad (4.10)$$

Furthermore, let $T_{0,i}(x)$ denote the workload-dependent timeout parameter for flow i which can be expressed via (4.2) as

$$T_{0,i}(x) = \max(T_{0,\min}, RTT_i(x) + 4\sigma_{RTT,i}), \quad (4.11)$$

where $\sigma_{RTT,i}$ stands for the standard deviation of RTT for flow i . The term $\sigma_{RTT,i}$ can be related to the standard deviation of the queuing delay $\sigma_{Q_{m,i}}$ and that of the resequencing delay $\sigma_{X_{m,s}}$ as follows:

$$\sigma_{RTT,i} = \sqrt{\sigma_{X_{m,s}}^2 + \sigma_{Q_{m,i}}^2}. \quad (4.12)$$

We refer reader to Chapter 3 for the formulation of $\sigma_{Q_{m,i}}$ and derive the resequencing statistics $X_{m,s}$ and $\sigma_{X_{m,s}}$ in the next section.

The overall rate of packets that are admitted into the queue denoted by $\lambda(x)$ can then be written as

$$\lambda(x) = \sum_{i=0}^{N-1} (1 - p(x)) \lambda_i(x), \quad (4.13)$$

where $\lambda_i(x)$ is the send rate of flow i when the queue occupancy takes the value x . We propose to use the PFTK TCP model (4.3) to write $\lambda_i(x)$ by replacing RTT and T_0 with their per-flow workload-dependent counterparts $RTT_i(x)$ and $T_{0,i}(x)$, respectively. In a similar fashion, p is replaced by \bar{p}_i , the average packet loss probability for flow i , as in (4.14),

$$\bar{p}_i = 1 - (1 - PER_{m,s})(1 - \bar{q}_i), \quad (4.14)$$

where \bar{q}_i denotes the queue average packet loss probability stemming only from AQM for flow i .

Errored packets in the first transmission attempt are retransmitted using HARQ-CC for which all retransmitted packets are identical. Retransmissions are assumed to be made in a Selective Repeat manner for which only the packets received in error are retransmitted after a retransmission delay of D_R unless Z number of retransmission opportunities are exhausted for each packet. PMF $f_{\mathbf{H}_{m,s}}(h)$ for the Random Variable (RV) $\mathbf{H}_{m,s}$ denoting the number of retransmissions of each FEC block can be expressed as follows:

$$f_{\mathbf{H}_{m,s}}(h) = \begin{cases} 1 - FER_{m,s,0}, & h = 0 \\ (1 - FER_{m,s,h}) \prod_{z=0}^{h-1} FER_{m,s,z}, & 0 < h < Z \\ \prod_{z=0}^{Z-1} FER_{m,s,z}, & h = Z. \end{cases} \quad (4.15)$$

Assuming loss events of building FEC blocks of a packet to be independent and identically distributed (iid) Bernoulli distributed, total number of retransmissions required for each packet, denoted by the RV $\mathbf{G}_{m,s}$ is the maximum of those of the F_m FEC blocks as shown in (4.16).

$$\mathbf{G}_{m,s} = \max_{F_m} \{\mathbf{H}_{m,s}\} \quad (4.16)$$

Retransmissions increase the workload of the transmitter which can be modeled as a virtual increase in the packet length. We let $f_{\mathbf{A}_{m,s}}(x)$ be the PDF of the virtual packet length denoted by $\mathbf{A}_{m,s}$ and relate it to PMF $f_{\mathbf{G}_{m,s}}(g)$ of $\mathbf{G}_{m,s}$ as follows:

$$f_{\mathbf{A}_{m,s}}(x) = \sum_{g=0}^Z f_{\mathbf{G}_{m,s}}(g) \delta(x - (g+1)L_m), \quad (4.17)$$

where $\delta()$ is the dirac delta function. Note that IEEE 802.16 *Wireless-MAN OFDMA PHY* air interface requires whole packet to be retransmitted even if a single FEC block is errored at the receiver which is captured by equation (4.17) [75]. Integrating $f_{\mathbf{A}_{m,s}}(x)$, we find $B_{m,s}(x)$ as in (4.18).

$$B_{m,s}(x) = \int_{y=0}^x f_{\mathbf{A}}(y) dy \quad (4.18)$$

Finally, we let $P_{m,s,z}$ denote the probability of failure of the z^{th} retransmission

and derive it from $f_{\mathbf{G}_{m,s}}(z)$ as follows:

$$P_{m,s,z} = \begin{cases} 1 - f_{\mathbf{G}_{m,s}}(0), & z = 0 \\ 1 - \frac{f_{\mathbf{G}_{m,s}}(z)}{\prod_{t=0}^{z-1} P_{m,s,t}}, & 0 < z < Z \\ \frac{PER_{m,s}}{\prod_{t=0}^{Z-1} P_{m,s,t}}, & z = Z. \end{cases} \quad (4.19)$$

As we present all components of (4.1), we refer reader to Chapter 3 for the remaining steps to reach a complete solution. We finalize this section by providing a method to numerically solve the integro-differential equation (4.1). For that purpose, queue occupancy is discretized with a discretization interval Δ such that $L/\Delta \gg 1$ is an integer. We then define $v_i = v(i\Delta)$, $\lambda_i = \lambda(i\Delta)$ and $B_i = B(i\Delta)$ for $i > 0$ and discretize (4.1) to obtain

$$v_i = \begin{cases} \frac{\lambda_0 V(0)(1-B_i) + \sum_{j=1}^{i-1} (1-B_{i-j}) \lambda_j v_j \Delta}{r - \lambda_i \Delta}, & i < l \\ \frac{\sum_{j=i-l+1}^{i-1} (1-B_{i-j}) \lambda_j v_j \Delta}{r - \lambda_i \Delta}, & \text{otherwise,} \end{cases} \quad (4.20)$$

where l is the integer such that $B(l\Delta) = 1$. Note that the identity (4.20) enables the calculation of v_i as a weighted sum of v_j 's for $j < i$. We propose to set $V(0) = 1$ and iteratively calculate v_i for $1 \leq i \leq K$ as in (4.20) where $\sum_{K+1}^{\infty} v_i \Delta = 0$. Throughout the chapter we safely set $K = (2th_{\max} + (Z+1)L_m)/\Delta$ and $\Delta = 20$ bits. We define $V = V(0) + \sum_{i=1}^K v_i \Delta$ and then normalize the quantities $V(0)$ and v_i as follows:

$$V(0) := V(0)/V, v_i := v_i/V, \quad 1 \leq i \leq K. \quad (4.21)$$

4.2.2 Approximate Resequencing Delay Model

The receiver maintains a resequencing buffer to re-order packets arriving out-of-order due to random retransmissions. The presumed resequencer in this analysis waits for the successful decoding of missing packets in its buffer and either upon their arrival or expiration of their timeouts imposed by the hard limit Z , releases all subsequent packets delayed for the arrival of these packets to the network. We note that the described resequencer is generic, since it does not adhere to a

particular implementation. In order to find the mean resequencing delay denoted by $X_{m,s}$, we first derive the associated PDF by taking similar steps with [155]. Briefly, the reference [155] models the resequencing delay caused by multipath data transfer between two hosts in a network, for which paths with distinct delays are randomly selected. Although the problem studied in [155] is very different, the proposed formulation is applicable to the problem at hand. We refer reader to the references [156], [157] and [158] for more comprehensive analysis on the subject.

The resequencing delay is defined as the time elapsed from the instant of reception of a packet by the receiver (either successfully or not) after the first transmission, until its disposal from the resequencing buffer. The resequencing delay, denoted by the RV $\mathbf{R}_{m,s}^i$ for the i^{th} packet can be expressed as follows.

$$\mathbf{R}_{m,s}^i = \max_{j \leq i} \{D_R \mathbf{G}_{m,s} - T_{m,s}(i - j)\}, \quad (4.22)$$

where $T_{m,s}$ is the mean interarrival time of packets to the receiver which are transmitted for the first time. Equation (4.22) formulates the resequencing delay of a packet as the maximum of either its own retransmission delay or the maximum amount of retransmission delay overlap of the preceding packets. Therefore, equation (4.22) has the inherent constraint $D_R Z > T_{m,s}(i - j)$, putting a limit on the number of preceding packets that may have a possible impact on the resequencing delay of the packet i . Assuming $\mathbf{R}_{m,s}^i$ to be iid, defining $k = i - j$ and dropping the packet indices, (4.22) can be rewritten as

$$\mathbf{R}_{m,s} = \max_{0 \leq k < \frac{D_R Z}{T_{m,s}}} \{D_R \mathbf{G}_{m,s} - T_{m,s}k\}. \quad (4.23)$$

$T_{m,s}$ not only depends on the packet length L_m , but also on the retransmission and transmitter queue statistics as follows:

$$T_{m,s} = \frac{L_m(1 + \mathbb{E}[\mathbf{G}_{m,s}])}{r_m(1 - V(0))}, \quad (4.24)$$

which is essentially the mean packet length divided by the mean capacity. Computing $X_{m,s} = \mathbb{E}[\mathbf{R}_{m,s}]$ and $\sigma_{X_{m,s}}^2 = \mathbb{V}[\mathbf{R}_{m,s}]$ based on (4.23) requires a few algebraic steps to derive the PDF of a RV standing for the maximum of a number of statistically independent RVs with known PDFs as for (4.16).

Table 4.1: Modulation and coding schemes of IEEE 802.16 used in this study.

m	0	1	2	3	4	5	6	7
V_m	4	4	16	16	64	64	64	64
R_m	1/2	3/4	1/2	3/4	1/2	2/3	3/4	5/6
$k_m(\text{bytes})$	60	54	60	54	54	48	54	60

4.3 Numerical Results

In this section, we evaluate the performance of the TAGLAWH scheme with a budget of Z retransmissions per packet, making its decisions irrespective of the parameters of the contending TCP flows to select the best MCS for HARQ-CC. More precisely, the proposed scheme chooses the MCS with the highest spectral efficiency having $P_{m,s,0} \leq th_P$, i.e., keeping the probability of failure in the first transmission below the threshold th_P . If no such MCS exists, TAGLAWH chooses MCS_0 . We conjecture th_P to be high enough to allow $PER_{m,s,0}$ to be calculated even from on-line statistics. We define a set of TCP traffic scenarios called $S_{N,F}$ with N flows, $N \in \{1, 2, 4, 8, 16\}$, each having a fixed RTT given by $RTT_{0,i} = 2(i+1)F/(N+1)$ where $F \in \{1, 4, 16, 64\}$ ms is the mean fixed RTT of all flows. $FER_{m,s,z}$ values are obtained through Coded Modulation Library (CML) PHY simulations based on IEEE 802.16e Wireless-MAN OFDMA PHY air interface [75]. Each MCS with Convolutional Turbo Codes (CTC) shown in Table 4.1 is simulated under the assumption of the ITU Vehicular-A channel [1] from a BS to an MS (downlink) with a velocity of 90 km/hr. The resulting $FER_{m,s,z}$ curves are shown in Fig.4.1 for an SNR range of $[0 \ 40]$ dB, sampled with 2 dB resolution. At least 10^7 FEC blocks are decoded to reach the presented FER values unless 400 FEC block error events are encountered.

Time Division Duplex (TDD) mode of WiMAX specification [154] has 35 downlink OFDM symbols each consisting of 768 data sub-carriers for a TDD frame with 10 MHz channel bandwidth and 5 ms duration offering an average PHY rate of $r = 5.376 \cdot 10^6$ sub-carriers/s. We fix the retransmission delay $D_R = 10$ ms as in [75] and the total of the two-way framing and the transmission delay $2D_F + L_m/r_m = 5$ ms.

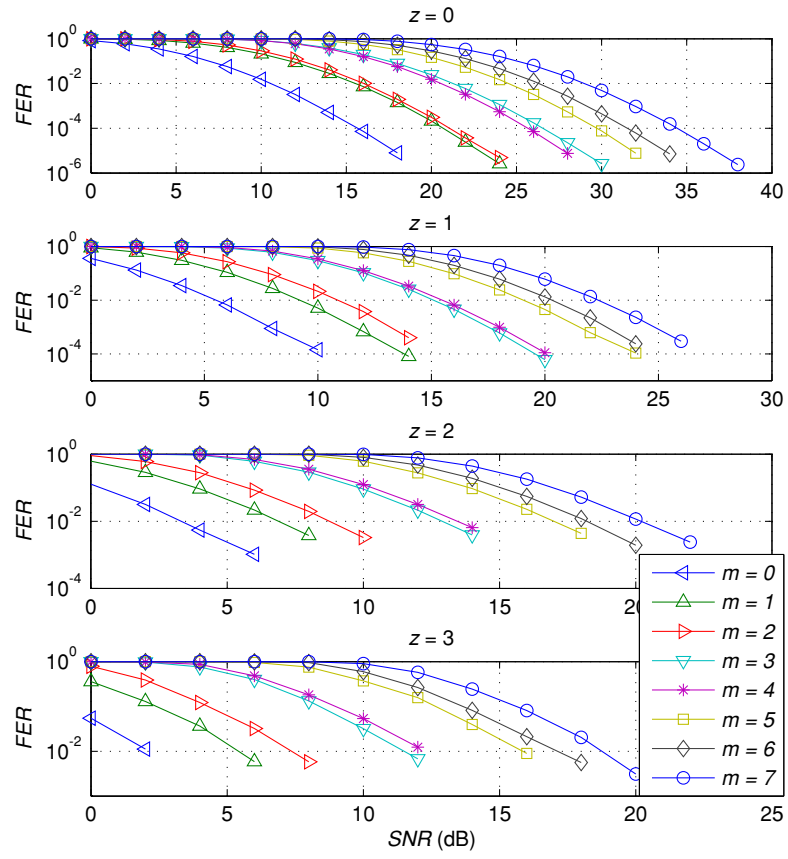


Figure 4.1: Simulated FER $FER_{m,s,z}$ for $Z = 3$ maximum number of allowed retransmissions and the ITU Vehicular-A channel.

Before evaluating the performance of TAGLAWH, we validate the proposed resequencing delay model with a number of MATLAB[®] simulations of a system consisting of: (i) a transmitter with a queue of packets to be retransmitted and having a new packet to send with a probability of $1 - V(0)$ whenever its retransmission queue is empty, (ii) a channel dropping packets as suggested by $P_{m,s,z}$ and (iii) a receiver with the aforementioned resequencing mechanism in Section 4.2.2. We generate sixteen test cases as shown in Table 4.2, by selecting queue occupancy atom $V(0) \in \{3 \cdot 10^{-3}, 3 \cdot 10^{-1}\}$, MCS index $m \in \{0, 2, 4, 7\}$ and SNR index s such that $P_{m,s,0} < \{3 \cdot 10^{-2}, 3 \cdot 10^{-1}\}$ is satisfied for minimum s . We present the simulation results along with the associated confidence intervals for 99% confidence level.

Table 4.2: Resequencing delay validation test cases and results for $Z = 3$. Results are presented with the 99% confidence intervals.

	$V(0)$	m	s	SNR (dB)	$P_{m,s,0}$	$X_{m,s}$ (ms)	$X_{m,s}$ -sim. (ms)	$\sigma_{X_{m,s}}$ (ms)	$\sigma_{X_{m,s}}$ -sim. (ms)
1	$3 \cdot 10^{-3}$	0	7	14	$1.26 \cdot 10^{-2}$	0.34	0.41 ± 0.04	1.55	1.80 ± 0.09
2	$3 \cdot 10^{-3}$	0	6	12	$7.84 \cdot 10^{-2}$	1.87	2.28 ± 0.08	3.28	3.77 ± 0.04
3	$3 \cdot 10^{-3}$	2	10	20	$7.66 \cdot 10^{-3}$	0.37	0.39 ± 0.06	1.58	1.62 ± 0.11
4	$3 \cdot 10^{-3}$	2	8	16	$2.25 \cdot 10^{-1}$	6.02	6.09 ± 0.05	3.53	3.57 ± 0.03
5	$3 \cdot 10^{-3}$	4	12	24	$1.51 \cdot 10^{-2}$	1.00	1.11 ± 0.10	2.46	2.63 ± 0.09
6	$3 \cdot 10^{-3}$	4	11	22	$8.79 \cdot 10^{-2}$	4.27	4.65 ± 0.09	3.74	3.92 ± 0.02
7	$3 \cdot 10^{-3}$	7	16	32	$2.34 \cdot 10^{-2}$	2.28	2.40 ± 0.12	3.32	3.43 ± 0.04
8	$3 \cdot 10^{-3}$	7	15	30	$1.15 \cdot 10^{-1}$	6.48	6.74 ± 0.13	3.13	3.17 ± 0.08
9	$3 \cdot 10^{-1}$	0	7	14	$1.26 \cdot 10^{-2}$	0.26	0.33 ± 0.02	1.38	1.65 ± 0.04
10	$3 \cdot 10^{-1}$	0	6	12	$7.84 \cdot 10^{-2}$	1.47	1.89 ± 0.05	3.08	3.62 ± 0.04
11	$3 \cdot 10^{-1}$	2	10	20	$7.66 \cdot 10^{-3}$	0.27	0.29 ± 0.03	1.38	1.43 ± 0.07
12	$3 \cdot 10^{-1}$	2	8	16	$2.25 \cdot 10^{-1}$	5.11	5.37 ± 0.07	3.87	3.90 ± 0.02
13	$3 \cdot 10^{-1}$	4	12	24	$1.51 \cdot 10^{-2}$	0.74	0.83 ± 0.05	2.18	2.36 ± 0.06
14	$3 \cdot 10^{-1}$	4	11	22	$8.79 \cdot 10^{-2}$	3.41	3.83 ± 0.12	3.73	3.99 ± 0.02
15	$3 \cdot 10^{-1}$	7	16	32	$2.34 \cdot 10^{-2}$	1.71	1.80 ± 0.08	3.03	3.15 ± 0.05
16	$3 \cdot 10^{-1}$	7	15	30	$1.15 \cdot 10^{-1}$	5.50	5.82 ± 0.10	3.54	3.63 ± 0.04

There is a slight disagreement between the simulations and the proposed analysis for both the first and the second order resequencing delay statistics which can be attributed to the approximate nature of the $T_{m,s}$ expression given in (4.24).

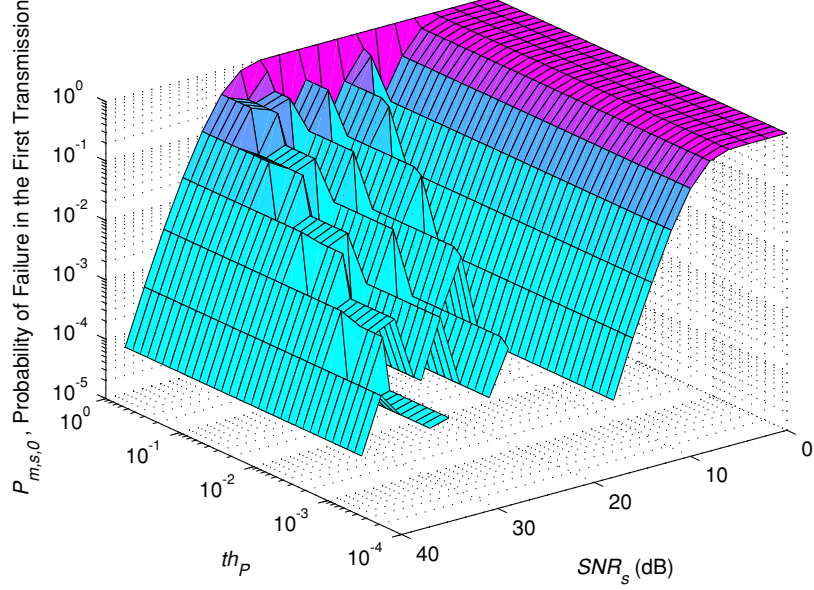


Figure 4.2: Probability of failure in the first transmission $P_{m,s,0}$ of TAGLAWH for varying SNR values SNR_s and threshold parameter th_P .

We also note that a packet to get retransmitted in simulation waits for an additional amount of time upon its NACK's arrival for the current transmission to finish, if any, a factor making the analytical results consistently less than those of the simulations. Overall, the accuracy of the proposed method is considered to serve well for the purposes of this study.

Next, we evaluate the performance of TAGLAWH using the presented analytical model. In Fig. 4.2, we show the resulting probability of failure in the first transmission $P_{m,s,0}$ of TAGLAWH with respect to SNR_s and th_P . TAGLAWH sticks to the most conservative MCS, MCS_0 , creating a waterfall-like region for relatively low SNR values. For increasing SNR, TAGLAWH switches to more aggressive MCSs manifesting itself as a staircase-like region until it reaches the most aggressive MCS, MCS_7 . As expected, boundary of these two regions is located at relatively lower SNR values for increasing values of th_P .

We call the policy whose MCS decision gives the highest throughput for each

and every value of SNR_s and traffic scenario $S_{N,F}$ as the Optimum Link Adaptation (OLA). In Fig. 4.3, aggregate TCP throughput of TAGLAWH normalized with that of OLA and averaged over all SNR_s values is presented for varying th_P and $S_{N,F}$ and for $Z = 3$ where traffic scenarios are indexed with the parameter idx for increasing average aggregate TCP throughput of OLA for the sake of visualization. We discard the SNR interval corresponding to $s \in [0, s_{\min} - 1]$ such that s_{\min} is the minimum index satisfying $P_{0,s_{\min},0} < 0.5$, in all statistical calculations over SNR_s , for Fig. 4.3 and also for other figures to come. We find $s_{\min} = 5$ corresponding to 10 dB SNR. As th_P increases, the performance of TAGLAWH reaches that of OLA regardless of the presumed traffic scenario. Owing to the retransmissions, $PER_{m,s}$ approaches zero for almost all values of th_P as evident from Fig. 4.1. Increasing th_P increases the resequencing delay $X_{m,s}$ and therefore the RTT of each TCP flow. The increase in RTT, however, is outweighed by the increase in channel capacity by choosing more aggressive MCSs on the average. The reason for relatively more insensitive behavior of TAGLAWH with respect to th_P for low idx values is that TCP sources cannot exploit the entire PHY capacity for aggressive MCSs reaching the limit imposed by their maximum TCP window size W_{\max} .

In Fig. 4.4, both the average and the minimum (worst case) normalized aggregate TCP throughput taken over all $S_{N,F}$ and SNR_s values are given for varying maximum number of allowed retransmissions Z . TCP throughput performance remains invariant of Z regardless of the threshold th_P , since the SNR range corresponding to $s \in [0, s_{\min} - 1]$ is excluded from the calculations. For the complementary range of interest, $s \in [s_{\min}, S - 1]$, the resulting $PER_{m,s}$ becomes negligible even after the first retransmission. In the light of the presented results, we recommend fixing th_P of TAGLAWH around 0.25, yielding an average of 4% and at worst 25% performance degradation compared to OLA. IEEE 802.16 does not enforce a particular value of th_P and this recommended value depends on the studied MCSs. Therefore, the proposed analysis should be repeated once the presumed PHY technology is changed.

Finally, both the average and the maximum (worst case) values of the mean resequencing delay $X_{m,s}$ are shown in Fig. 4.5 again for varying th_P and Z . For

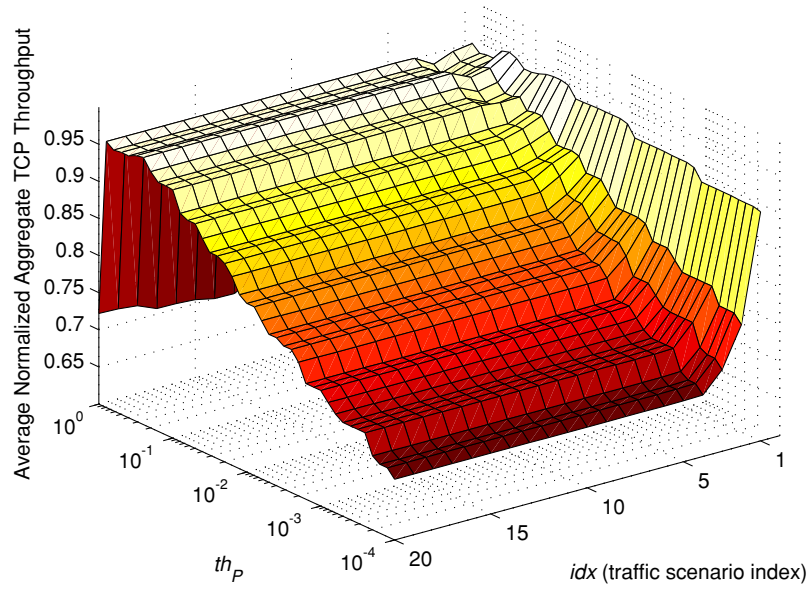


Figure 4.3: Normalized aggregate TCP throughput of TAGLAWH averaged over all SNR values SNR_s for varying traffic scenarios $S_{N,F}$ and threshold parameter th_P , and for $Z = 3$ maximum number of allowed retransmissions.

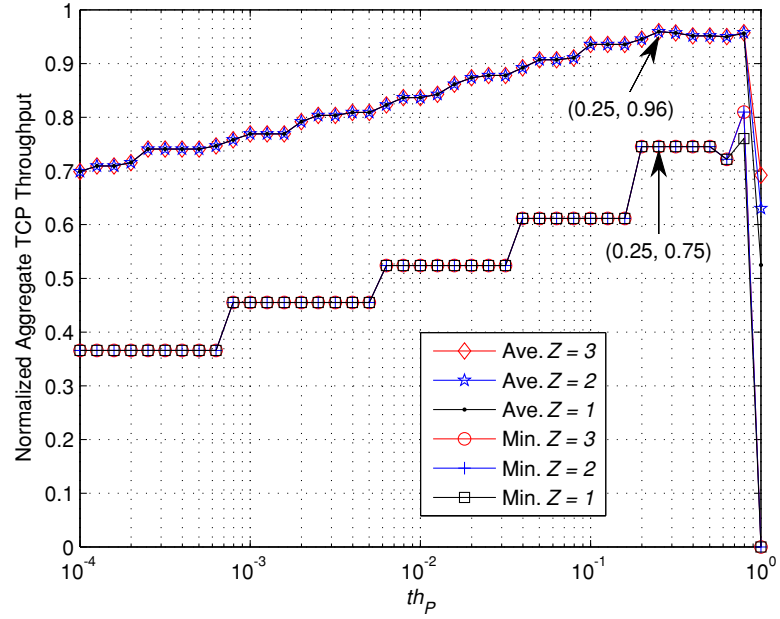


Figure 4.4: Average and minimum (worst case) normalized aggregate TCP throughput of TAGLawH taken over all SNR values SNR_s and traffic scenarios $S_{N,F}$ for varying threshold parameter th_P and maximum number of allowed retransmissions Z .

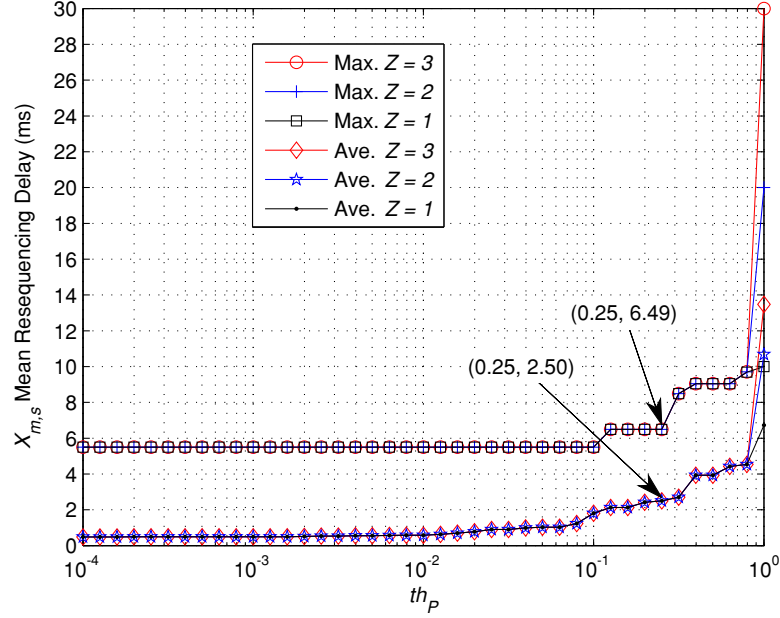


Figure 4.5: Average and maximum (worst case) mean resequencing delay $X_{m,s}$ of TAGLAWH taken over all SNR values SNR_s and traffic scenarios $S_{N,F}$ for varying threshold parameter th_P and maximum number of allowed retransmissions Z .

the same arguments made for the results of Fig. 4.4, $X_{m,s}$ remains unaffected from the choice of Z until th_P approaches 1, for which the minimum normalized aggregate TCP throughput drops down to 0. For the proposed value of $th_P = 0.25$, the maximum (worst case) and the average values of $X_{m,s}$ are computed to be around 6.49 ms and 2.50 ms, respectively. As long as the wireless link of interest remains the bottleneck link for all TCP flows it is serving for, th_P parameter of TAGLAWH can be optimized for throughput without paying much attention to increasing RTT due to the resequencing delay. For the estimation of the resulting throughput at a particular instance of the channel condition and the traffic scenario, however, the resequencing delay needs to be taken into account.

Chapter 5

Queue-Aware Link Adaptation (QAWLA)

This chapter is organized as follows. In Section 5.1, problem description of the Queue-Aware Link Adaptation (QAWLA) scheme is given. In Section 5.2, we present the general Dual-Regime Wireless Link (DRWL) framework along with the presumed assumptions and the particular QAWLA mechanism we propose for link adaptation. Section 5.3 presents the fixed-point model for the DRWL framework. In Section 5.4, traffic and wireless link scenarios used in the numerical experiments are described. Section 5.5 addresses the validation of the proposed fixed-point model using extensive ns-3 simulations. In Section 5.6, we provide numerical examples to validate the effectiveness of the proposed QAWLA scheme.

5.1 Problem Description

A Packet Error Rate (PER)-based Adaptive Modulation and Coding (AMC) mechanism driven solely by the physical layer (PHY) parameters, referred to as a Traffic-AGnostic Link Adaptation (TAGLA) in this chapter and also in Chapter 3, may lead to one of the two above-mentioned undesirable situations. Target PER

of such schemes can only be optimized if the system parameters of interest are precisely known, e.g., the number of contending TCP flows, their Round-Trip Times (RTTs), etc., in addition to the PHY parameters as shown in Chapter 3 and in [159]. However, estimation of such system parameters is highly difficult in practice [160]. As a remedy, we propose the framework of Dual-Regime Wireless Link (DRWL) for which the queue occupancy level is taken into consideration in the process of Modulation and Coding Scheme (MCS) selection, as opposed to using other system parameters that are hard to estimate. Specifically, we use a conservative (aggressive) MCS when the queue occupancy is below (above) a certain queue threshold in DRWL. Reducing the probability of empty queues and hence the link being under-utilized by TCP sources because of wireless packet losses is the rationale behind DRWL. We view DRWL as a general framework which does not produce a unique policy but instead comprises a set of policies out of which we propose one particular subset of policies called Queue-Aware Link Adaptation (QAWLA) in our numerical examples. Actually, the QAWLA policy attempts to maintain two particular per-regime PER values and therefore belongs to the DRWL framework.

5.2 Dual-Regime Wireless Link

We envision a point-to-point wireless link employing Active Queue Management (AQM) which maintains a shorter average queue length than its drop-tail counterpart. One of the most popular AQM schemes is Random Early Detection (RED) for which an arriving packet is dropped with a probability depending on the average queue occupancy [66]. The RED scheme interprets “the average queue occupancy exceeding a minimum queue threshold denoted by th_{\min} ” as an onset of network congestion and reacts by linearly increasing its drop probability from 0 up to the value p_{\max} until the maximum queue threshold denoted by th_{\max} is reached. Beyond th_{\max} , the arriving packets are dropped deterministically. The performance of RED is known to be sensitive to the choice of its parameters p_{\max} and th_{\max} and as a remedy, the so-called gentle variant of RED denoted by GRED has been proposed having a continuous drop probability function $q(x)$ as follows

[68],[64]:

$$q(x) = \begin{cases} 0, & 0 \leq x < th_{\min} \\ \frac{x-th_{\min}}{th_{\max}-th_{\min}}p_{\max}, & th_{\min} \leq x < th_{\max} \\ p_{\max} + \frac{x-th_{\max}}{th_{\max}}(1-p_{\max}), & th_{\max} \leq x < 2th_{\max} \\ 1, & \text{otherwise,} \end{cases} \quad (5.1)$$

where x denotes the queue occupancy. The drop probability function $q(x)$ in equation (5.1) is illustrated in Fig. 5.1 by a red line. We use GRED in this study for buffer management but other AQM schemes could also be employed.

The wireless link is assumed to carry N long-lived TCP-Reno flows using First-In-First-Out (FIFO) scheduling with a common packet size L . Each flow $i, i \in \{0, 1, \dots, N-1\}$, is assumed to have a fixed (yet arbitrary) RTT denoted by $RTT_{0,i}$, taking into account the propagation delays of all links on the path of the flow i . We assume all flows are bottlenecked at this wireless link and packet losses on other links are assumed to be negligible. We therefore do not attempt to model networks of AQM router links but rather focus on a single AQM bottleneck link in this chapter. Queuing and transmission delays as well as the error rates of the TCP ACK packets are assumed to be negligibly small and will be ignored by the analytical model assuming TCP ACK prioritization to be employed and enhanced wireless protection to be established at the reverse path of the flows [144],[145].

For link adaptation purposes, we introduce in this study a threshold B and subsequently partition the queue of the wireless link into two different regimes, namely $\mathcal{R}_1 = [0, B)$ and $\mathcal{R}_2 = (B, 2th_{\max})$ along with the boundary $\mathcal{B} = \{B\}$. The queue is served with a transmission rate r_1 (r_2) with a wireless PER denoted by PER_1 (PER_2) when the buffer occupancy x resides in regime \mathcal{R}_1 (\mathcal{R}_2) such that $r_1 \leq r_2$ and $PER_1 \leq PER_2$. In the above-mentioned definition, the strict inequality case is definitely more interesting but we let DRWL to be more general by allowing equalities. We present an overlaid illustration of the proposed DRWL and the GRED AQM scheme in Fig. 5.1. This DRWL can be generalized to a multi-regime scenario by further partitioning the queue into more than two

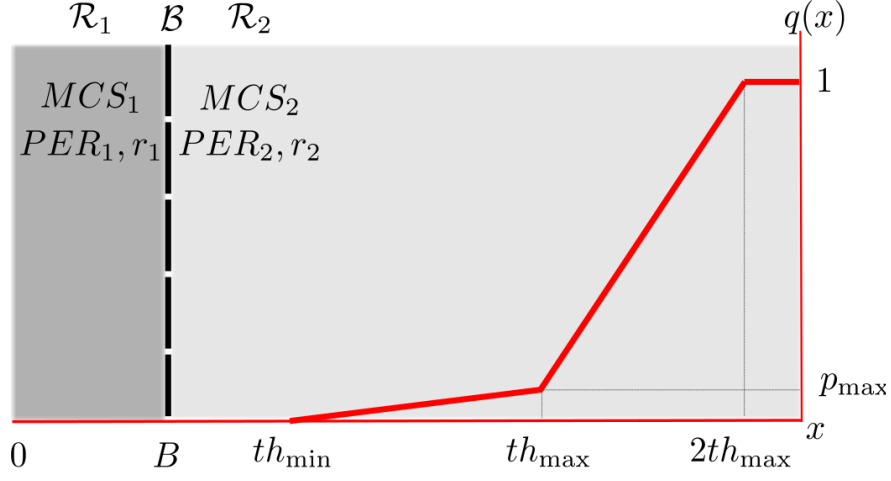


Figure 5.1: Illustration of DRWL with the x -axis representing the queue occupancy x .

regimes, but we limit our scope only to DRWL in this study. The DRWL framework consists of a set of queue-aware link adaptation mechanisms out of which we propose a particular subset of policies next. For this purpose, we consider M different candidate PHY MCSs denoted by mcs_m where $m \in \{0, 1, \dots, M-1\}$ that are supported by the wireless link's air interface. When a packet gets to be transmitted, we use a dedicated MCS at each regime, namely MCS_1 and MCS_2 , when the queue length at the epoch of packet transmission resides in \mathcal{R}_1 and \mathcal{R}_2 , respectively. If the queue occupancy resides at \mathcal{B} , either MCS_1 or MCS_2 can be used. When MCS_j equals mcs_m for regime j , $j \in \{1, 2\}$, and for SNR level snr_s , $s \in \{0, 1, \dots, S-1\}$, packets are transmitted with a bit rate of $r_j = g_m$ and errored at the receiver with a probability denoted by $PER_j = per_{m,s}$ where g_m is the bit rate of mcs_m seen by the link layer and $per_{m,s}$ is the packet error rate when mcs_m is used at SNR level snr_s .

In this study, we propose a particular DRWL mechanism denoted by $QAWLA(th_{PER}, H, B)$ in terms of three parameters th_{PER} , H , and B . In this PER-based LA mechanism, the MCS with the highest spectral efficiency whose resulting PER denoted by $per_{m,s}$ is such that $per_{m,s} < th_{PER}$ for a threshold parameter th_{PER} at a particular SNR level snr_s , is chosen for regime \mathcal{R}_2 . MCS decision for \mathcal{R}_1 is given in the same manner with \mathcal{R}_2 , but with a lower threshold

th_{PER}/H for some $H \geq 1$. It is clear that $QAWLA(th_{PER}, H, B)$ belongs to the DRWL framework for the entire range of its parameter set. For the particular QAWLA mechanism with $H = 1$, we have $MCS_1 = MCS_2$ irrespective of the queue occupancy at the same channel conditions and is therefore referred to as $TAGLA(th_{PER})$, i.e., Traffic AGnostic Link Adaptation (TAGLA). In the next section, we develop a fixed-point analytical model of the generic DRWL by means of which we evaluate the performance of the specific QAWLA scheme to be used in the numerical examples.

5.3 Fixed-Point Analytical Model of DRWL

In line with the majority of the existing work on TCP modeling, we propose to use the so-called ‘‘PFTK’’ TCP formula which relates the packet sending rate of a TCP flow to the packet loss rate seen by the flow [5]. Let p , λ , L , and T_0 denote the packet loss rate, packet send rate in packets/s, packet size in bits, and the retransmission timeout parameter of a TCP source, respectively. For the timeout parameter, we use

$$T_0 = \max(T_{0,\min}, RTT + 4\sigma_{RTT}), \quad (5.2)$$

where RTT and σ_{RTT} are the smoothed estimates for the RTT and its standard deviation, respectively, and $T_{0,\min}$ is a minimum limit imposed on the timeout parameter [2]. Let W_u denote the random variable associated with the unconstrained window size of the TCP source. Also let $W_{\max} = W/L$ and b denote the maximum window size in units of packets and the number of packets to wait before sending a cumulative ACK packet by the TCP receiver, respectively, where W is the receiver’s buffer size. The reference [5] proposes the following identity, known as the PFTK formula, for the TCP send rate λ if the TCP flow faces a packet loss rate p :

$$\lambda = \begin{cases} \frac{\frac{1-p}{p} + E[W_u] + \tilde{Q}(E[W_u])\frac{1}{1-p}}{RTT(\frac{b}{2}E[W_u] + 1) + \tilde{Q}(E[W_u])T_0\frac{f(p)}{1-p}}, & E[W_u] < W_{\max} \\ \frac{\frac{1-p}{p} + W_{\max} + \tilde{Q}(W_{\max})\frac{1}{1-p}}{RTT(\frac{b}{8}W_{\max} + \frac{1-p}{pW_{\max}} + 2) + \tilde{Q}(W_{\max})T_0\frac{f(p)}{1-p}}, & \text{otherwise,} \end{cases} \quad (5.3)$$

where

$$f(p) = 1 + p + 2p^2 + 4p^3 + 8p^4 + 16p^5 + 32p^6, \quad (5.4)$$

$$\tilde{Q}(w) = \min(1, \frac{(1 - (1 - p)^3)(1 + (1 - p)^3)(1 - (1 - p)^{(w-3)})}{1 - (1 - p)^w}), \quad (5.5)$$

and

$$E[W_u] = \frac{2 + b}{3b} + \sqrt{\frac{8(1 - p)}{3bp} + \left(\frac{2 + b}{3b}\right)^2}. \quad (5.6)$$

Note that the equation (5.3) provides a closed-form expression for the TCP send rate λ provided the parameters p and RTT are available. In this study, we assume all TCP flows use the same minimum timeout parameter $T_{0,\min}$ and the term $RTT + 4\sigma_{RTT}$ in (5.2) is much smaller than $T_{0,\min}$ which yields $T_0 = T_{0,\min}$. Exploiting this assumption, we simplify equation (5.3) to be used in sequel as follows:

$$\lambda = \begin{cases} \frac{1}{RTTP_1 + P_2}, & E[W_u] < W_{\max} \\ \frac{1}{RTTP_{1,c} + P_{2,c}}, & \text{otherwise,} \end{cases} \quad (5.7)$$

where P_1 and P_2 ($P_{1,c}$ and $P_{2,c}$) are functions that represent the packet loss rate dependency of the unconstrained (constrained) TCP packet sending rate as defined below:

$$P_1 = \frac{\frac{b}{2}E[W_u] + 1}{\frac{1-p}{p} + E[W_u] + \tilde{Q}(E[W_u])\frac{1}{1-p}}, \quad (5.8)$$

$$P_2 = \frac{\tilde{Q}(E[W_u])T_0\frac{f(p)}{1-p}}{\frac{1-p}{p} + E[W_u] + \tilde{Q}(E[W_u])\frac{1}{1-p}}, \quad (5.9)$$

$$P_{1,c} = \frac{\frac{b}{8}W_{\max} + \frac{1-p}{pW_{\max}} + 2}{\frac{1-p}{p} + W_{\max} + \tilde{Q}(W_{\max})\frac{1}{1-p}}, \quad (5.10)$$

$$P_{2,c} = \frac{\tilde{Q}(W_{\max})T_0\frac{f(p)}{1-p}}{\frac{1-p}{p} + W_{\max} + \tilde{Q}(W_{\max})\frac{1}{1-p}}. \quad (5.11)$$

Since the pairs (r_1, PER_1) and (r_2, PER_2) are not necessarily identical, it may be possible that the combined AQM-AMC policy may push the buffer occupancy from \mathcal{R}_1 outward to \mathcal{R}_2 and vice versa, making the boundary B the fixed-point. This can be viewed as the queue occupancy hovering in close vicinity of the boundary B , visiting both regimes infinitely often but transmitting packets in \mathcal{R}_1 and \mathcal{R}_2 , with probabilities $(1 - \alpha)$ and α , respectively, at the steady-state.

For higher (lower) values of α , a larger ratio of packets admitted into the queue finds the queue in the \mathcal{R}_2 (\mathcal{R}_1) regime. Consequently, the queue is modeled to be served with a transmission rate of $r(x, \alpha)$ when the queue occupancy is x :

$$r(x, \alpha) = \begin{cases} r_1, & 0 \leq x < B \\ r_1(1 - \alpha) + r_2\alpha, & x = B \\ r_2, & B < x < 2th_{\max} \end{cases} \quad (5.12)$$

and the average wireless loss probability, denoted by $PER(x, \alpha)$, can be written as follows:

$$PER(x, \alpha) = \begin{cases} PER_1, & 0 \leq x < B \\ \frac{PER_1 r_1(1 - \alpha) + PER_2 r_2 \alpha}{r(B, \alpha)}, & x = B \\ PER_2, & B < x < 2th_{\max} \end{cases} \quad (5.13)$$

Note that when $x = B$, the transmission rate and wireless loss probability also depend on the parameter α which needs to be calculated. Based on the philosophy of DRWL, we assume $PER_1 \leq PER_2 < 1$ in which case the TCP receivers get service from both regimes and $r_1 \leq r_2$. Lost packets are not retransmitted and loss events are assumed to be independent and identically distributed (iid) following the Bernoulli wireless loss model. Assuming AQM and wireless packet losses to be independent from each other, the overall loss probability can then be expressed as

$$p(x, \alpha) = 1 - (1 - PER(x, \alpha))(1 - q(x)). \quad (5.14)$$

All flows are exposed to a queuing delay $x/r(x, \alpha)$ and a transmission delay $L/r(x, \alpha)$ at the router. Without loss of generality, we let D_F account for the one-way framing and processing delays. Moreover, D_F is multiplied by a factor of two in order to cover both forward and reverse (TCP ACK messages) path delays. Taking into account the propagation delays of all links on the path of the flow i , we have the following expression for the overall RTT of flow i :

$$RTT_i(x, \alpha) = RTT_{0,i} + 2D_F + x/r(x, \alpha) + L/r(x, \alpha). \quad (5.15)$$

We take similar steps with [12] in relating the PFTK TCP model given in (5.3) with the queue occupancy x but also considering the dual-regime nature of

the queue. The overall rate of bits that are admitted into the queue denoted by $\kappa(x, \alpha)$ can then be written as

$$\kappa(x, \alpha) = L(1 - q(x)) \sum_{i=0}^{N-1} \lambda_i(x, \alpha), \quad (5.16)$$

where $\lambda_i(x, \alpha)$ is the packet send rate of flow i when the queue takes the value x and we propose to use the PFTK TCP formula (5.3) to write $\lambda_i(x, \alpha)$ with RTT and p being replaced with $RTT_i(x, \alpha)$ and $p(x, \alpha)$, respectively. The goal of the fixed-point model is to find the steady-state buffer occupancy denoted by x^* which can be viewed as an approximation to the mean queue occupancy in the actual system. Assuming that the queue has a steady-state solution at $(x, \alpha) = (x^*, \alpha^*)$, the following fixed-point identity should hold:

$$\kappa(x^*, \alpha^*) \begin{cases} = r(x^*, \alpha^*), & x^* > 0 \\ < r_1, & x^* = 0. \end{cases} \quad (5.17)$$

Given the steady-state solution (x^*, α^*) , the aggregate TCP throughput of the system denoted by T is given by the following identity:

$$T = (1 - PER(x^*, \alpha^*)) \kappa(x^*, \alpha^*). \quad (5.18)$$

Next, we take the preliminary steps leading to the proof for existence and uniqueness of the solution to DRWL for $r_1 < r_2$ and $PER_1 < PER_2$. For the particular case when $r_1 = r_2$ and $PER_1 = PER_2$, we refer the reader to [12]. Recalling equation (5.7) and replacing the terms P_1 , P_2 , $P_{1,c}$ and $P_{2,c}$ therein with their x and α dependent counterparts $P_1(x, \alpha)$, $P_2(x, \alpha)$, $P_{1,c}(x, \alpha)$ and $P_{2,c}(x, \alpha)$, respectively, as well as the RTT term with its per-flow counterpart $RTT_i(x, \alpha)$, we express the per-flow TCP send rate as follows:

$$\lambda_i(x, \alpha) = \begin{cases} \frac{1}{RTT_i(x, \alpha) P_1(x, \alpha) + P_2(x, \alpha)}, & E[W_u] < W_{\max} \\ \frac{1}{RTT_i(x, \alpha) P_{1,c}(x, \alpha) + P_{2,c}(x, \alpha)}, & \text{otherwise,} \end{cases} \quad (5.19)$$

Since TCP packet sending rate is a Monotonically Decreasing (MD) function of packet loss rate regardless of the RTT, the functions $P_1(\cdot)$ and $P_2(\cdot)$, and additionally $P_{1,c}(\cdot)$ and $P_{2,c}(\cdot)$, are Monotonically Non-Decreasing (MND) in x , given

that $p(x, \alpha)$ in (5.14) is MND. The MND property of $p(x, \alpha)$ is implied by the inequality $PER_1 < PER_2$ inherited from DRWL and the fact that $q(\cdot)$ is MND. Without loss of generality, we provide the proof for existence and uniqueness only for the unconstrained TCP packet sending rate using the functions $P_1(\cdot)$ and $P_2(\cdot)$. The aggregate bit arrival rate to the queue can then be written using (5.19) as:

$$\begin{aligned} L \sum_{i=0}^{N-1} \lambda_i(x, \alpha) &= \sum_{i=0}^{N-1} \frac{L}{(RTT_{0,i} + 2D_F + \frac{x+L}{r(x, \alpha)})P_1(x, \alpha) + P_2(x, \alpha)} \quad (5.20) \\ &= \frac{r(x, \alpha)}{G(x, \alpha)}, \end{aligned}$$

where $G(x, \alpha)$ equals

$$\left(\sum_{i=0}^{N-1} \frac{L}{((RTT_{0,i} + 2D_F)r(x, \alpha) + x + L)P_1(x, \alpha) + P_2(x, \alpha)r(x, \alpha)} \right)^{-1}, \quad (5.21)$$

and is a strictly positive Monotonically Increasing (MI) function provided that $r(x, \alpha)$ in (5.12) is MND which is true since $r_1 < r_2$. With these definitions, the identity (5.17) can further be simplified as follows:

$$G(x^*, \alpha^*) \begin{cases} = 1 - q(x^*), & x^* > 0 \\ > 1, & x^* = 0, \end{cases} \quad (5.22)$$

which is the main identity we refer to in this study that needs to be satisfied at the steady-state. Next, we present the proof for existence and uniqueness of a solution to DRWL in Theorems 5.3.1 and 5.3.2, for both $\mathcal{R}_j, j \in \{1, 2\}$ and \mathcal{B} , respectively.

Theorem 5.3.1. *There exists a unique solution x^* to the dual-regime queue provided that $r_1 < r_2$, $PER_1 < PER_2$, $\kappa(2th_{\max}, \alpha) < r_2$ and $q(x)$ is an MND continuous function of x .*

Proof. The condition $\kappa(2th_{\max}, \alpha) < r_2$ guarantees that full-queue never occurs. It is clear that the identity $G(2th_{\max}, \alpha) > 1 - q(2th_{\max}) = 0$ holds. Since the function $1 - q(x)$ is monotonically non-increasing and continuous, $G(x, \alpha)$ is monotonically increasing in x given that $r_1 < r_2$ and $PER_1 < PER_2$; either

$G(x^*, \alpha^*) = 1 - q(x^*)$ for some (x^*, α^*) where $x^* \in (0, 2th_{\max}]$ and $\alpha^* \in [0, 1]$; or $G(0, \alpha) > 1 - q(0) = 1$ for $x^* = 0$ must be satisfied. Uniqueness of x^* follows from $G(x, \alpha)$ being monotonically increasing and $1 - q(x)$ being monotonically non-increasing. \square

Theorem 5.3.2. *Provided $r_1 < r_2$ and $PER_1 < PER_2$, the solution to the dual-regime queue is unique in α when $x^* = B$.*

Proof. Note that $G(B, \alpha)$ is monotonically increasing in α at $x = B$. Let (B, α^*) be a solution, then for any $\alpha' \neq \alpha^*$, $G(B, \alpha') \neq G(B, \alpha^*) = 1 - q(B)$, which concludes the proof. \square

We also outline an algorithm to numerically solve the dual-regime queue in Algorithm 1. Once the solution is assured to reside in either of the two regimes \mathcal{R}_1 or \mathcal{R}_2 , or at the boundary \mathcal{B} , then a binary search is performed for the unknowns x^* and α^* , respectively, in the corresponding domain. We note that the case of $r_1 = r_2$ and $PER_1 = PER_2$ can also be solved by Algorithm 1.

Algorithm 1 solveDualRegimeWirelessLink

```

1: if  $\kappa(0, \alpha) < r_1$  then ▷ Solution is empty queue.
2:    $x^* \leftarrow 0$ 
3:    $T \leftarrow (1 - PER(0, \alpha))\kappa(0, \alpha)$ 
4: else if  $\kappa(B, 0) < r(B, 0)$  then ▷ Solution is in  $\mathcal{R}_1$ .
5:    $x^* \leftarrow \text{BINARYSEARCH}(x, \mathcal{R}_1)$  ▷ Perform binary search for  $x$  in  $\mathcal{R}_1$ .
6:    $T \leftarrow (1 - PER(x^*, \alpha))\kappa(x^*, \alpha)$ 
7: else if  $\kappa(B, 1) < r(B, 1)$  then ▷ Solution is at  $\mathcal{B}$ .
8:    $\alpha^* \leftarrow \text{BINARYSEARCH}(\alpha, \mathcal{B})$  ▷ Perform binary search for  $\alpha$  at  $\mathcal{B}$ .
9:    $x^* \leftarrow B$ 
10:   $T \leftarrow (1 - PER(B, \alpha^*))\kappa(B, \alpha^*)$ 
11: else ▷ Solution is in  $\mathcal{R}_2$ .
12:    $x^* \leftarrow \text{BINARYSEARCH}(x, \mathcal{R}_2)$  ▷ Perform binary search for  $x$  in  $\mathcal{R}_2$ .
13:    $T \leftarrow (1 - PER(x^*, \alpha))\kappa(x^*, \alpha)$ 
14: end if

```

Table 5.1: Modulation and coding schemes of IEEE 802.16 used in this study.

m	0	1	2	3	4	5	6	7
V_m	4	4	16	16	64	64	64	64
R_m	1/2	3/4	1/2	3/4	1/2	2/3	3/4	5/6
$k_m(\text{bytes})$	60	54	60	54	54	48	54	60

5.4 Wireless Link and Traffic Scenarios

In our numerical examples, we use the following parameters. For the fixed packet size, we set $L = 1500$ bytes. For GRED, the parameters th_{\min} and th_{\max} are set to 30 and 90, respectively, in units of packets, and p_{\max} is set to 0.1 as in [12]. For TCP parameters, we set $T_{0,\min} = 1$ s as in [161], $b = 2$ and $W = 64$ Kbytes as in [2]. For the PHY, we use the *Wireless-MAN OFDMA PHY* which specifies a cellular system comprising a Base Station (BS) and a number of Mobile Stations (MSs) [75] but which can alternatively be used as a point-to-point wireless link as in [149],[150]. For *Wireless-MAN OFDMA PHY*, we carry out simulations with the Coded Modulation Library (CML) to obtain the $per_{m,s}$ values for given mcs_m and snr_s [153]. For this purpose, we choose eight MCSs that use Convolutional Turbo Codes (CTC) which are enumerated in Table 5.1 according to an MCS index m , $m \in \{0, 1, \dots, 7\}$, for use in the current study which differ according to their modulation order V_m (i.e., the number of points in the constellation diagram), code rate R_m , and Forward Error Correction (FEC) block length k_m .

Assuming FEC block error events of a packet to be iid Bernoulli distributed, the quantity $per_{m,s}$ can be derived from the FEC block Error Rate (FER) denoted by $fer_{m,s}$ as follows:

$$per_{m,s} = 1 - (1 - fer_{m,s})^{\lceil L/k_m \rceil}. \quad (5.23)$$

For the sake of completeness, we present $per_{m,s}$ vs. snr_s curves obtained using CML in Figs. 5.2 and 5.3, for the Additive White Gaussian Noise (AWGN) and ITU Vehicular-A channels, respectively, the latter corresponding to an MS with velocity 90 km/hr., which is referred to as the ITU-A channel for the rest of the chapter [1]. SNR ranges of [0 dB, 22 dB] and [0 dB, 40 dB] are sampled with a resolution of 0.5 dB and 2 dB, respectively, to obtain the corresponding

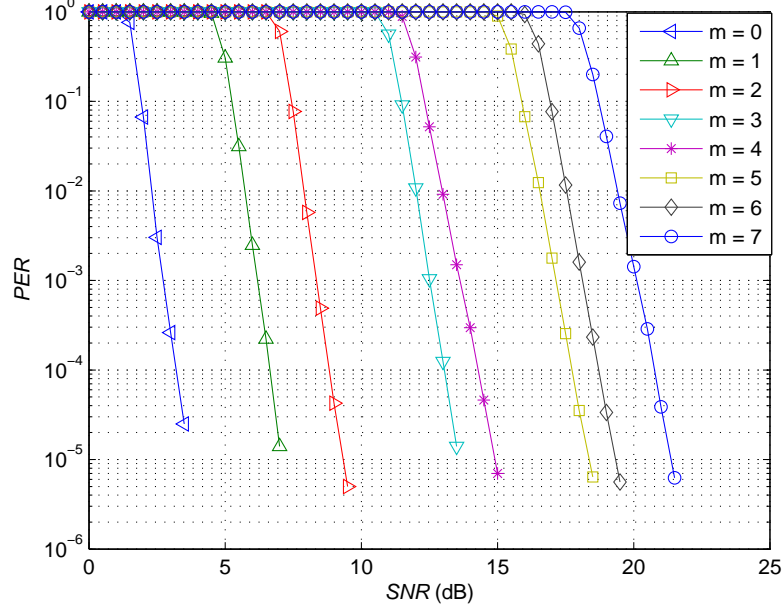


Figure 5.2: Simulated PER $per_{m,s}$ for different values of the MCS index m and the AWGN channel.

snr_s values for the AWGN and the ITU-A channels. At least 10^7 FEC blocks are decoded to reach the PER values illustrated in these figures unless 400 FEC block error events are encountered.

The Time Division Duplex (TDD) mode as specified by WiMAX [154] uses 35 downlink (DL) OFDM symbols with 768 data sub-carriers per symbol for a channel bandwidth of 10 MHz [75] and a TDD frame duration of 5 ms, resulting in an average PHY rate of $c = 5.376 \cdot 10^6$ sub-carriers/s. The raw bit rate c_m of the IEEE 802.16 *Wireless-MAN OFDMA PHY* air interface can then be calculated in bps as $c_m = c \log_2(V_m)R_m$. The padding inefficiency caused by the need for FEC block alignment of packets reduces the raw bit rate down to the link layer bit rate $g_m = c_m L / (k_m \lceil L/k_m \rceil)$ for MCS mcs_m . Note that MCSs in Table 5.1 are ordered based on their raw bit rates. These eight different MCSs lead to $\frac{8 \cdot 7}{2} - 1 = 27$ possible DRWL policies which satisfy the condition $r_1 < r_2$ and $PER_1 < PER_2$, excluding in particular the dual-regime policy $(MCS_1, MCS_2) = (mcs_3, mcs_4)$ having the same link layer bit rate (i.e., $g_3 = g_4$) but with interchanging PER performances for the AWGN and the ITU-A channels. Taking into consideration

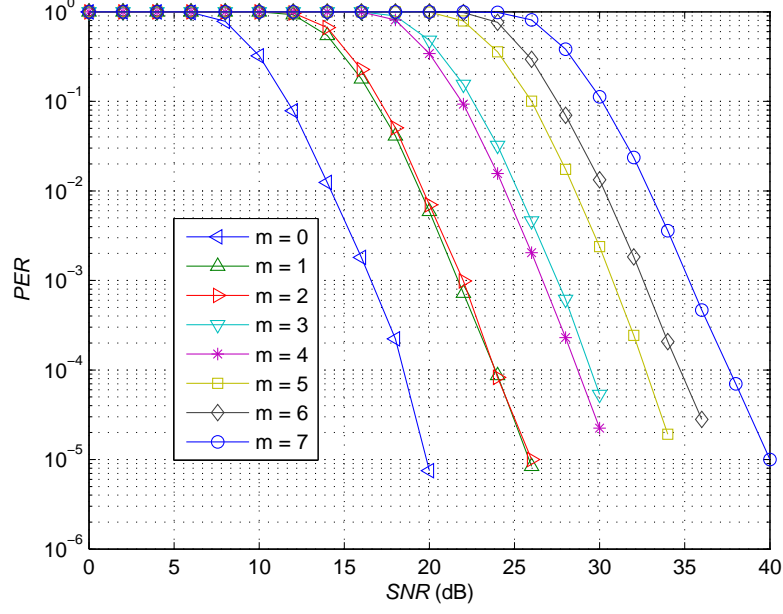


Figure 5.3: Simulated PER $per_{m,s}$ for different values of the MCS index m and the ITU-A channel.

the remaining policies for which $r_1 = r_2$ and $PER_1 = PER_2$, an overall of $27 + 8 = 35$ distinct policies are studied in the numerical examples. In order to account for framing and processing delays of the system, D_F is set to 2.5 ms.

We study traffic scenarios spanning a wide range of N and $RTT_{0,i}$ values. In particular, we study two groups of traffic scenarios having fixed and uniformly spaced $RTT_{0,i}$ values denoted by $SF_{N,F}$ and $SU_{N,F}$, respectively, where $N \in \{1, 2, 4, 8, 16\}$ and $F \in \{1, 5, 10, 20, 40, 60, 80, 100\}$ ms. In scenario $SF_{N,F}$, there are N long-lived TCP flows and all flows have the same $RTT_{0,i}$ of F ms. On the other hand, in scenario $SU_{N,F}$, there are again N flows but each with a different $RTT_{0,i} = 2(i+1)F/(N+1)$ leading to an average fixed RTT of F ms. Note that scenarios represented by $SF_{1,F}$ and $SU_{1,F}$ are identical, thus leading to an overall of seventy two unique traffic scenarios.

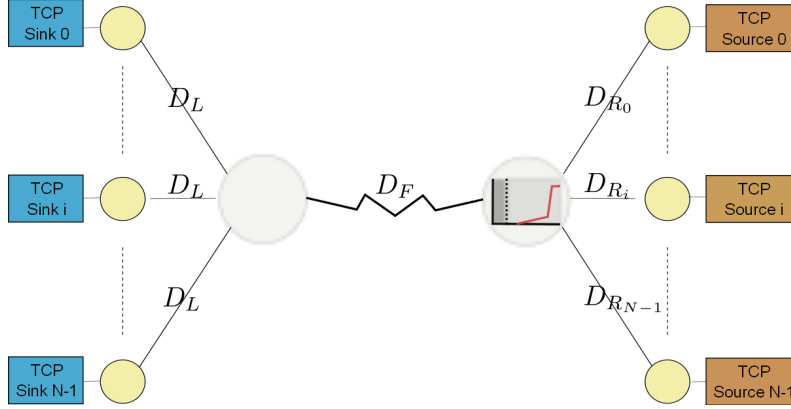


Figure 5.4: ns-3 simulation topology.

5.5 Validation of the Analytical Model

The proposed fixed-point analytical model for DRWL is validated using the ns-3 network simulator [2] for a subset of scenarios described in Section 5.4. Particularly, we employ the scenarios $SU_{N,F}$ for $N \in \{1, 4, 16\}$, $F \in \{1, 40\}$ ms, and $snr_s \in \{22, 26, 30\}$ dB for the ITU-A channel, totaling eighteen distinct scenarios indexed by the parameter idx . Table 5.2 summarizes the parameters used for each scenario including the per-regime PER values (PER_1, PER_2) , and per-regime bit rates (r_1, r_2) . We prefer to use a dumb-bell topology, which is a common topology to study TCP congestion algorithms in bottleneck links, involving N TCP-Reno flows in our simulations as shown in Fig. 5.4 [146],[147]. The ingress link for flow i , $0 \leq i < N$, has a one-way propagation delay D_{R_i} whereas the egress link for the same flow has a one-way propagation delay D_L . We set $D_L = \min_i(RTT_{0,i})/4$ and $D_{R_i} = RTT_{0,i}/2 - D_L$. All ingress and egress links have a capacity of 1 Gbps leaving the central wireless link in the middle as the bottleneck link with one-way propagation delay $D_F = 2.5$ ms. Note that the central link is of DRWL-type with its MCS selection policy dictated by Table 5.2.

TCP flow statistics are obtained using the *FlowMonitor* which is a monitoring framework developed for ns-3 [148]. The *RateErrorModel* class of ns-3 is used to simulate PERs. Simulations are terminated after five minutes but the first thirty seconds corresponding to transients are ignored. Each simulation is repeated ten

Table 5.2: The list of eighteen traffic scenarios indexed with idx used for validation of the fixed-point analytical model proposed for DRWL for the ITU-A channel model.

idx	Traffic Scenario	SNR (dB)	MCS_1	MCS_2	r_1 (Mbps)	r_2 (Mbps)	PER_1	PER_2
1	$SU_{1,1}$	22	mcs_1	mcs_3	8	16	$7.19 \cdot 10^{-4}$	$1.55 \cdot 10^{-1}$
2	$SU_{1,1}$	26	mcs_4	mcs_5	16	21	$2.04 \cdot 10^{-3}$	$1.00 \cdot 10^{-1}$
3	$SU_{1,1}$	30	mcs_4	mcs_5	16	21	$2.24 \cdot 10^{-5}$	$2.39 \cdot 10^{-3}$
4	$SU_{1,40}$	22	mcs_0	mcs_1	5.376	8	0	$7.19 \cdot 10^{-4}$
5	$SU_{1,40}$	26	mcs_0	mcs_1	5.376	8	0	$8.40 \cdot 10^{-6}$
6	$SU_{1,40}$	30	mcs_0	mcs_7	5.376	26.88	0	$1.12 \cdot 10^{-1}$
7	$SU_{4,1}$	22	mcs_1	mcs_2	8	10.752	$7.19 \cdot 10^{-4}$	$9.85 \cdot 10^{-4}$
8	$SU_{4,1}$	26	mcs_2	mcs_5	10.752	21	$1.00 \cdot 10^{-5}$	$1.00 \cdot 10^{-1}$
9	$SU_{4,1}$	30	mcs_5	mcs_7	21	26.88	$2.39 \cdot 10^{-3}$	$1.12 \cdot 10^{-1}$
10	$SU_{4,40}$	22	mcs_1	mcs_2	8	10.752	$7.19 \cdot 10^{-4}$	$9.85 \cdot 10^{-4}$
11	$SU_{4,40}$	26	mcs_3	mcs_6	16	24	$4.62 \cdot 10^{-3}$	$2.95 \cdot 10^{-1}$
12	$SU_{4,40}$	30	mcs_3	mcs_7	16	26.88	$5.32 \cdot 10^{-5}$	$1.12 \cdot 10^{-1}$
13	$SU_{16,1}$	22	mcs_2	mcs_4	10.752	16	$9.85 \cdot 10^{-4}$	$9.32 \cdot 10^{-2}$
14	$SU_{16,1}$	26	mcs_2	mcs_6	10.752	24	$1.00 \cdot 10^{-5}$	$2.95 \cdot 10^{-1}$
15	$SU_{16,1}$	30	mcs_2	mcs_6	10.752	24	0	$1.33 \cdot 10^{-2}$
16	$SU_{16,40}$	22	mcs_1	mcs_4	8	16	$7.19 \cdot 10^{-4}$	$9.32 \cdot 10^{-2}$
17	$SU_{16,40}$	26	mcs_3	mcs_5	16	21	$4.62 \cdot 10^{-3}$	$1.00 \cdot 10^{-1}$
18	$SU_{16,40}$	30	mcs_3	mcs_5	16	21	$5.32 \cdot 10^{-5}$	$2.39 \cdot 10^{-3}$

times and the average results are reported together with the 99% confidence intervals. Aggregate TCP throughput results of ns-3 simulations and the analytical model proposed in this chapter are presented for each scenario in Tables 5.3, 5.4 and 5.5 for B being equal to 10, 20, and 30 respectively, all in units of packets. In these tables, we also provide the regime of the solution point (i.e., whether x^* resides in \mathcal{R}_1 , \mathcal{R}_2 , or at the boundary \mathcal{B}) and the α^* parameter, whenever the solution is at \mathcal{B} , obtained by the analysis. Overall results exhibit a remarkable level of agreement in the aggregate TCP throughput between simulations and the fixed-point analytical model especially for B equals 20 or 30. For $B = 10$, which is closer to the vicinity of the empty queue, the analytical model tends to be optimistic for scenarios with high PER values for \mathcal{R}_2 (e.g. idx equals 2, 11, 12 and 17). In order to better understand this behavior, we first let the discrete random variable K denote the number of packets waiting in the queue for transmission with the Probability Mass Function (PMF) u_k defined as $u_k = Pr(K = k)$ where $k \in [0, 2th_{\max})$. Subsequently, we present the empirical PMF u_k obtained from ns-3 simulations for three different regime boundary values when the scenario index is fixed at $idx = 2$ in Fig. 5.5. Note that in ns-3, which is an event based simulator, it is more convenient to probe the queue occupancy in units of packets

Table 5.3: Aggregate TCP throughput T obtained with ns-3 simulations and the fixed-point analytical model for $B = 10$. Results for ns-3 simulations are presented with the 99% confidence intervals.

idx	T (ns3) (Mbps)	T (analysis) (Mbps)	Solution Domain	α^*
1	7.7536 ± 0.0535	8.0208	\mathcal{B}	$4.81 \cdot 10^{-3}$
2	13.2888 ± 0.4525	15.9673	\mathcal{R}_1	N/A
3	18.5577 ± 0.0686	18.2195	\mathcal{B}	$4.48 \cdot 10^{-1}$
4	6.5931 ± 0.0939	6.5793	\mathcal{B}	$4.60 \cdot 10^{-1}$
5	7.9630 ± 0.0169	7.9999	\mathcal{R}_2	N/A
6	4.9082 ± 0.0531	5.3999	\mathcal{B}	$1.29 \cdot 10^{-3}$
7	10.7244 ± 0.0013	10.7414	\mathcal{R}_2	N/A
8	11.3006 ± 0.0171	11.1503	\mathcal{B}	$4.90 \cdot 10^{-2}$
9	20.1596 ± 0.0843	21.0230	\mathcal{B}	$2.51 \cdot 10^{-2}$
10	10.6419 ± 0.0119	10.7412	\mathcal{R}_2	N/A
11	10.6183 ± 0.1630	12.0195	\mathcal{R}_1	N/A
12	14.2814 ± 0.1153	16.0956	\mathcal{B}	$1.23 \cdot 10^{-2}$
13	11.6557 ± 0.0193	11.6082	\mathcal{B}	$2.30 \cdot 10^{-1}$
14	11.0416 ± 0.0092	11.0528	\mathcal{B}	$4.88 \cdot 10^{-2}$
15	23.5724 ± 0.0224	23.6809	\mathcal{R}_2	N/A
16	8.9470 ± 0.0216	9.0075	\mathcal{B}	$1.56 \cdot 10^{-1}$
17	14.4627 ± 0.0720	16.1824	\mathcal{B}	$8.65 \cdot 10^{-2}$
18	20.8878 ± 0.0041	20.9496	\mathcal{R}_2	N/A

rather than the continuous occupancy level x . The analytical queue occupancy, however, is a real number which is found to be 3.9049 in units of packets for all values of B . By its very nature, the fixed-point approach makes the location of \mathcal{B} irrelevant to the solution once the solution resides in either \mathcal{R}_1 or \mathcal{R}_2 . Accordingly, for decreasing B , the probability of queue becoming empty obtained from simulations increases which is not accounted by the model for this particular case.

In Fig. 5.6, the empirical queue occupancy PMF obtained with ns-3 simulations is depicted together with the corresponding analytical solution for $B = 20$ corresponding to six scenarios with $idx \in \{3, 4, 11, 13, 14, 18\}$. When idx equals 11 and 18, the model finds the solution in \mathcal{R}_1 and \mathcal{R}_2 , respectively, and for idx equals 3, 4, 13, or 14, the solution turns out to be at \mathcal{B} . The shape of the PMFs obtained via ns-3 for scenarios with analytical solution at \mathcal{B} , demonstrates the effectiveness of the proposed approach in capturing the behavior of the queue around the regime boundary. In the light of all simulation results, we let $B \geq 20$ in all the remaining numerical examples so that the empty queue regime is avoided and furthermore the fixed-point model performs remarkably well.

Table 5.4: Aggregate TCP throughput T obtained with ns-3 simulations and the fixed-point analytical model for $B = 20$. Results for ns-3 simulations are presented with the 99% confidence intervals.

idx	T (ns3) (Mbps)	T (analysis) (Mbps)	Solution Domain	α^*
1	7.9566 ± 0.0315	8.0001	\mathcal{B}	$1.06 \cdot 10^{-3}$
2	15.0448 ± 0.2067	15.9673	\mathcal{R}_1	N/A
3	17.2953 ± 0.1523	17.2050	\mathcal{B}	$2.44 \cdot 10^{-1}$
4	5.8687 ± 0.0183	5.5724	\mathcal{B}	$7.50 \cdot 10^{-2}$
5	6.1174 ± 0.0069	6.0328	\mathcal{B}	$2.50 \cdot 10^{-1}$
6	4.9370 ± 0.0696	5.3797	\mathcal{B}	$1.98 \cdot 10^{-4}$
7	10.6713 ± 0.0099	10.7414	\mathcal{R}_2	N/A
8	11.1897 ± 0.0077	11.0506	\mathcal{B}	$3.67 \cdot 10^{-2}$
9	20.9866 ± 0.0253	20.9979	\mathcal{B}	$1.65 \cdot 10^{-2}$
10	10.2652 ± 0.0249	10.7412	\mathcal{R}_2	N/A
11	12.7334 ± 0.1325	12.0195	\mathcal{R}_1	N/A
12	15.6795 ± 0.0350	16.0741	\mathcal{B}	$9.53 \cdot 10^{-3}$
13	11.5683 ± 0.0102	11.5174	\mathcal{B}	$2.06 \cdot 10^{-1}$
14	11.0345 ± 0.0066	11.0222	\mathcal{B}	$4.39 \cdot 10^{-2}$
15	23.1019 ± 0.0520	23.6811	\mathcal{R}_2	N/A
16	8.9518 ± 0.0165	8.8827	\mathcal{B}	$1.36 \cdot 10^{-1}$
17	15.9371 ± 0.0321	16.1458	\mathcal{B}	$7.41 \cdot 10^{-2}$
18	20.6509 ± 0.0187	20.9499	\mathcal{R}_2	N/A

Table 5.5: Aggregate TCP throughput T obtained with ns-3 simulations and the fixed-point analytical model for $B = 30$. Results for ns-3 simulations are presented with the 99% confidence intervals.

idx	T (ns3) (Mbps)	T (analysis) (Mbps)	Solution Domain	α^*
1	7.9785 ± 0.0162	7.9942	\mathcal{R}_1	N/A
2	15.4886 ± 0.0857	15.9674	\mathcal{R}_1	N/A
3	15.9636 ± 0.2527	16.2673	\mathcal{B}	$5.41 \cdot 10^{-2}$
4	5.3673 ± 0.0000	5.3760	\mathcal{R}_1	N/A
5	5.3673 ± 0.0000	5.3760	\mathcal{R}_1	N/A
6	5.3673 ± 0.0000	5.3760	\mathcal{R}_1	N/A
7	9.8443 ± 0.0336	10.7416	\mathcal{R}_2	N/A
8	11.0671 ± 0.0080	10.9739	\mathcal{B}	$2.73 \cdot 10^{-2}$
9	21.0011 ± 0.0053	20.9776	\mathcal{B}	$9.51 \cdot 10^{-3}$
10	9.1072 ± 0.0330	10.7412	\mathcal{R}_2	N/A
11	12.9934 ± 0.0867	12.0195	\mathcal{R}_1	N/A
12	15.9259 ± 0.0378	16.0586	\mathcal{B}	$7.56 \cdot 10^{-3}$
13	11.4676 ± 0.0120	11.4330	\mathcal{B}	$1.84 \cdot 10^{-1}$
14	11.0026 ± 0.0043	10.9937	\mathcal{B}	$3.93 \cdot 10^{-2}$
15	20.8078 ± 0.1013	23.6811	\mathcal{R}_2	N/A
16	8.8136 ± 0.0159	8.7706	\mathcal{B}	$1.19 \cdot 10^{-1}$
17	16.1202 ± 0.0134	16.1126	\mathcal{B}	$6.29 \cdot 10^{-2}$
18	19.5952 ± 0.0287	20.9496	\mathcal{R}_2	N/A

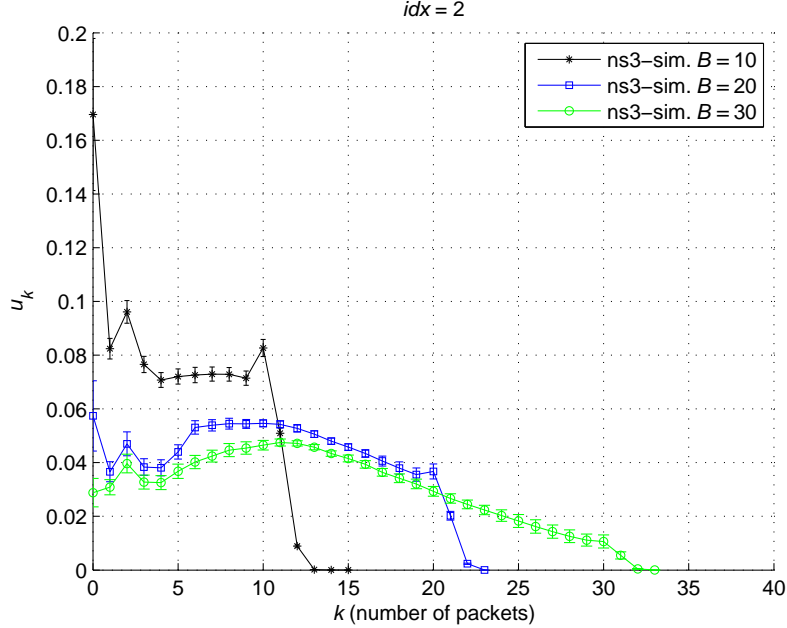


Figure 5.5: The empirical queue occupancy PMF u_k for the scenario with $idx = 2$ for varying $B \in \{10, 20, 30\}$, all having the same fixed-point solution with a queue occupancy level of 3.9049 packets.

5.6 Performance Evaluation of QAWLA

For each snr_s and th_{PER} value, we choose MCSs for both TAGLA and QAWLA policies. Out of all DRWL policies, we pick the one, called *optimum*, that produces the maximum TCP throughput for each snr_s value and traffic scenario, which is solely used for benchmarking due to the off-line nature of finding the *optimum* policy. For all figures to be presented, aggregate TCP throughput values of TAGLA and QAWLA are normalized with respect to the corresponding throughput values of *optimum*. In Figs. 5.7 and 5.8, normalized aggregate TCP throughput of TAGLA and QAWLA are averaged over all traffic scenarios and snr_s values to give the mean normalized aggregate TCP throughput $\mathbf{T_M}$ for the AWGN and the ITU-A channels, respectively, and plotted as a function of the threshold parameter th_{PER} for different values of H and B parameters of the QAWLA policy. Owing to shadow fading, the channel SNR is assumed to be a Normal random variable with a mean of 12 dB (26 dB) and a standard deviation

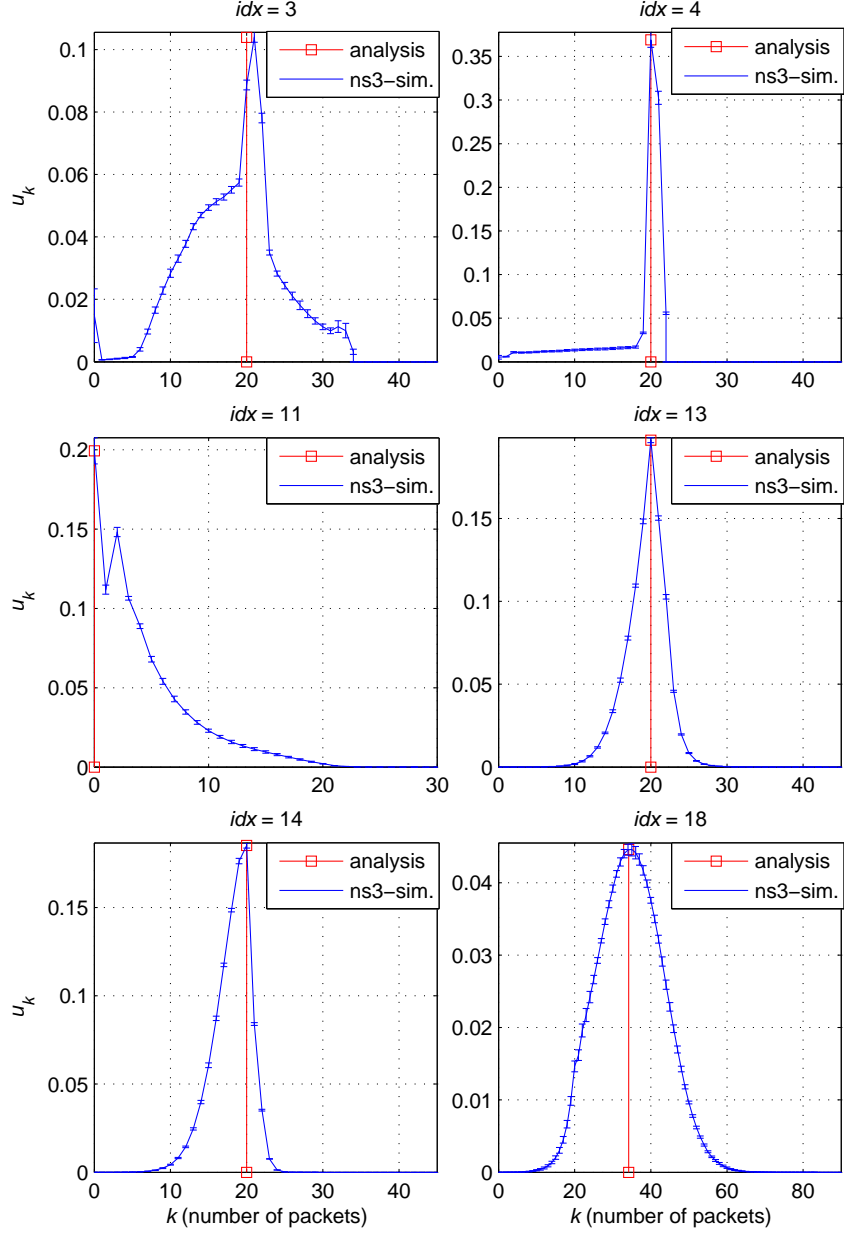


Figure 5.6: The empirical queue occupancy PMF u_k for scenarios with $idx \in \{3, 4, 11, 13, 14, 18\}$ and $B = 20$. Analytical results are also depicted.

of 8 dB for the AWGN (ITU-A) channel. We first discretize the Normal distribution with a resolution of 0.5 dB (2 dB) and then truncate over the support of [2dB, 22dB] ([14dB, 40dB]) for the AWGN (ITU-A) channel for averaging purposes over the snr_s values. The minimum SNR value for the support of each channel type is selected such that mcs_0 has a packet error rate less than 0.1.

For both channel types, but more prominently for the ITU-A channel, the choice of $H = 100$ yields the best results in terms of peak normalized throughput and the degree of robustness for increasing th_{PER} values. Note that QAWLA with $B = 40 > th_{\min} = 30$ performs worse than TAGLA for low values of th_{PER} , since AQM packet losses force the queue to be confined in \mathcal{R}_1 having lower capacity for the QAWLA scheme. Only for values of th_{PER} well exceeding the level of 10^{-2} , can the wireless packet losses start to dominate making \mathcal{R}_1 a desirable regime with its lower PER values for QAWLA. The remaining choices of $B \leq th_{\min}$ reveal the true potential of QAWLA in both channels, while the $B = 20$ choice performing slightly better than the choice of $B = 30$ owing to its lower average queuing delay. For the rest of the numerical examples, we fix $H = 100$ and $B = 20$ and study the selection of the th_{PER} parameter of the $QAWLA(th_{PER}, 100, 20)$ policy.

In real-life implementations, both TAGLA and QAWLA policies require real time PER estimations to successfully operate. This information, however, may not be precise due to rapidly changing wireless channel conditions and/or the accuracy of the particular implementations used in channel quality measurements. In Figs. 5.9 and 5.10, throughput results of TAGLA and QAWLA based on the MCS decisions given as if the channel SNR values were 2 dB higher than the actual values, resulting in an over-rated channel assessment are also given. The same averaging steps described for Figs. 5.7 and 5.8 are employed for Figs. 5.9 and 5.10 in obtaining the presented throughput results. QAWLA appears to be relatively insensitive to the choice of th_{PER} compared to TAGLA and significantly improves TAGLA for over-rated channels as well. Both TAGLA and QAWLA performances deteriorate in case an over-rated channel assessment is made, but the deterioration is more severe for the AWGN channel scenario as its $per_{m,s}$ vs. snr_s curves are steeper than those of the ITU-A channel scenario. The optimum choice of the parameter th_{PER} appears to be dependent on the channel

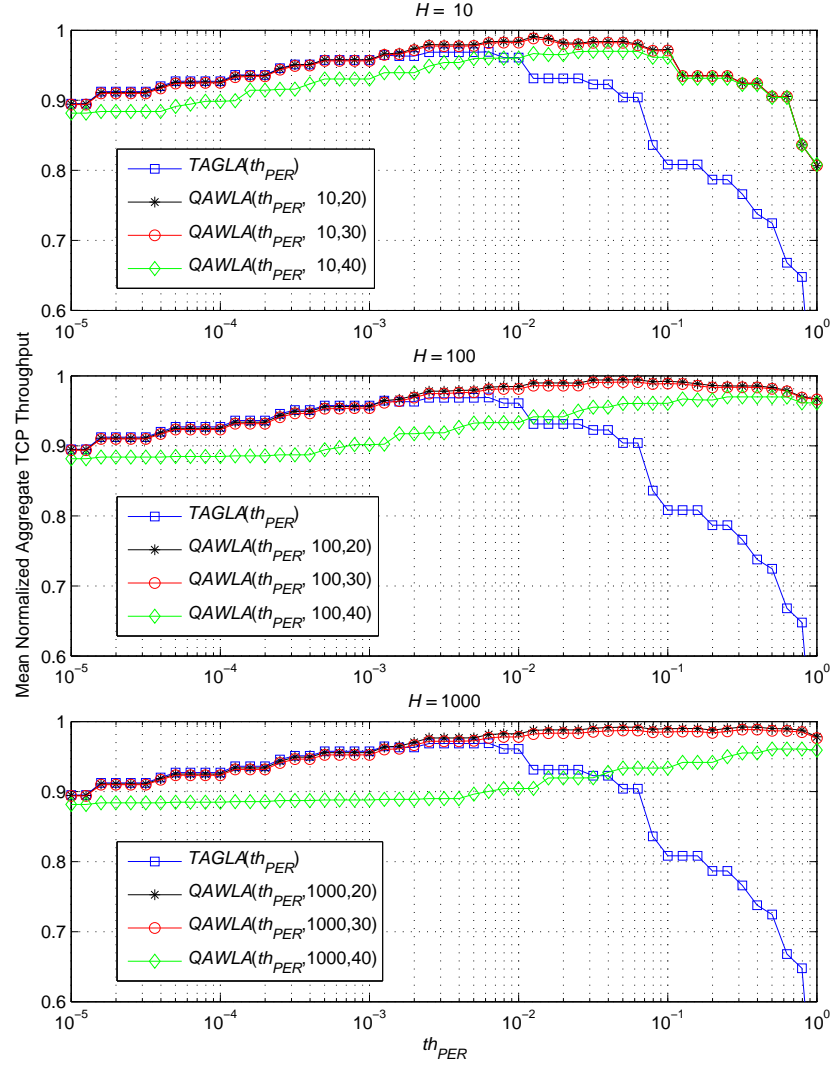


Figure 5.7: Mean normalized aggregate TCP throughput $\mathbf{T_M}$ of TAGLA and QAWLA as a function of th_{PER} with $H \in \{10, 100, 1000\}$ and $B \in \{20, 30, 40\}$ for the AWGN channel.

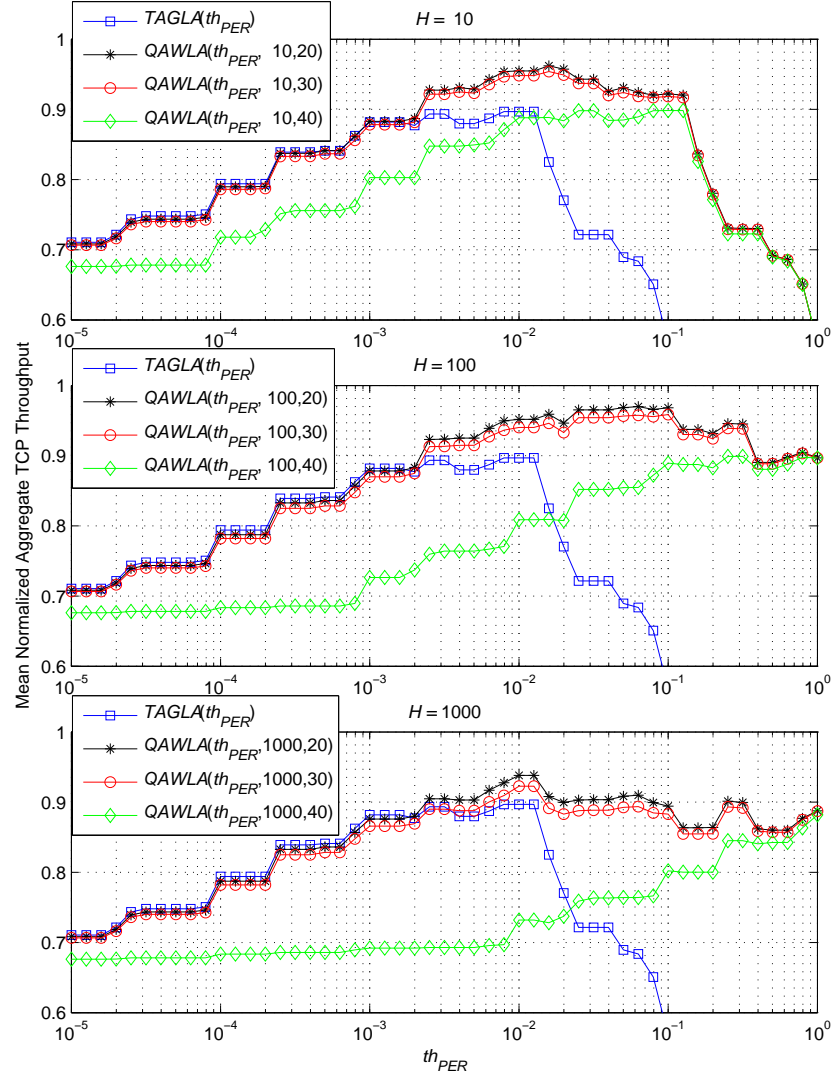


Figure 5.8: Mean normalized aggregate TCP throughput $\mathbf{T_M}$ of TAGLA and QAWLA as a function of th_{PER} with $H \in \{10, 100, 1000\}$ and $B \in \{20, 30, 40\}$ for the ITU-A channel.

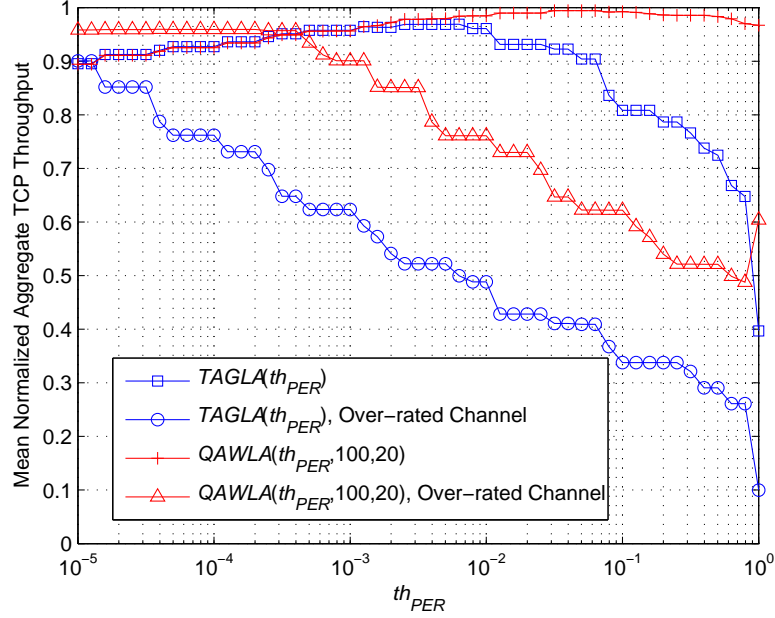


Figure 5.9: Mean normalized aggregate TCP throughput $\mathbf{T_M}$ of TAGLA and QAWLA as a function of th_{PER} with $H = 100$ and $B = 20$ for the AWGN channel.

type and the precision of the SNR estimate. Both TAGLA and QAWLA benefit from relatively lower values of th_{PER} for the over-rated ITU-A channel, making them to be more conservative which in turn compensates the error in the channel estimation. This phenomenon, however, is less pronounced for QAWLA and even unobservable for TAGLA for the AWGN channel owing to its steeper $per_{m,s}$ vs. snr_s curves.

As an alternative metric, we define the worst case normalized aggregate TCP throughput $\mathbf{T_W}$. In order to calculate $\mathbf{T_W}$, we first find the minimum value of the normalized aggregate TCP throughput for each traffic scenario over the aforementioned SNR values and then take average of these minimum values over the entire traffic scenario set. In Figs. 5.11 and 5.12, $\mathbf{T_W}$ for TAGLA and QAWLA are depicted. The results clearly demonstrate that the worst case throughput performances of TAGLA are considerably improved with QAWLA. Unlike the over-rated channel case, the worst case throughput performances of both channels under TAGLA and QAWLA policies exhibit a similar trend. The worst

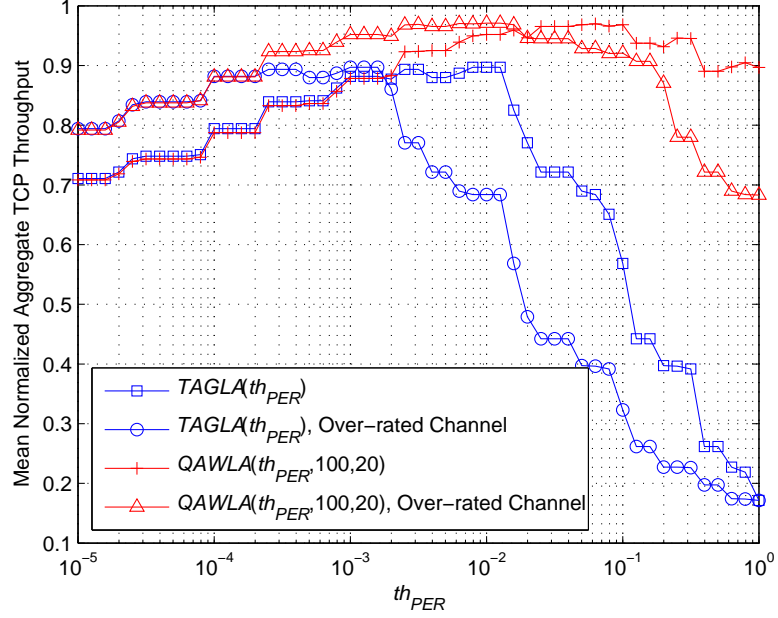


Figure 5.10: Mean normalized aggregate TCP throughput T_M of TAGLA and QAWLA as a function of th_{PER} with $H = 100$ and $B = 20$ for the ITU-A channel.

case performance T_W of both channel types appear to peak in the vicinity of $th_{PER} = 5 \times 10^{-2}$. This behavior is the consequence of the interplay between the bit rate and the packet loss rate of the chosen MCSs controlled by the parameter th_{PER} . Moreover, the corresponding policy $QAWLA(5 \times 10^{-2}, 100, 20)$ performs close to *optimum* for both channel types as far as the mean performance T_M is concerned and therefore appears to be a reasonable choice for the given AQM setting and the set of MCSs used in this study.

Finally, we compare the normalized aggregate TCP throughput performances of TAGLA and QAWLA in Table 5.6 based on the metrics T_M and T_W where the former is given for both the perfect channel and the Over-Rated Channel (ORC) assessment scenarios. For the sake of fairness, performance of each policy is evaluated for its own preferred value of th_{PER} . To this end, we fix $th_{PER} = 3.2 \times 10^{-3}$ for TAGLA which maximizes the average of T_M for the AWGN and the ITU-A channels. We note that this particular choice of th_{PER} is also consistent with the suggested value of 5×10^{-3} for TAGLA in Chapter 3.

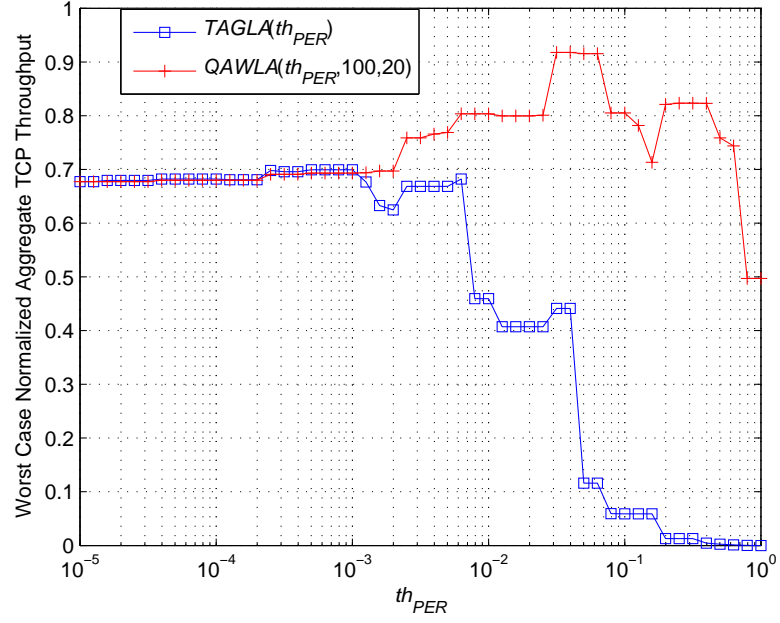


Figure 5.11: Worst case normalized aggregate TCP throughput $\mathbf{T_w}$ of TAGLA and QAWLA as a function of th_{PER} with $H = 100$ and $B = 20$ for the AWGN channel.

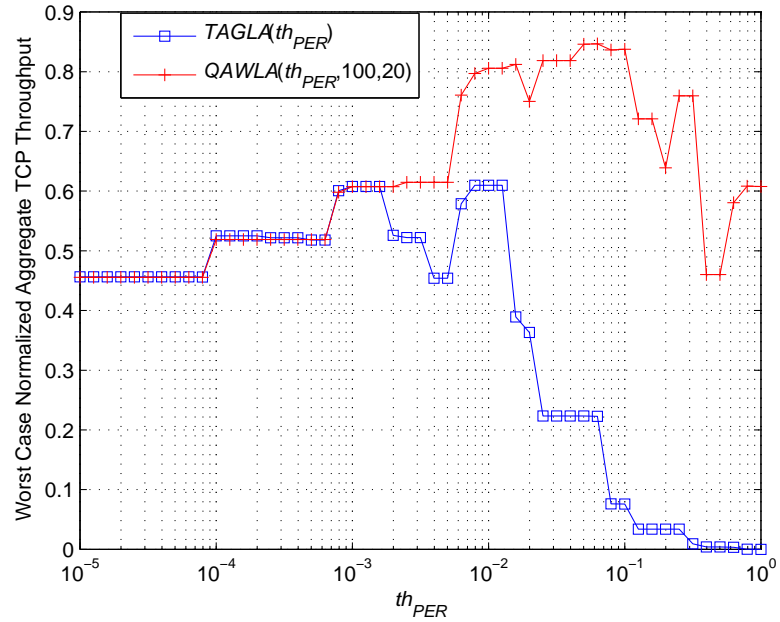


Figure 5.12: Worst case normalized aggregate TCP throughput $\mathbf{T_w}$ of TAGLA and QAWLA as a function of th_{PER} with $H = 100$ and $B = 20$ for the ITU-A channel.

Table 5.6: Comparison of the mean ($\mathbf{T_M}$) and the worst case ($\mathbf{T_W}$) normalized aggregate TCP throughput performances of TAGLA and QAWLA for the AWGN and the ITU-A channels.

	AWGN			ITU-A		
	$\mathbf{T_M}$	$\mathbf{T_M}$ (ORC)	$\mathbf{T_W}$	$\mathbf{T_M}$	$\mathbf{T_M}$ (ORC)	$\mathbf{T_W}$
$QAWLA(5 \times 10^{-2}, 100, 20)$	0.99	0.62	0.92	0.97	0.93	0.85
$TAGLA(3.2 \times 10^{-3})$	0.97	0.52	0.67	0.89	0.77	0.52

Chapter 6

Energy Efficient Queue-Aware Link Adaptation with HARQ (EnQAWLAwH)

This chapter is organized as follows. In Section 6.1, problem description of the Energy efficient Queue-Aware Link Adaptation scheme with HARQ (EnQAWLAwH) is given. In Section 6.2, the proposed analytical model for Dual-Regime Wireless Networks (DRWNs) is presented with simulation-based validation of the model provided in Section 6.3. In Section 6.4, the performance of the proposed EnQAWLAwH link adaptation scheme is evaluated for a wide variety of wireless, traffic and network scenarios.

6.1 Problem Description

In a network of wireless links, each TCP flow has a bottleneck link but there may be network links which may not be a bottleneck for any of the TCP flows. For such non-bottleneck links associated with low queue occupancies, it may well be possible to conserve energy by reducing the transmission power which is the basic

principle underlying the proposed Energy efficient Queue-AWare Link Adaptation scheme with HARQ (EnQAWLAWH). EnQAWLAWH is distributed and requires no coordination between the network nodes. Basically, EnQAWLAWH takes the “instantaneous queue occupancy staying below a certain queue threshold” as an implicit indication that the contending flows are bottlenecked elsewhere. Whenever such a situation arises, EnQAWLAWH simultaneously falls back to a Modulation and Coding Scheme (MCS) with a lower service rate and reduces the transmission power so that the new MCS choice will still perform sufficiently well. One can give the following example in order to appreciate the rationale behind EnQAWLAWH. Consider the link queue of a wireless transmitter which is kept occupied less than half of the time with a certain service rate. Without changing the arrival rate to the queue, halving its capacity is expected to at most double the percentage of time the link is occupied. On the other hand, halving the capacity will allow one to reduce the SNR of the receiver down to a level less than half of its current value in linear scale with regards to the Shannon’s channel capacity formula. Eventually, energy which is the power integral over time will decrease at the expense of potentially increased queue occupancy. Contrary to the fixed arrival rate in the aforementioned example, this study focuses on TCP traffic which reduces its packet sending rate for increased Round-Trip Times (RTTs) induced by increased queuing delays. Therefore, an analytical model is required to evaluate the performance of EnQAWLAWH with TCP traffic. In this chapter, we present a fixed-point analytical model of a Dual-Regime Wireless Network (DRWN), which is essentially a multi-hop wireless network comprising an interconnection of Point-To-Point (PTP) links. In this network, each PTP link is of Dual-Regime Wireless Link (DRWL)-type running the proposed EnQAWLAWH link adaptation (LA) scheme.

6.2 Analytical Model

In this section, we present an analytical model to obtain the queue occupancy level x of each link for a network of PTP DRWL-type links after which we evaluate the

key performance metrics of the proposed EnQAWLAwH scheme, such as network-wide TCP-level throughput and average power consumption. Throughout this study, we assume the following:

- N persistent TCP-Reno flows with arbitrary routes share a network of wireless links with arbitrary topology.
- Each flow n , $n \in \{0, 1, \dots, N-1\}$, uses a common packet size C .
- Incoming packets from the TCP flows are dropped at each node according to the Gentle RED [68] AQM scheme [66] whose drop policy is given below:

$$q(x) = \begin{cases} 0, & 0 \leq x < th_{\min} \\ \frac{x-th_{\min}}{th_{\max}-th_{\min}} p_{\max}, & th_{\min} \leq x < th_{\max} \\ p_{\max} + \frac{x-th_{\max}}{th_{\max}} (1 - p_{\max}), & th_{\max} \leq x < 2th_{\max} \\ 1, & \text{otherwise.} \end{cases} \quad (6.1)$$

- The transmitter of each unidirectional link l , $l \in \{0, 1, \dots, L-1\}$, in the network runs the same LA policy independently from each other, i.e., without any collaboration.
- The links are in Single-Input-Single-Output (SISO) configuration.
- The network is interference-free, i.e., transmissions on a particular link do not interfere with others which can be ensured by the use of separate frequency bands in nearby links or by the deployment of directive antennas.
- Variation of the Power Amplifier (PA) inefficiency within the transmission power range of interest is negligible. This assumption holds either for an ideal PA, or for a switching PA architecture [77] by which the most efficient PA is selected based on the desired transmission power. Moreover, transmission power dominates circuit power.
- Type-II HARQ with Chase Combining (HARQ-CC) is used to recover independent and identically distributed (iid) wireless packet losses. Selective

Repeat retransmission policy is in place to retransmit only the errored packets after a retransmission delay of D_R with the number of retransmissions upper bounded by Z . The transmission power is kept constant throughout the retransmissions.

- A resequencing mechanism is employed at each node in order to cope with out-of-order successful packet transmissions.
- There exist M alternative MCSs denoted by mcs_m , $m \in \{0, 1, \dots, M-1\}$, to choose among for each regime. Each MCS has a Forward Error Correction (FEC) block Error Rate (FER) denoted by $fer_{m,s,z}$ at SNR level snr_s , $s \in \{0, 1, \dots, S-1\}$, and at retransmission index, $z \in \{0, 1, \dots, Z\}$.
- A packet consists of multiple FEC blocks and the successful retransmission of a packet requires all building FEC blocks to be successfully transmitted. We denote by $P_{m,s,z}$ the probability of failure of a packet at retransmission index z meaning at least one of the building FEC blocks has not been successfully transmitted yet. An expression for $P_{m,s,z}$ will be given in the sequel.
- TCP ACK packets are prioritized throughout the network [144],[145]. Therefore, the associated queuing, transmission and retransmission delays as well as packet error rates for ACK packets are negligible.

Based on the above assumptions we describe the LA framework as follows:

- All of the links are of DRWL-type which is ensured by dividing the associated queue into two regimes namely $\mathcal{R}_1 = \{x : x < B\}$ and $\mathcal{R}_2 = \{x : x > B\}$ across the boundary \mathcal{B} residing at queue occupancy threshold B i.e., $\mathcal{B} = \{x : x = B\}$ as shown in Fig. 6.1.
- Packets transmitted from \mathcal{R}_i (i.e., when the queue occupancy is in \mathcal{R}_i), $i \in \{1, 2\}$, employ a transmission power \mathcal{P}_i (in units of Watts) and an MCS denoted by MCS_i resulting in an SNR level SNR_i , a transmission rate r_i and a wireless packet loss rate PER_i . When there exists no active

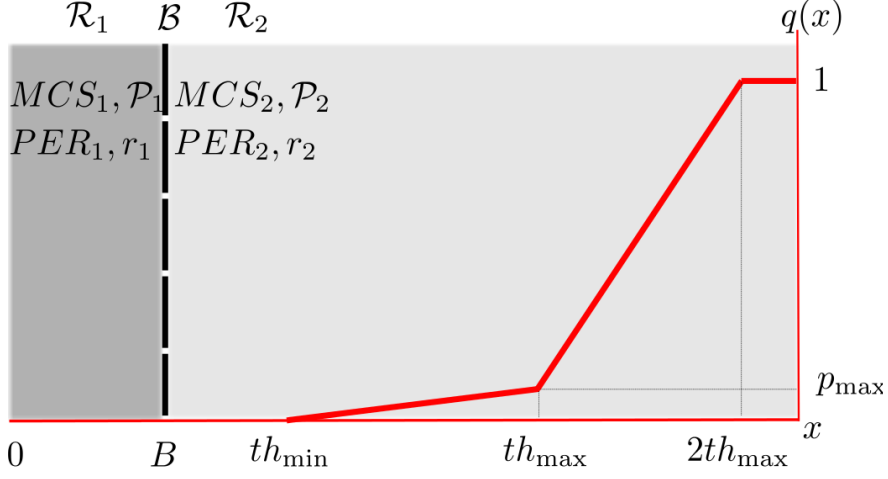


Figure 6.1: Illustration of DRWL with the x -axis representing the queue occupancy x .

packet transmission, the power consumption is assumed to be zero as in Discontinuous Transmission (DTX) scheme [127].

In the light of the presented framework, we describe the proposed EnQAWLAWH(B, Ω, th_P, Z) LA scheme as follows:

- I Set $\mathcal{P}_2 = \mathcal{P}_{\max}$ where \mathcal{P}_{\max} is the maximum output power.
- II For the resulting SNR level snr_{s_2} dB choose $MCS_2 = mcs_{m_2}$ for \mathcal{R}_2 with the highest spectral efficiency such that $P_{m_2, s_2, 0} \leq th_P$.
- III Set $MCS_1 = mcs_{m_1} = \max\{0, MCS_2 - \Omega\}$ where $\Omega \in \mathbb{Z}^+$ is the MCS offset parameter.
- IV Find $SNR_1 = snr_{s_1}$ dB such that $P_{m_1, s_1, 0} < P_{m_2, s_2, 0}$ is satisfied for minimum s_1 and set the transmission power of \mathcal{R}_1 by backing off \mathcal{P}_2 by a factor of $\zeta = 10^{(snr_{s_2} - snr_{s_1})/10}$, i.e., $\mathcal{P}_1 = \mathcal{P}_2 / \zeta$.

In the numerical examples of this study, we will fix $(th_P, Z) = (0.25, 3)$ as suggested in Chapter 4 for the ITU-A channel [1] and study the performance of the EnQAWLAWH scheme as a function of different choices of the (B, Ω) pair.

6.2.1 Analytical Model of DRWN

At the steady state, the transmission queue of a DRWL can be in one of the two regimes \mathcal{R}_i or at the boundary \mathcal{B} . A solution at \mathcal{B} corresponds to the queue constantly going back and forth between \mathcal{R}_1 and \mathcal{R}_2 , spending $(1 - \alpha)$ and α of its time in these two regimes, respectively. We formulate this behavior at \mathcal{B} for the average transmission rate and PER of link l as follows:

$$r_l(x, \alpha) = \begin{cases} r_1, & 0 \leq x < B \\ r_1(1 - \alpha) + r_2\alpha, & x = B \\ r_2, & B < x < 2th_{\max} \end{cases} \quad (6.2)$$

$$PER_l(x, \alpha) = \begin{cases} PER_1, & 0 \leq x < B \\ \frac{PER_1 r_1(1 - \alpha) + PER_2 r_2 \alpha}{r(B, \alpha)}, & x = B \\ PER_2, & B < x < 2th_{\max} \end{cases} \quad (6.3)$$

The total packet loss probability stemming from both wireless channel and GRED queue admission policy on link l can then be written as follows:

$$p_l(x, \alpha) = 1 - (1 - PER_l(x, \alpha))(1 - q(x)). \quad (6.4)$$

Let $X(x, \alpha)$ denote the resequencing delay. Subsequently, the RTT of link l is given below:

$$RTT_l(x, \alpha) = \underbrace{2D_F}_{\text{two-way framing}} + \underbrace{\frac{x}{r(x, \alpha)}}_{\text{queuing}} + \underbrace{\frac{C}{r(x, \alpha)}}_{\text{transmission}} + \underbrace{X(x, \alpha)}_{\text{resequencing}}. \quad (6.5)$$

The set of links the flow n traverses and the set of flows the link l is traversed by, are denoted by \mathcal{L}_n and \mathcal{N}_l , respectively. Let $\Psi_{n,l}$ denote the overall external packet loss rate which the flow n experiences at links other than the link l , i.e., $\mathcal{L}_n \setminus l$:

$$\Psi_{n,l} = 1 - \prod_{j \in \mathcal{L}_n \setminus l} (1 - p_j(x, \alpha)). \quad (6.6)$$

Similarly, let $\Upsilon_{n,l}$ and $\Lambda_{n,l}$ denote the external RTT and the rate limit, respectively, of the flow n for the link l :

$$\Upsilon_{n,l} = \sum_{j \in \mathcal{L}_n \setminus l} RTT_j(x, \alpha). \quad (6.7)$$

$$\Lambda_{n,l} = \min_{j \in \mathcal{L}_n \setminus l} T_{n,j}(x, \alpha). \quad (6.8)$$

Let $\lambda_{n,l}(x, \alpha)$ denote the rate of the flow n (in units of packets/s) arriving at link l . Then, we denote by $T_{n,l}(x, \alpha)$ the throughput that the flow n experiences at link l :

$$T_{n,l}(x, \alpha) = (1 - PER_l(x, \alpha))\kappa_{n,l}(x, \alpha), \quad (6.9)$$

where the notation

$$\kappa_{n,l}(x, \alpha) = (1 - q(x)) \min(C\lambda_{n,l}(x, \alpha), \Lambda_{n,l}) \quad (6.10)$$

denotes the rate of the flow n admitted into the transmission queue of link l .

Let λ denote the packet sending rate of a flow in packets/s. We use well known ‘‘PFTK’’ [5] formula (6.11) to relate packet loss p and RTT seen by a flow to its λ as follows:

$$\lambda = \begin{cases} \frac{\frac{1-p}{p} + E[W_u] + \tilde{Q}(E[W_u])\frac{1}{1-p}}{RTT(\frac{b}{2}E[W_u] + 1) + \tilde{Q}(E[W_u])T_0\frac{f(p)}{1-p}}, & E[W_u] < W_{\max} \\ \frac{\frac{1-p}{p} + W_{\max} + \tilde{Q}(W_{\max})\frac{1}{1-p}}{RTT(\frac{b}{8}W_{\max} + \frac{1-p}{pW_{\max}} + 2) + \tilde{Q}(W_{\max})T_0\frac{f(p)}{1-p}}, & \text{otherwise,} \end{cases} \quad (6.11)$$

where

$$f(p) = 1 + p + 2p^2 + 4p^3 + 8p^4 + 16p^5 + 32p^6, \quad (6.12)$$

$$\tilde{Q}(w) = \min(1, \frac{(1 - (1-p)^3)(1 + (1-p)^3)(1 - (1-p)^{(w-3)})}{1 - (1-p)^w}), \quad (6.13)$$

and

$$E[W_u] = \frac{2+b}{3b} + \sqrt{\frac{8(1-p)}{3bp} + \left(\frac{2+b}{3b}\right)^2}. \quad (6.14)$$

The terms $W_{\max} = W/C$ in equation (6.11) and b in (6.14) stand for the maximum window size in units of packets and the number of packets a cumulative ACK packet is given by the TCP receiver where W is the receiver buffer size in bytes. Let σ_{RTT} denote standard deviation of RTT , timeout parameter T_0 in (6.11) can be expresses as follows:

$$T_0 = \max(T_{0,\min}, RTT + 4\sigma_{RTT}), \quad (6.15)$$

where $T_{0,\min}$ is the minimum possible value of T_0 [2]. Throughout the numerical examples of this study, we set $th_{\min} = 30C$, $th_{\max} = 90C$, $p_{\max} = 0.1$ as in [12],

$D_R = 5$ ms as in [75], $T_{0,\min} = 1$ s as in [161], $b = 2$, $W = 64$ Kbytes as in [2], $2D_F = 5$ ms and $C = 1500$ bytes.

For the flow n and link l , we replace p in (6.11)-(6.14) with $1 - (1 - p_l(x, \alpha))(1 - \Psi_{n,l})$ and RTT in (6.11) with $RTT_l(x, \alpha) + \Upsilon_{n,l}$ in order to find the solution point (x_l^*, α_l^*) such that the following equality holds:

$$\kappa_l(x_l^*, \alpha_l^*) = r_l(x_l^*, \alpha_l^*), \quad (6.16)$$

where

$$\kappa_l(x_l^*, \alpha_l^*) = \sum_{n \in \mathcal{N}_l} \kappa_{n,l}(x_l^*, \alpha_l^*) \quad (6.17)$$

is the aggregate bit arrival rate into the queue from all flows. We solve the network by successively and iteratively solving each link until its solution points (x_l^*, α_l^*) for all links l are obtained as outlined in Algorithm 2. In order to prevent oscillations between the fixed-point iterations, we exponentially smooth p_l , RTT_l and $T_{n,l}$ with the smoothing parameters ϵ_1 , ϵ_2 and ϵ_3 , respectively. Let $p_l^{(k)}$, $RTT_l^{(k)}$ and $T_{n,l}^{(k)}$ denote what are obtained at the k^{th} network solver iteration. Then, smoothing is performed as follows:

$$p_l^{(k+1)'} = \epsilon_1 p_l^{(k)'} + (1 - \epsilon_1) p_l^{(k)}, \quad (6.18)$$

$$RTT_l^{(k+1)'} = \epsilon_2 RTT_l^{(k)'} + (1 - \epsilon_2) RTT_l^{(k)}, \quad (6.19)$$

$$T_{n,l}^{(k+1)'} = \epsilon_3 T_{n,l}^{(k)'} + (1 - \epsilon_3) T_{n,l}^{(k)}, \quad (6.20)$$

where the primed variables denote the smoothed versions of the corresponding variables. Individual convergence status of p_l , RTT_l and $T_{n,l}$ are tracked by the change ratio parameters ς_1 , ς_2 and ς_3 , respectively, as shown below:

$$\varsigma_1 = \max_l \{ |p_l^{(k+1)'} - p_l^{(k)'}| / p_l^{(k)'} \}, \quad (6.21)$$

$$\varsigma_2 = \max_l \{ |RTT_l^{(k+1)'} - RTT_l^{(k)'}| / RTT_l^{(k)'} \}, \quad (6.22)$$

$$\varsigma_3 = \max_{n,l} \{ |T_{n,l}^{(k+1)'} - T_{n,l}^{(k)'}| / T_{n,l}^{(k)'} \}. \quad (6.23)$$

Finally, the iterations are terminated by checking the overall convergence flag ν expressed below:

$$\nu = \begin{cases} 1, & \varsigma_1 < \xi_1 \text{ and } \varsigma_2 < \xi_2 \text{ and } \varsigma_3 < \xi_3 \\ 0, & \text{otherwise,} \end{cases} \quad (6.24)$$

where ξ_1 , ξ_2 and ξ_3 are the tolerances for packet loss rate, RTT and throughput, respectively. Throughout this study, we set $(\epsilon_1, \epsilon_2, \epsilon_3) = (0.9, 0.7, 0.7)$ and $(\xi_1, \xi_2, \xi_3) = (0.01, 0.01, 0.01)$. In Algorithm 2, the 3-tuples $\omega_{n,l}^{(k)} \triangleq (p_l^{(k)}, RTT_l^{(k)}, T_{n,l}^{(k)})$ and $\omega_{n,l}^{(k)'} \triangleq (p_l^{(k)'}, RTT_l^{(k)'}, T_{n,l}^{(k)'})$ are used for the sake of convenience.

Algorithm 2 solveDualRegimeWirelessNetwork

```

1:  $\omega_{n,l}^{(0)'} \leftarrow (0, 0, \infty)$ 
2:  $\nu \leftarrow 0$ 
3:  $k \leftarrow 0$ 
4: while  $\nu = 0$  do
5:    $[\Psi_{n,l}, \Upsilon_{n,l}, \Lambda_{n,l}] \leftarrow \text{EVALEXTERNALLINKPARAMS}(\omega_{n,l}^{(k)'}, \mathcal{L}_n)$   $\triangleright$  eq. (6.6), (6.7), (6.8).
6:   for all links  $l \in \{0, 1, \dots, L-1\}$  do
7:     if  $\mathcal{N}_l \in \emptyset$  then
8:       continue
9:     end if
10:     $[\omega_{n,l}^{(k)}, x_l^*, \alpha_l^*] \leftarrow \text{SOLVEDRWL}(\Psi_{n,l}, \Upsilon_{n,l}, \Lambda_{n,l}, \mathcal{N}_l)$   $\triangleright$  eq. 6.16.
11:  end for
12:   $[\omega_{n,l}^{(k+1)'}, \nu] \leftarrow \text{SMOOTHDRWLPARAMS}(\omega_{n,l}^{(k)}, \omega_{n,l}^{(k)'})$   $\triangleright$  eq. (6.18), (6.19), (6.20), (6.24).
13:   $k \leftarrow k + 1$ 
14: end while

```

Obtaining a complete network-wide solution using fixed-point iterations, we now derive the physical layer (PHY) related parameters. Let $f_{\mathbf{H}_{m,s}}(h)$ expressed below denote the Probability Density Function (PDF) of the Random Variable (RV) $\mathbf{H}_{m,s}(h)$ representing the number of retransmissions required to successfully transmit a FEC block where m and s representing mcs_m and snr_s , respectively.

$$f_{\mathbf{H}_{m,s}}(h) = \begin{cases} 1 - fer_{m,s,0}, & h = 0 \\ (1 - fer_{m,s,h}) \prod_{z=0}^{h-1} fer_{m,s,z}, & 0 < h < Z \\ \prod_{z=0}^{Z-1} fer_{m,s,z}, & h = Z. \end{cases} \quad (6.25)$$

Each packet with length C consists of $F_m = \lceil C/k_m \rceil$ number of FEC blocks where k_m is the length of a FEC block for MCS mcs_m . Assuming loss events of FEC blocks to be iid Bernoulli distributed, total number of retransmissions required for each packet denoted by the RV $\mathbf{G}_{m,s}$, is the maximum of those of the F_m FEC blocks as follows:

$$\mathbf{G}_{m,s} = \max_{F_m} \{\mathbf{H}_{m,s}\} \quad (6.26)$$

The resulting wireless packet loss rate $per_{m,s}$ after Z retransmissions is then given as follows:

$$per_{m,s} = 1 - \left(1 - \prod_{z=0}^Z fer_{m,s,z}\right)^{F_m}. \quad (6.27)$$

The Time Division Duplex (TDD) mode as specified by WiMAX [154] uses 35 out of 47 OFDM symbols for downlink with 768 data sub-carriers per OFDM symbol for a channel bandwidth of 10 MHz [75] and a TDD frame duration of 5 ms, resulting in an average PHY rate of $c = 5.376 \cdot 10^6$ sub-carriers/s. In order to maintain symmetry among all links within the network including the links in opposite direction (i.e., sharing the same TDD frame), we set the PHY rate of each link to c , keeping the TDD frame duration fixed. This assignment requires the channel bandwidth of each link to increase in direct proportion with the increase in the total number of OFDM symbols per TDD frame, which is equal to 70/47. The raw bit rate c_m of the IEEE 802.16 *Wireless-MAN OFDMA PHY* air interface of each link can then be calculated in bps as $c_m = c \log_2(V_m)R_m$ where V_m and R_m denote the modulation order and code rate of mcs_m , respectively. The combined retransmission and padding inefficiency $\eta = C/(k_m F_m)$ caused by the need for FEC block alignment of packets reduce the raw bit rate down to the link layer bit rate $g_{m,s}$ as follows:

$$g_{m,s} = \frac{c_m \eta}{1 + \mathbb{E}[\mathbf{G}_{m,s}]}. \quad (6.28)$$

Using $\mathbf{G}_{m,s}$, we express probability of failure in the z^{th} retransmission denoted by $P_{m,s,z}$ as follows:

$$P_{m,s,z} = \begin{cases} 1 - f_{\mathbf{G}_{m,s}}(0), & z = 0 \\ 1 - \frac{f_{\mathbf{G}_{m,s}}(z)}{\prod_{t=0}^{z-1} P_{m,s,t}}, & 0 < z < Z \\ \frac{per_{m,s}}{\prod_{t=0}^{Z-1} P_{m,s,t}}, & z = Z. \end{cases} \quad (6.29)$$

6.2.2 Approximate DRWL Resequencing Delay Model

For the sake of notational simplicity, we drop the link identifier l in this section focusing on a single link. We use the same resequencing delay model presented

in Section 4.2.2 to calculate X_1 and X_2 for \mathcal{R}_1 and \mathcal{R}_2 , respectively, except for a slight modification for the “empty queue” solution. Unlike the presumed queuing model of Chapters 3 and 4 which facilitates the computation of queue occupancy PDF for the entire range of queue occupancy, the fixed-point model of this chapter and Chapter 5 ends up with a single queue occupancy level for which empty queue is one of the candidates. Let $A(x, \alpha)$ denote the mean interarrival time of packets which is given by the following equation for DRWL framework.

$$A(x, \alpha) = \begin{cases} \frac{C}{\kappa(0, \alpha)}, & x = 0, \\ \frac{C}{r(x, \alpha)}, & \text{otherwise,} \end{cases} \quad (6.30)$$

where $\kappa(x, \alpha)$ is the overall rate of bits admitted into the queue as found in equation (6.17). Taking similar steps with Section 4.2.2, the resequencing delay can then be expressed as follows:

$$\mathbf{R}(x, \alpha) = \max_{0 \leq k < \frac{D_R Z}{A(x, \alpha)}} \{D_R \mathbf{G}(x, \alpha) - A(x, \alpha)k\}, \quad (6.31)$$

where the PDF of the RV $\mathbf{G}(x, \alpha)$ denoting the total number of retransmissions required for a packet is formulated as follows:

$$f_{\mathbf{G}(x, \alpha)}(g) = \begin{cases} f_{\mathbf{G}_1}(g), & 0 \leq x < B \\ \frac{f_{\mathbf{G}_1}(g)r_1(1-\alpha) + f_{\mathbf{G}_2}(g)r_2\alpha}{r(x, \alpha)}, & x = B \\ f_{\mathbf{G}_2}(g), & B < x < 2th_{\max}. \end{cases} \quad (6.32)$$

In the above expression, RVs \mathbf{G}_1 and \mathbf{G}_2 denote the total number of retransmissions required for a packet for \mathcal{R}_1 and \mathcal{R}_2 , respectively, and can be derived using equation (6.26). The PDF of the total number of retransmissions at \mathcal{B} is taken to be weighted sum of those of \mathbf{G}_1 and \mathbf{G}_2 with $r_1(1 - \alpha)/r(x, \alpha)$ and $r_2\alpha/r(x, \alpha)$, respectively. Finally, $X(x, \alpha) = \mathbb{E}[\mathbf{R}(x, \alpha)]$ gives the mean resequencing delay. On the basis of equation (6.32), $X(x, \alpha)$ can then be written as follows:

$$X(x, \alpha) = \begin{cases} X_1, & 0 \leq x < B \\ X_B, & x = B \\ X_2, & B < x < 2th_{\max}, \end{cases} \quad (6.33)$$

where X_B is the resequencing delay at \mathcal{B} .

Proof for existence and uniqueness for DRWL with single transmission opportunity presented in Chapter 5 can be extended to DRWL with multiple transmission opportunities by proving $X(x, \alpha)$ to be a non-decreasing function of the queue occupancy x in \mathcal{R}_1 and \mathcal{R}_2 and a non-decreasing function of α at \mathcal{B} as in Theorems 6.2.1 and 6.2.2, respectively.

Theorem 6.2.1. *The inequality $X_1 \leq X_2$ is satisfied provided that $r_1 < r_2$ and $F_{\mathbf{G}_1}(g) \geq F_{\mathbf{G}_2}(g)$ for all g .*

Proof. The mean resequencing delay X_1 for empty queue is smaller than that of any other solution point in \mathcal{R}_1 since $A(0, \alpha) < A(x, \alpha)$ for $x \neq 0$. Therefore, without loss of generality (WLOG) we provide the proof assuming $x \neq 0$ for \mathcal{R}_1 . Let the RV $\mathbf{\Gamma}_{i,k}$ be equal to $D_R \mathbf{G}_i - \frac{Ck}{r_i}$ for regime \mathcal{R}_i . Then, using equations (6.30) and (6.31), the inequality of interest $X_1 \leq X_2$ can be rewritten as follows:

$$\mathbb{E}[\max_k \mathbf{\Gamma}_{1,k}] \leq \mathbb{E}[\max_k \mathbf{\Gamma}_{2,k}]. \quad (6.34)$$

Also, let $\mathbf{\Gamma}_{i,k}^+$ be the RV whose PDF is given as follows:

$$f_{\mathbf{\Gamma}_{i,k}^+}(\gamma) = \begin{cases} f_{\mathbf{\Gamma}_{i,k}}(\gamma), & \gamma > 0 \\ \int_{-\infty}^0 f_{\mathbf{\Gamma}_{i,k}}(\gamma') d\gamma', & \gamma = 0, \end{cases} \quad (6.35)$$

where $f_{\mathbf{\Gamma}_{i,k}}(\gamma)$ denotes the PDF of the RV $\mathbf{\Gamma}_{i,k}$. Since the minimum possible value of $\max_k \mathbf{\Gamma}_{i,k}$ is equal to $\min \mathbf{\Gamma}_{i,0} = 0$, the inequality (6.34) and the following inequality imply one another:

$$\mathbb{E}[\max_k \mathbf{\Gamma}_{1,k}^+] \leq \mathbb{E}[\max_k \mathbf{\Gamma}_{2,k}^+]. \quad (6.36)$$

Fubini's Theorem relates the mean value of a non-negative RV denoted by Ξ directly to its Cumulative Distribution Function (CDF) $F_{\Xi}(\tau)$ as follows:

$$\mathbb{E}[\Xi] = \int_0^\infty 1 - F_{\Xi}(\tau) d\tau \quad (6.37)$$

Exploiting equation (6.37), the inequality (6.36) can be decomposed as follows:

$$\int_0^\infty 1 - \prod_k F_{\mathbf{\Gamma}_{1,k}^+}(\gamma) d\gamma \leq \int_0^\infty 1 - \prod_k F_{\mathbf{\Gamma}_{2,k}^+}(\gamma) d\gamma. \quad (6.38)$$

Note that the following inequality is a sufficient (but not necessary) condition for (6.38) to hold:

$$F_{\mathbf{r}_{1,k}^+}(\gamma) \geq F_{\mathbf{r}_{2,k}^+}(\gamma), \text{ for all } k \text{ and } \gamma. \quad (6.39)$$

Observe that $F_{\mathbf{r}_{i,k}^+}(\gamma)$ is a shifted and scaled transformation of $F_{\mathbf{G}_i}(g)$. Provided that $r_1 < r_2$ and $F_{\mathbf{G}_1}(g) \geq F_{\mathbf{G}_2}(g)$ for all g , condition (6.39) is satisfied which completes the proof. \square

Conditions of Theorem 6.2.1 are numerically ensured to be satisfied for all numerical examples studied in this chapter.

Theorem 6.2.2. $X(B, \alpha') \leq X(B, \alpha^\dagger)$ for $\alpha' < \alpha^\dagger$ provided that $r_1 < r_2$ and $F_{\mathbf{G}_1}(g) \geq F_{\mathbf{G}_2}(g)$ for all g .

Proof. Let $F_{\mathbf{G}'}(g)$ and $F_{\mathbf{G}_\dagger}(g)$ be CDFs of RVs denoting the number of retransmissions for α' and α^\dagger , respectively. Using equation (6.32), the following inequality holds since $\alpha' < \alpha^\dagger$ and $F_{\mathbf{G}_1}(g) \geq F_{\mathbf{G}_2}(g)$:

$$F_{\mathbf{G}'}(g) \geq F_{\mathbf{G}_\dagger}(g). \quad (6.40)$$

Note also that $r(B, \alpha') < r(B, \alpha^\dagger)$ which together with inequality (6.40) constitutes the two assumptions of Theorem 6.2.1 yielding the inequality $X(B, \alpha') \leq X(B, \alpha^\dagger)$ is satisfied. \square

The proofs presented in Chapter 5 and hereby lead to the existence and uniqueness of a solution only for a single DRWL with multiple transmission opportunities. Nevertheless, network-wide convergence to a solution could be achieved for each numerical example of this study.

6.2.3 Network Performance Metrics

We now present the expressions for network-wide throughput and power which are indicative of the total revenue and operational cost of a network operator,

respectively. Let FT_n be the throughput which the flow n gets from the network. Obviously, the following must hold for all n and l such that $l \in \mathcal{L}_n$:

$$FT_n = T_{n,l}(x_l^*, \alpha_l^*). \quad (6.41)$$

For the sake of completeness, the aggregate throughput of link l can be obtained as shown below:

$$LT_l = \sum_{n \in \mathcal{N}_l} T_{n,l}(x_l^*, \alpha_l^*). \quad (6.42)$$

Using (6.41), the network-wide aggregate TCP throughput denoted by NT can be found as follows:

$$NT = \sum_n FT_n. \quad (6.43)$$

Let LP_l be the power consumption of link l as shown below:

$$LP_l = \begin{cases} \mathcal{P}_{\max}, & x^* \in \mathcal{R}_2 \\ \mathcal{P}_{\max}((1 - \alpha^*)/\zeta + \alpha^*), & x^* \in \mathcal{B} \\ \mathcal{P}_{\max}/\zeta, & x^* \in \mathcal{R}_1 \text{ and } x^* \neq 0 \\ \mathcal{P}_{\max}\rho/\zeta, & x^* \in \mathcal{R}_1 \text{ and } x^* = 0, \end{cases} \quad (6.44)$$

where

$$\rho = \frac{\kappa(0, \alpha)}{r(0, \alpha)} \quad (6.45)$$

is the load of the link when its queue is empty. Assuming all links transmit at equal power in \mathcal{R}_2 , the total network power consumption denoted by NP can then be calculated as follows:

$$NP = \sum_l LP_l. \quad (6.46)$$

We identify NT and NP presented in equations (6.43) and (6.46), respectively, as the key network performance metrics. Note that they can also be used for a Single-Regime Wireless Network (SRWN), by means of eroding \mathcal{B} via letting $\Omega = 0$ and $PER_1 = PER_2$. In this case, the EnQAWLAWH scheme degenerates to the TAGLAWH scheme presented in Chapter 4. SRWN will be the primary source of benchmark in Section 6.4 where the performance of the EnQAWLAWH scheme

is evaluated. Using (6.43) and (6.46), the network energy per bit performance metric denoted by $NEpB$ can be written as:

$$NEpB_D = NP_D/NT_D \quad (6.47)$$

and

$$NEpB_S = NP_S/NT_S. \quad (6.48)$$

for DRWN and SRWN with the associated subscripts D and S , respectively.

The EnQAWLAwH scheme with its dual-regime nature slows down the link whenever it “considers” necessary, which may result in a lower NT_D than NT_S . We let $NTLP$ denote the percentage network throughput loss to keep track of such cases which is expressed as follows:

$$NTLP = 100(1 - NT_D/NT_S). \quad (6.49)$$

Since the primary objective of the EnQAWLAwH scheme is to reduce NP_D compared to NP_S , we let $NPRP$ denote the percentage network power reduction as shown below:

$$NPRP = 100(1 - NP_D/NP_S). \quad (6.50)$$

Both $NTLP$ and $NPRP$ are unitless and thus can be weighted with a weight factor $\beta \in [0, 1]$ to obtain the network performance gain percentage Θ as follows:

$$\Theta(\beta) = -\beta NTLP + (1 - \beta) NPRP, \quad (6.51)$$

for which $\beta = 0$ and $\beta = 1$ boundary values correspond to ignoring loss in throughput and reduction in power, respectively. For any value of β , the higher Θ is, the better the overall network performance gets. While Equation (6.51) is one way to assess the interplay between power and throughput, percentage network energy per bit reduction denoted by $NEpBRP$ is another alternative as given below:

$$NEpBRP = 100(1 - NEpB_D/NEpB_S). \quad (6.52)$$

Although $NEpBRP$ is a performance metric that the communications community may be more familiar with, we believe it falls short in exposing a possible degradation in network-wide throughput.

Table 6.1: Modulation and coding schemes of IEEE 802.16 used in this study.

m	0	1	2	3	4	5	6	7
V_m	4	4	16	16	64	64	64	64
R_m	1/2	3/4	1/2	3/4	1/2	2/3	3/4	5/6
$k_m(\text{bytes})$	60	54	60	54	54	48	54	60

6.3 Validation of the Analytical Model

In this section, the proposed EnQAWLAWH scheme is validated using the chosen subset of MCSs shown in Table 6.1 from the IEEE 802.16 standard. Assuming all links to follow the AWGN wireless channel model, the FER vs. SNR curves of these MCSs with Convolutional Turbo Codes (CTC) for the AWGN channel are depicted in Fig. 6.2 for $Z = 3$ maximum number of allowed retransmissions. At least $4 \cdot 10^7$ FEC blocks are decoded to reach the presented FER values unless 400 FEC block error events are encountered. Since mcs_4 has the same spectral efficiency with mcs_3 but higher FER values for all retransmission attempts and all SNR values, it is discarded in MCS selection for both \mathcal{R}_1 and \mathcal{R}_2 . The final samples on some of the presented FER curves turn out to be higher than the preceding ones. Especially the discarded MCS mcs_4 exhibits this trend which we attribute to insufficient number of realizations achieved at high retransmission indices. We ignore these errors due to low probability of reaching high retransmission indices for the selected parameter value $th_P = 0.25$ of the EnQAWLAWH scheme.

As preferred in Chapter 4, the approximate resequencing delay model for DRWL is validated with a number of MATLAB[®] simulations. Since the presented approximate model in Section 6.2.2 for \mathcal{R}_1 and \mathcal{R}_2 are essentially the same with the one presented in Section 4.2.2, the focus in this section is kept on the validation of the model at \mathcal{B} . Recall that mcs_{m_1} (mcs_{m_2}) and snr_{s_1} (snr_{s_2}) are the values of MCS_1 (MCS_2) and SNR_1 (SNR_2) maintained by the EnQAWLAWH scheme, respectively. The simulator running in MATLAB[®] consists of: (i) a transmitter with a queue of packets to be retransmitted and a new packet whenever its retransmission queue is empty with a link-layer transmission rate of g_{m_1,s_1} (g_{m_2,s_2}) as in (6.28) with probability $1 - \alpha$ (α), (ii) a channel dropping

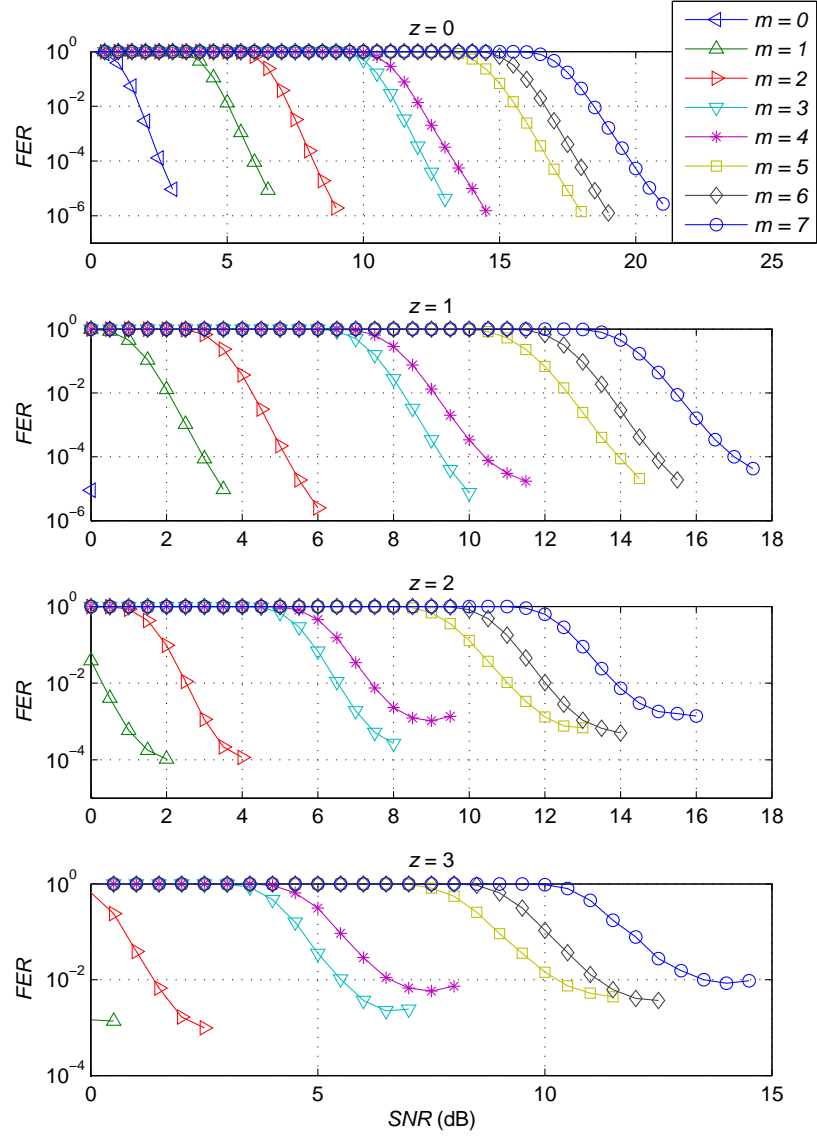


Figure 6.2: Simulated FER $fer_{m,s,z}$ for $Z = 3$ maximum number of allowed retransmissions and the AWGN channel.

packets by either $P_{m_1, s_1, z}$ or $P_{m_2, s_2, z}$ as in (6.29) depending on the regime the packet is initially transmitted from and (iii) a receiver with the same resequencing mechanism described in Section 4.2.2. We generate eighteen test cases as shown in Table 6.2 by selecting $\alpha \in \{1 \cdot 10^{-2}, 5 \cdot 10^{-1}, 9.9 \cdot 10^{-1}\}$, $m_2 \in \{5, 6, 7\}$ and $\Omega \in \{3, 5\}$. For all test cases, we choose s_1 and s_2 such that the condition $P_{m_1, s_1, 0} < P_{m_2, s_2, 0} \leq th_P = 0.25$ is satisfied for minimum s_1 and s_2 . We present the simulation results along with the associated confidence intervals for 99% confidence level.

Table 6.2: DRWL resequencing delay validation test cases and results for $Z = 3$. Results are presented with the 99% confidence intervals.

	α	$m_1(2)$	$s_1(2)$	$snr^{s_1(2)}$ (dB)	$P_{m_1(2), s_1(2), 0}$	$X_{1(2)}$ (ms)	X_B (ms)	$X_{B\text{-sim.}}$ (ms)	σX_B (ms)	$\sigma X_{B\text{-sim.}}$ (ms)
1	$1.00 \cdot 10^{-2}$	2(5)	16(32)	8.0(16.0)	$5.89 \cdot 10^{-3} (7.60 \cdot 10^{-2})$	0.08(1.47)	0.10	0.11 ± 0.02	0.59	0.67 ± 0.05
2	$1.00 \cdot 10^{-2}$	0(5)	4(32)	2.0(16.0)	$6.94 \cdot 10^{-2} (7.60 \cdot 10^{-2})$	0.53(1.47)	0.54	0.86 ± 0.03	1.38	1.95 ± 0.02
3	$1.00 \cdot 10^{-2}$	3(6)	24(34)	12.0(17.0)	$9.72 \cdot 10^{-3} (7.97 \cdot 10^{-2})$	0.18(1.67)	0.20	0.22 ± 0.03	0.83	0.89 ± 0.05
4	$1.00 \cdot 10^{-2}$	1(6)	11(34)	5.5(17.0)	$3.06 \cdot 10^{-2} (7.97 \cdot 10^{-2})$	0.32(1.67)	0.34	0.45 ± 0.02	1.09	1.35 ± 0.02
5	$1.00 \cdot 10^{-2}$	3(7)	23(37)	11.5(18.5)	$9.05 \cdot 10^{-2} (2.02 \cdot 10^{-1})$	1.39(3.15)	1.42	1.55 ± 0.03	1.83	1.95 ± 0.01
6	$1.00 \cdot 10^{-2}$	2(7)	15(37)	7.5(18.5)	$7.85 \cdot 10^{-2} (2.02 \cdot 10^{-1})$	0.94(3.15)	0.98	1.17 ± 0.04	1.66	1.91 ± 0.02
7	$5.00 \cdot 10^{-1}$	2(5)	16(32)	8.0(16.0)	$5.89 \cdot 10^{-3} (7.60 \cdot 10^{-2})$	0.08(1.47)	0.86	0.75 ± 0.04	1.56	1.56 ± 0.03
8	$5.00 \cdot 10^{-1}$	0(5)	4(32)	2.0(16.0)	$6.94 \cdot 10^{-2} (7.60 \cdot 10^{-2})$	0.53(1.47)	1.04	0.99 ± 0.02	1.68	1.90 ± 0.02
9	$5.00 \cdot 10^{-1}$	3(6)	24(34)	12.0(17.0)	$9.72 \cdot 10^{-3} (7.97 \cdot 10^{-2})$	0.18(1.67)	1.01	1.00 ± 0.04	1.64	1.72 ± 0.03
10	$5.00 \cdot 10^{-1}$	1(6)	11(34)	5.5(17.0)	$3.06 \cdot 10^{-2} (7.97 \cdot 10^{-2})$	0.32(1.67)	1.08	0.98 ± 0.04	1.69	1.82 ± 0.02
11	$5.00 \cdot 10^{-1}$	3(7)	23(37)	11.5(18.5)	$9.05 \cdot 10^{-2} (2.02 \cdot 10^{-1})$	1.39(3.15)	2.47	2.56 ± 0.06	1.88	2.06 ± 0.01
12	$5.00 \cdot 10^{-1}$	2(7)	15(37)	7.5(18.5)	$7.85 \cdot 10^{-2} (2.02 \cdot 10^{-1})$	0.94(3.15)	2.36	2.30 ± 0.03	1.91	2.19 ± 0.01
13	$9.90 \cdot 10^{-1}$	2(5)	16(32)	8.0(16.0)	$5.89 \cdot 10^{-3} (7.60 \cdot 10^{-2})$	0.08(1.47)	1.45	1.51 ± 0.04	1.81	1.88 ± 0.01
14	$9.90 \cdot 10^{-1}$	0(5)	4(32)	2.0(16.0)	$6.94 \cdot 10^{-2} (7.60 \cdot 10^{-2})$	0.53(1.47)	1.46	1.52 ± 0.04	1.82	1.90 ± 0.01
15	$9.90 \cdot 10^{-1}$	3(6)	24(34)	12.0(17.0)	$9.72 \cdot 10^{-3} (7.97 \cdot 10^{-2})$	0.18(1.67)	1.65	1.80 ± 0.04	1.85	1.97 ± 0.01
16	$9.90 \cdot 10^{-1}$	1(6)	11(34)	5.5(17.0)	$3.06 \cdot 10^{-2} (7.97 \cdot 10^{-2})$	0.32(1.67)	1.65	1.80 ± 0.03	1.85	1.98 ± 0.01
17	$9.90 \cdot 10^{-1}$	3(7)	23(37)	11.5(18.5)	$9.05 \cdot 10^{-2} (2.02 \cdot 10^{-1})$	1.39(3.15)	3.14	3.45 ± 0.03	1.68	1.77 ± 0.02
18	$9.90 \cdot 10^{-1}$	2(7)	15(37)	7.5(18.5)	$7.85 \cdot 10^{-2} (2.02 \cdot 10^{-1})$	0.94(3.15)	3.14	3.46 ± 0.03	1.68	1.77 ± 0.02

Analytical results reveal an acceptable level of agreement with those of simulation. In accordance with its single-regime counterpart, DRWL resequencing model slightly overestimates the mean and the standard deviation of the resequencing delay which can be attributed to its approximate nature and the way simulations are performed. During simulations, the packet to be retransmitted waits for an additional time until the completion of the current transmission even if a NACK arrives at the transmitter. This phenomenon brings in an upward bias to the results of the simulations as seen in Table 6.2. Although the fixed-point model presented in this chapter is indifferent to standard deviation of the resequencing delay, associated results of the test cases in Table 6.2 are presented for the sake of completeness. Analytically obtained X_i values for the chosen parameters of \mathcal{R}_i are also given in Table 6.2 as they constitute reference intervals to the corresponding X_B values of \mathcal{B} .

In Fig. 6.3, the simulation topology constructed to validate the proposed analytical model in the ns-3 simulation environment is depicted [2]. We prefer simulating a dumb-bell topology with a DRWL-type center link connected to conventional single-regime leaf links dedicated exclusively to each and every flow contending the center link c . Single-regime leaf links serve the purpose of independently varying flow parameters like packet loss ratio, RTT and rate limit. In accordance with the presented analytical model in Section 6.2.1, Algorithm 2 iteratively solves each DRWL link by taking packet loss ratio, RTT and rate limit imposed by the complementary part of the network into account as suggested by equations (6.6), (6.7) and (6.8). At each iteration a single DRWL is solved inside the innermost loop of Algorithm 2, which is the part of the algorithm we validate in this study. In Fig. 6.3, left leaf links are error-free and rate unlimited with a one-way delay of D_L ms whereas each right leaf link has a D_{R_n} ms one-way delay together with a V_{R_n} bps rate limit and a packet loss rate of P_{R_n} through the link in the forward direction, i.e., from TCP sources to sinks, for $n \in \{0, 1, \dots, N-1\}$.

We define five sets of scenarios for validation, namely A, B, C, D and E, each having eighteen test scenarios indexed with the parameter idx totaling ninety test scenarios. For each test scenario:

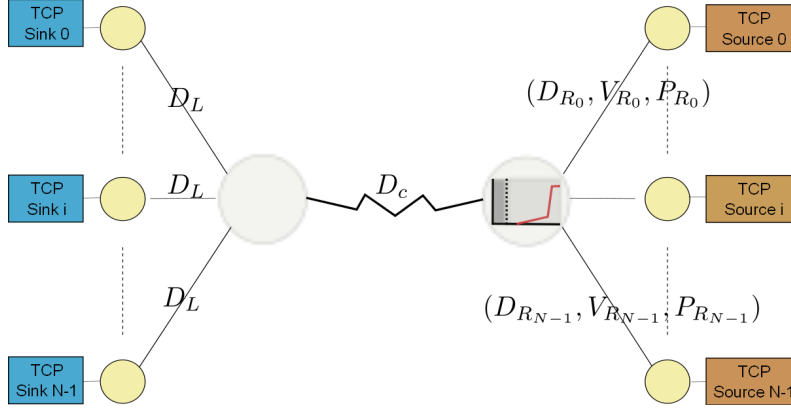


Figure 6.3: ns-3 simulation topology.

- Encouraged by the level of success attained by the approximate DRWL resequencing delay model and the relatively lower values of the resequencing delay obtained therefrom, we implement a single transmission approximation of the center DRWL for the sake of simplicity. In other words, we implement neither a retransmission nor a resequencing mechanism but only the average resequencing delay $X(x^*, \alpha^*)$ as $D_c = D_F + X(x^*, \alpha^*)/2$. Accordingly, we simulate the resulting PER values after the final retransmission is made in \mathcal{R}_i which converge to 0 for the presumed pair $(th_P, Z) = (0.25, 3)$ and the AWGN channel as evident from Fig. 6.2.
- Number of TCP flows N and the average RTT contribution of their right and left leaf links in total of F ms are represented by $SU_{N,F}$ where the flow n is assigned an individual total leaf link RTT of $RTT_{0,n} = 2(n+1)F/(N+1)$ ms. WLOG, we fix $D_L = \min_n(RTT_{0,n})/4$ and $D_{R_n} = RTT_{0,n}/2 - D_L$.
- The flow n 's right leaf link packet loss rate is chosen as follows:

$$P_{R_n} = \begin{cases} 0, & N = 1 \\ 0, & N > 1 \text{ and } n < N/2 \\ \frac{\chi_2 - \chi_1}{N/2 - 1}(n - N/2) + \chi_1, & \text{otherwise,} \end{cases} \quad (6.53)$$

where N is an even integer when $N > 1$ and where χ_1 and χ_2 are the maximum and the minimum values, respectively, that P_{R_n} can take.

- The flow n 's right leaf link rate limit is chosen as follows:

$$V_{R_n} = \begin{cases} \frac{r_2}{N} \frac{\Phi_1}{100}, & N = 1 \\ \frac{r_2}{N} \left(\frac{\Phi_2 - \Phi_1}{100} \frac{n}{\hat{N} - 1} + \frac{\Phi_1}{100} \right), & N > 1 \text{ and } n < \hat{N} \\ \infty, & \text{otherwise,} \end{cases} \quad (6.54)$$

where,

$$\hat{N} = \begin{cases} N, & \chi_1 = \chi_2 = 0 \\ N/2, & \text{otherwise.} \end{cases} \quad (6.55)$$

Φ_1 and Φ_2 in equation (6.54) denote the percentage maximum and minimum values of service rate, respectively, that the flows can take from their equal share from the capacity of \mathcal{R}_2 of the center link c . The condition (6.55) enforces half of the flows to be rate limited when the other half have error-prone access links as defined by (6.53), all of the flows otherwise.

TCP flow statistics are acquired using the *FlowMonitor* monitoring framework developed for ns-3 [148] and the *RateErrorModel* class of ns-3 is used to induce packet errors. Simulations are run for five minutes and all statistics are acquired after thirty seconds pass. For test scenarios with $P_{R_n} \neq 0$ for any n and/or for which solution domain of the center link c is \mathcal{R}_2 where packets may be dropped by the GRED AQM policy, simulations are repeated ten times and the average results are reported together with the 99% confidence intervals for aggregate DRWN TCP throughput NT_D .

Parameters of Scenario Sets A, B, and C are chosen to be the same as detailed in Table 6.3 except for the corresponding boundary \mathcal{B} being located at $B = 2C$, $B = 4C$ and $B = 8C$, respectively. For these scenario sets, we rate limit the flows without inducing any packet loss and vary SNR_2 and Ω parameters. Resulting MCS_i , r_i and $P_{m_i, s_i, 0}$ values are also shown in Table 6.3 and in the corresponding Tables 6.4 and 6.5 of Scenario Sets D and E, respectively. For Scenario Set D, we fix $\chi_1 = \chi_2 = 0$, $SNR_2 = 18.5$ dB, $(B, \Omega, th_P, Z) = (4C, 3, 0.25, 3)$ and vary the rate limit across the scenarios. The reason we give emphasis on this particular choice of the (B, Ω) pair is that they turn out to be a preferable operating point for the EnQAWLAwH scheme as will be discussed in Section 6.4. Finally for Sce-

Table 6.3: The list of eighteen traffic scenarios of Scenario Sets A, B and C with $B = 2C$, $B = 4C$ and $B = 8C$, respectively, and with $(th_P, Z) = (0.25, 3)$ used for validation of the fixed-point analytical model proposed for DRWL for the AWGN channel model.

idx	Traffic Scenario	$\Phi_{1,2}$ (%)	$\chi_{1,2}$	SNR_2 (dB)	Ω	$MCS_{1(2)}$	$r_{1(2)}$ (Mbps)	$P_{m_{1(2)}, s_{1(2)}, 0}$
1	$SU_{1,1}$	80	0	18.5	3	$mcs_3(7)$	14.67(22.36)	$9.05 \cdot 10^{-2}(2.02 \cdot 10^{-1})$
2	$SU_{1,1}$	80	0	16.0	4	$mcs_1(5)$	7.76(19.52)	$3.06 \cdot 10^{-2}(7.60 \cdot 10^{-2})$
3	$SU_{1,40}$	80	0	18.5	5	$mcs_2(7)$	9.97(22.36)	$7.85 \cdot 10^{-2}(2.02 \cdot 10^{-1})$
4	$SU_{1,40}$	80	0	16.0	3	$mcs_2(5)$	10.69(19.52)	$5.89 \cdot 10^{-3}(7.60 \cdot 10^{-2})$
5	$SU_{1,160}$	80	0	18.5	7	$mcs_0(7)$	5.03(22.36)	$6.94 \cdot 10^{-2}(2.02 \cdot 10^{-1})$
6	$SU_{1,160}$	80	0	16.0	2	$mcs_3(5)$	15.85(19.52)	$9.72 \cdot 10^{-3}(7.60 \cdot 10^{-2})$
7	$SU_{4,1}$	80,40	0,0	18.5	4	$mcs_3(7)$	14.67(22.36)	$9.05 \cdot 10^{-2}(2.02 \cdot 10^{-1})$
8	$SU_{4,1}$	80,40	0,0	16.0	5	$mcs_0(5)$	5.03(19.52)	$6.94 \cdot 10^{-2}(7.60 \cdot 10^{-2})$
9	$SU_{4,40}$	80,40	0,0	18.5	3	$mcs_3(7)$	14.67(22.36)	$9.05 \cdot 10^{-2}(2.02 \cdot 10^{-1})$
10	$SU_{4,40}$	80,40	0,0	16.0	4	$mcs_1(5)$	7.76(19.52)	$3.06 \cdot 10^{-2}(7.60 \cdot 10^{-2})$
11	$SU_{4,160}$	80,40	0,0	18.5	6	$mcs_1(7)$	7.76(22.36)	$3.06 \cdot 10^{-2}(2.02 \cdot 10^{-1})$
12	$SU_{4,160}$	80,40	0,0	16.0	1	$mcs_3(5)$	15.85(19.52)	$9.72 \cdot 10^{-3}(7.60 \cdot 10^{-2})$
13	$SU_{16,1}$	80,40	0,0	18.5	5	$mcs_2(7)$	9.97(22.36)	$7.85 \cdot 10^{-2}(2.02 \cdot 10^{-1})$
14	$SU_{16,1}$	80,40	0,0	16.0	3	$mcs_2(5)$	10.69(19.52)	$5.89 \cdot 10^{-3}(7.60 \cdot 10^{-2})$
15	$SU_{16,40}$	80,40	0,0	18.5	4	$mcs_3(7)$	14.67(22.36)	$9.05 \cdot 10^{-2}(2.02 \cdot 10^{-1})$
16	$SU_{16,40}$	80,40	0,0	16.0	5	$mcs_0(5)$	5.03(19.52)	$6.94 \cdot 10^{-2}(7.60 \cdot 10^{-2})$
17	$SU_{16,160}$	80,40	0,0	18.5	7	$mcs_0(7)$	5.03(22.36)	$6.94 \cdot 10^{-2}(2.02 \cdot 10^{-1})$
18	$SU_{16,160}$	80,40	0,0	16.0	1	$mcs_3(5)$	15.85(19.52)	$9.72 \cdot 10^{-3}(7.60 \cdot 10^{-2})$

Table 6.4: The list of eighteen traffic scenarios of Scenario Set D with $(B, \Omega, th_P, Z) = (4C, 3, 0.25, 3)$ used for validation of the fixed-point analytical model proposed for DRWL for the AWGN channel model.

idx	Traffic Scenario	$\Phi_{1,2}$ (%)	$\chi_{1,2}$	SNR_2 (dB)	Ω	$MCS_{1(2)}$	$r_{1(2)}$ (Mbps)	$P_{m_{1(2)}, s_{1(2)}, 0}$
1	$SU_{1,1}$	60	0	18.5	3	$mcs_3(7)$	14.67(22.36)	$9.05 \cdot 10^{-2}(2.02 \cdot 10^{-1})$
2	$SU_{1,1}$	40	0	18.5	3	$mcs_3(7)$	14.67(22.36)	$9.05 \cdot 10^{-2}(2.02 \cdot 10^{-1})$
3	$SU_{1,40}$	60	0	18.5	3	$mcs_3(7)$	14.67(22.36)	$9.05 \cdot 10^{-2}(2.02 \cdot 10^{-1})$
4	$SU_{1,40}$	40	0	18.5	3	$mcs_3(7)$	14.67(22.36)	$9.05 \cdot 10^{-2}(2.02 \cdot 10^{-1})$
5	$SU_{1,160}$	60	0	18.5	3	$mcs_3(7)$	14.67(22.36)	$9.05 \cdot 10^{-2}(2.02 \cdot 10^{-1})$
6	$SU_{1,160}$	40	0	18.5	3	$mcs_3(7)$	14.67(22.36)	$9.05 \cdot 10^{-2}(2.02 \cdot 10^{-1})$
7	$SU_{4,1}$	80,60	0,0	18.5	3	$mcs_3(7)$	14.67(22.36)	$9.05 \cdot 10^{-2}(2.02 \cdot 10^{-1})$
8	$SU_{4,1}$	60,40	0,0	18.5	3	$mcs_3(7)$	14.67(22.36)	$9.05 \cdot 10^{-2}(2.02 \cdot 10^{-1})$
9	$SU_{4,40}$	80,60	0,0	18.5	3	$mcs_3(7)$	14.67(22.36)	$9.05 \cdot 10^{-2}(2.02 \cdot 10^{-1})$
10	$SU_{4,40}$	60,40	0,0	18.5	3	$mcs_3(7)$	14.67(22.36)	$9.05 \cdot 10^{-2}(2.02 \cdot 10^{-1})$
11	$SU_{4,160}$	80,60	0,0	18.5	3	$mcs_3(7)$	14.67(22.36)	$9.05 \cdot 10^{-2}(2.02 \cdot 10^{-1})$
12	$SU_{4,160}$	60,40	0,0	18.5	3	$mcs_3(7)$	14.67(22.36)	$9.05 \cdot 10^{-2}(2.02 \cdot 10^{-1})$
13	$SU_{16,1}$	80,60	0,0	18.5	3	$mcs_3(7)$	14.67(22.36)	$9.05 \cdot 10^{-2}(2.02 \cdot 10^{-1})$
14	$SU_{16,1}$	60,40	0,0	18.5	3	$mcs_3(7)$	14.67(22.36)	$9.05 \cdot 10^{-2}(2.02 \cdot 10^{-1})$
15	$SU_{16,40}$	80,60	0,0	18.5	3	$mcs_3(7)$	14.67(22.36)	$9.05 \cdot 10^{-2}(2.02 \cdot 10^{-1})$
16	$SU_{16,40}$	60,40	0,0	18.5	3	$mcs_3(7)$	14.67(22.36)	$9.05 \cdot 10^{-2}(2.02 \cdot 10^{-1})$
17	$SU_{16,160}$	80,60	0,0	18.5	3	$mcs_3(7)$	14.67(22.36)	$9.05 \cdot 10^{-2}(2.02 \cdot 10^{-1})$
18	$SU_{16,160}$	60,40	0,0	18.5	3	$mcs_3(7)$	14.67(22.36)	$9.05 \cdot 10^{-2}(2.02 \cdot 10^{-1})$

Table 6.5: The list of eighteen traffic scenarios of Scenario Set E with $(B, \Omega, th_P, Z) = (4C, 3, 0.25, 3)$ used for validation of the fixed-point analytical model proposed for DRWL for the AWGN channel model.

idx	Traffic Scenario	$\Phi_{1,2}$ (%)	$\chi_{1,2}$	SNR_2 (dB)	Ω	$MCS_{1(2)}$	$r_{1(2)}$ (Mbps)	$P_{m_{1(2)}, s_{1(2)}, 0}$
1	$SU_{4,1}$	80,40	$10^{-2}, 10^{-4}$	18.5	3	$mcs_{3(7)}$	14.67(22.36)	$9.05 \cdot 10^{-2}(2.02 \cdot 10^{-1})$
2	$SU_{4,1}$	80,60	$10^{-2}, 10^{-3}$	18.5	3	$mcs_{3(7)}$	14.67(22.36)	$9.05 \cdot 10^{-2}(2.02 \cdot 10^{-1})$
3	$SU_{4,1}$	60,40	$10^{-3}, 10^{-4}$	18.5	3	$mcs_{3(7)}$	14.67(22.36)	$9.05 \cdot 10^{-2}(2.02 \cdot 10^{-1})$
4	$SU_{4,40}$	80,40	$10^{-2}, 10^{-4}$	18.5	3	$mcs_{3(7)}$	14.67(22.36)	$9.05 \cdot 10^{-2}(2.02 \cdot 10^{-1})$
5	$SU_{4,40}$	80,60	$10^{-2}, 10^{-3}$	18.5	3	$mcs_{3(7)}$	14.67(22.36)	$9.05 \cdot 10^{-2}(2.02 \cdot 10^{-1})$
6	$SU_{4,40}$	60,40	$10^{-3}, 10^{-4}$	18.5	3	$mcs_{3(7)}$	14.67(22.36)	$9.05 \cdot 10^{-2}(2.02 \cdot 10^{-1})$
7	$SU_{4,160}$	80,40	$10^{-2}, 10^{-4}$	18.5	3	$mcs_{3(7)}$	14.67(22.36)	$9.05 \cdot 10^{-2}(2.02 \cdot 10^{-1})$
8	$SU_{4,160}$	80,60	$10^{-2}, 10^{-3}$	18.5	3	$mcs_{3(7)}$	14.67(22.36)	$9.05 \cdot 10^{-2}(2.02 \cdot 10^{-1})$
9	$SU_{4,160}$	60,40	$10^{-3}, 10^{-4}$	18.5	3	$mcs_{3(7)}$	14.67(22.36)	$9.05 \cdot 10^{-2}(2.02 \cdot 10^{-1})$
10	$SU_{16,1}$	80,40	$10^{-2}, 10^{-4}$	18.5	3	$mcs_{3(7)}$	14.67(22.36)	$9.05 \cdot 10^{-2}(2.02 \cdot 10^{-1})$
11	$SU_{16,1}$	80,60	$10^{-2}, 10^{-3}$	18.5	3	$mcs_{3(7)}$	14.67(22.36)	$9.05 \cdot 10^{-2}(2.02 \cdot 10^{-1})$
12	$SU_{16,1}$	60,40	$10^{-3}, 10^{-4}$	18.5	3	$mcs_{3(7)}$	14.67(22.36)	$9.05 \cdot 10^{-2}(2.02 \cdot 10^{-1})$
13	$SU_{16,40}$	80,40	$10^{-2}, 10^{-4}$	18.5	3	$mcs_{3(7)}$	14.67(22.36)	$9.05 \cdot 10^{-2}(2.02 \cdot 10^{-1})$
14	$SU_{16,40}$	80,60	$10^{-2}, 10^{-3}$	18.5	3	$mcs_{3(7)}$	14.67(22.36)	$9.05 \cdot 10^{-2}(2.02 \cdot 10^{-1})$
15	$SU_{16,40}$	60,40	$10^{-3}, 10^{-4}$	18.5	3	$mcs_{3(7)}$	14.67(22.36)	$9.05 \cdot 10^{-2}(2.02 \cdot 10^{-1})$
16	$SU_{16,160}$	80,40	$10^{-2}, 10^{-4}$	18.5	3	$mcs_{3(7)}$	14.67(22.36)	$9.05 \cdot 10^{-2}(2.02 \cdot 10^{-1})$
17	$SU_{16,160}$	80,60	$10^{-2}, 10^{-3}$	18.5	3	$mcs_{3(7)}$	14.67(22.36)	$9.05 \cdot 10^{-2}(2.02 \cdot 10^{-1})$
18	$SU_{16,160}$	60,40	$10^{-3}, 10^{-4}$	18.5	3	$mcs_{3(7)}$	14.67(22.36)	$9.05 \cdot 10^{-2}(2.02 \cdot 10^{-1})$

nario Set E, we again fix $SNR_2 = 18.5$ dB and $(B, \Omega, th_P, Z) = (4C, 3, 0.25, 3)$, but vary both packet loss rate and rate limit by means of (χ_1, χ_2) and (Φ_1, Φ_2) , respectively. As discussed already, PER_i converges to 0 for the selected En-QAWLawH parameters. Therefore, packet losses are supposed to be caused solely by the GRED AQM scheme in proportion of the congestion level. Packet loss rates of AQM, on the other hand, are expected to be in the vicinity of 10^{-2} at most as will be discussed in Section 6.4.

In Tables 6.6-6.9, ns-3 simulation results are tabulated for Scenario Sets A-E, respectively. We not only compare the network-wide throughput results of ns-3 simulations and the proposed analysis denoted by NT_D -ns3 and NT_D -anal., respectively, but also present the percentage throughput error of the center link c , the percentage average absolute flow throughput error and the percentage energy per bit error of center link c which are denoted by Δ_{LT} , Δ_{FT} and Δ_{LE} , respectively, as defined below:

$$\Delta_{LT} = 100 \frac{\sum_n FT_n\text{-ns3} - \sum_n FT_n\text{-anal.}}{\sum_n FT_n\text{-ns3}}, \quad (6.56)$$

Table 6.6: TCP throughput and energy statistics obtained with ns-3 simulations and the fixed-point analytical model for Scenario Set A.

idx	NT_D -ns3 (Mbps)	NT_D -anal. (Mbps)	Δ_{LT} (%)	Δ_{FT} (%)	Δ_{LE} (%)	Solution Domain	α^*	X -anal. (ms)
1	17.8630	17.8885	-0.1	0.1	0.1	\mathcal{B}	$4.18 \cdot 10^{-1}$	2.32
2	15.5912	15.6137	-0.1	0.1	0.1	\mathcal{B}	$6.68 \cdot 10^{-1}$	1.14
3	10.3653	10.5858	-2.1	2.1	-11.5	\mathcal{B}	$4.98 \cdot 10^{-2}$	1.13
4	10.6738	10.8248	-1.4	1.4	-6.7	\mathcal{B}	$1.54 \cdot 10^{-2}$	0.11
5	3.0839	3.1243	-1.3	1.3	0.2	\mathcal{R}_1	N/A	0.42
6	3.1481	3.1618	-0.4	0.4	0.2	\mathcal{R}_1	N/A	0.06
7	13.3910	13.4164	-0.2	0.2	11.4	\mathcal{R}_1	N/A	1.31
8	11.6872	11.7103	-0.2	0.2	0.1	\mathcal{B}	$4.61 \cdot 10^{-1}$	1.00
9	13.3918	13.4164	-0.2	0.2	0.6	\mathcal{R}_1	N/A	1.31
10	11.6879	11.7103	-0.2	0.2	0.2	\mathcal{B}	$3.36 \cdot 10^{-1}$	0.77
11	12.5126	12.7740	-2.1	2.5	-2.2	\mathcal{B}	$3.43 \cdot 10^{-1}$	1.76
12	11.5992	11.7103	-1.0	1.2	1.0	\mathcal{R}_1	N/A	0.14
13	13.3678	13.4164	-0.4	0.4	3.8	\mathcal{B}	$2.78 \cdot 10^{-1}$	1.84
14	11.6639	11.7103	-0.4	0.4	8.7	\mathcal{B}	$1.16 \cdot 10^{-1}$	0.28
15	13.3686	13.4164	-0.4	0.4	31.6	\mathcal{R}_1	N/A	1.31
16	11.6646	11.7103	-0.4	0.4	0.4	\mathcal{B}	$4.61 \cdot 10^{-1}$	1.00
17	13.3714	13.4164	-0.3	0.3	0.3	\mathcal{B}	$4.84 \cdot 10^{-1}$	2.25
18	11.6670	11.7103	-0.4	0.4	9.6	\mathcal{R}_1	N/A	0.14

$$\Delta_{FT} = \frac{100}{N} \sum_n \frac{|FT_n\text{-ns3} - FT_n\text{-anal.}|}{FT_n\text{-ns3}}, \quad (6.57)$$

$$\Delta_{LE} = 100 \frac{LP_c\text{-ns3}/LT_c\text{-ns3} - LP_c\text{-anal.}/LT_c\text{-anal.}}{LP_c\text{-ns3}/LT_c\text{-ns3}}. \quad (6.58)$$

$LP_c\text{-ns3}$ in (6.58) is calculated by weighting the power consumptions $1/\zeta$ and 1 associated with \mathcal{R}_1 and \mathcal{R}_2 , respectively, by the percentage of time link c spends in each regime leaving out the periods the queue remains idle in \mathcal{R}_1 . For the sake of completeness, we present α^* for scenarios whose solution domains are \mathcal{B} and the analytically calculated resequencing delay $X\text{-anal.}$ for all scenarios. Distribution of $X\text{-anal.}$ values in Tables 6.6-6.9 verifies with the preferred range of parameters in validating the approximate DRWL resequencing delay model.

Except for the test scenario with $idx = 15$ of Table 6.6 having relatively small B and test scenarios with $idx \in \{4, 5, 16, 17\}$ of Table 6.10 with relatively high loss probabilities (i.e., $\chi_1 = 10^{-2}$), results of ns-3 simulations and analytical model are in remarkable agreement from both energy and throughput point of view. In Section 6.4, we show that the maximum packet loss rate $\chi_1 = 10^{-2}$ chosen for the simulations of Scenario Set E is rarely experienced in the studied scenarios therein. The overall simulation results validate the analytical model, which lead us to evaluating the performance of the EnQAWLAWH scheme in the

Table 6.7: TCP throughput and energy statistics obtained with ns-3 simulations and the fixed-point analytical model for Scenario Set B.

idx	NT_D -ns3 (Mbps)	NT_D -anal. (Mbps)	Δ_{LT} (%)	Δ_{FT} (%)	Δ_{LE} (%)	Solution Domain	α^*	X-anal. (ms)
1	17.8630	17.8885	-0.1	0.1	0.1	\mathcal{B}	$4.18 \cdot 10^{-1}$	2.32
2	15.5911	15.6137	-0.1	0.1	0.1	\mathcal{B}	$6.68 \cdot 10^{-1}$	1.14
3	9.9549	10.0979	-1.4	1.4	-10.4	\mathcal{B}	$1.04 \cdot 10^{-2}$	0.98
4	10.6738	10.6891	-0.1	0.1	0.1	\mathcal{R}_1	N/A	0.08
5	3.0837	3.1243	-1.3	1.3	0.2	\mathcal{R}_1	N/A	0.42
6	3.1481	3.1618	-0.4	0.4	0.2	\mathcal{R}_1	N/A	0.06
7	13.3910	13.4164	-0.2	0.2	0.2	\mathcal{R}_1	N/A	1.31
8	11.6872	11.7103	-0.2	0.2	0.1	\mathcal{B}	$4.61 \cdot 10^{-1}$	1.00
9	13.3918	13.4164	-0.2	0.2	0.2	\mathcal{R}_1	N/A	1.31
10	11.6880	11.7103	-0.2	0.2	0.1	\mathcal{B}	$3.36 \cdot 10^{-1}$	0.77
11	12.4293	12.7360	-2.5	2.9	-2.7	\mathcal{B}	$3.41 \cdot 10^{-1}$	1.75
12	11.5986	11.7103	-1.0	1.2	0.1	\mathcal{R}_1	N/A	0.14
13	13.3678	13.4164	-0.4	0.4	0.8	\mathcal{B}	$2.78 \cdot 10^{-1}$	1.84
14	11.6638	11.7103	-0.4	0.4	3.7	\mathcal{B}	$1.16 \cdot 10^{-1}$	0.28
15	13.3687	13.4164	-0.4	0.4	6.1	\mathcal{R}_1	N/A	1.31
16	11.6648	11.7103	-0.4	0.4	0.3	\mathcal{B}	$4.61 \cdot 10^{-1}$	1.00
17	13.3713	13.4164	-0.3	0.3	0.3	\mathcal{B}	$4.84 \cdot 10^{-1}$	2.25
18	11.6670	11.7103	-0.4	0.4	0.7	\mathcal{R}_1	N/A	0.14

Table 6.8: TCP throughput and energy statistics obtained with ns-3 simulations and the fixed-point analytical model for Scenario Set C.

idx	NT_D -ns3 (Mbps)	NT_D -anal. (Mbps)	Δ_{LT} (%)	Δ_{FT} (%)	Δ_{LE} (%)	Solution Domain	α^*	X-anal. (ms)
1	17.8630	17.8885	-0.1	0.1	0.1	\mathcal{B}	$4.18 \cdot 10^{-1}$	2.32
2	15.5912	15.6137	-0.1	0.1	0.1	\mathcal{B}	$6.68 \cdot 10^{-1}$	1.14
3	9.9549	9.9693	-0.1	0.1	0.1	\mathcal{R}_1	N/A	0.94
4	10.6738	10.6891	-0.1	0.1	0.1	\mathcal{R}_1	N/A	0.08
5	3.0837	3.1243	-1.3	1.3	0.2	\mathcal{R}_1	N/A	0.42
6	3.1481	3.1618	-0.4	0.4	0.2	\mathcal{R}_1	N/A	0.06
7	13.3910	13.4164	-0.2	0.2	0.2	\mathcal{R}_1	N/A	1.31
8	11.6871	11.7103	-0.2	0.2	0.2	\mathcal{B}	$4.61 \cdot 10^{-1}$	1.00
9	13.3918	13.4164	-0.2	0.2	0.2	\mathcal{R}_1	N/A	1.31
10	11.6879	11.7103	-0.2	0.2	0.2	\mathcal{B}	$3.36 \cdot 10^{-1}$	0.77
11	12.2683	12.5927	-2.6	3.0	-3.0	\mathcal{B}	$3.31 \cdot 10^{-1}$	1.72
12	11.5986	11.7103	-1.0	1.2	0.1	\mathcal{R}_1	N/A	0.14
13	13.3678	13.4164	-0.4	0.4	0.3	\mathcal{B}	$2.78 \cdot 10^{-1}$	1.84
14	11.6639	11.7103	-0.4	0.4	0.4	\mathcal{B}	$1.16 \cdot 10^{-1}$	0.28
15	13.3687	13.4164	-0.4	0.4	0.4	\mathcal{R}_1	N/A	1.31
16	11.6646	11.7103	-0.4	0.4	0.3	\mathcal{B}	$4.61 \cdot 10^{-1}$	1.00
17	13.3714	13.4164	-0.3	0.3	0.3	\mathcal{B}	$4.84 \cdot 10^{-1}$	2.25
18	11.6670	11.7103	-0.4	0.4	0.3	\mathcal{R}_1	N/A	0.14

Table 6.9: TCP throughput and energy statistics obtained with ns-3 simulations and the fixed-point analytical model for Scenario Set D.

idx	NT_D -ns3 (Mbps)	NT_D -anal. (Mbps)	Δ_{LT} (%)	Δ_{FT} (%)	Δ_{LE} (%)	Solution Domain	α^*	X -anal. (ms)
1	13.3967	13.4164	-0.1	0.1	0.2	\mathcal{R}_1	N/A	1.31
2	8.9305	8.9443	-0.2	0.2	0.2	\mathcal{R}_1	N/A	0.99
3	10.8019	11.1627	-3.3	3.3	0.1	\mathcal{R}_1	N/A	1.15
4	8.9312	8.9443	-0.1	0.1	0.1	\mathcal{R}_1	N/A	0.99
5	3.1328	3.1514	-0.6	0.6	0.2	\mathcal{R}_1	N/A	0.55
6	3.1169	3.1514	-1.1	1.1	0.2	\mathcal{R}_1	N/A	0.55
7	15.6241	15.6525	-0.2	0.2	0.2	\mathcal{B}	$1.28 \cdot 10^{-1}$	1.72
8	11.1578	11.1803	-0.2	0.2	0.2	\mathcal{R}_1	N/A	1.16
9	15.6252	15.6525	-0.2	0.2	0.2	\mathcal{B}	$1.28 \cdot 10^{-1}$	1.72
10	11.1586	11.1803	-0.2	0.2	0.2	\mathcal{R}_1	N/A	1.16
11	12.6811	12.9789	-2.3	2.5	0.2	\mathcal{R}_1	N/A	1.28
12	10.7681	10.9381	-1.6	1.9	0.2	\mathcal{R}_1	N/A	1.14
13	15.6009	15.6525	-0.3	0.3	4.1	\mathcal{B}	$1.28 \cdot 10^{-1}$	1.72
14	11.1347	11.1803	-0.4	0.4	6.8	\mathcal{R}_1	N/A	1.16
15	15.6020	15.6525	-0.3	0.3	2.9	\mathcal{B}	$1.28 \cdot 10^{-1}$	1.72
16	11.1355	11.1803	-0.4	0.4	1.8	\mathcal{R}_1	N/A	1.16
17	15.6053	15.6525	-0.3	0.3	2.0	\mathcal{B}	$1.28 \cdot 10^{-1}$	1.72
18	11.1378	11.1803	-0.4	0.4	1.8	\mathcal{R}_1	N/A	1.16

Table 6.10: TCP throughput and energy statistics obtained with ns-3 simulations and the fixed-point analytical model for Scenario Set E. Results for ns-3 simulations are presented with the 99% confidence intervals.

idx	NT_D -ns3 (Mbps)	NT_D -anal. (Mbps)	Δ_{LT} (%)	Δ_{FT} (%)	Δ_{LE} (%)	Solution Domain	α^*	X -anal. (ms)
1	21.9645 ± 0.1152	22.3395	-1.7	10.8	-1.4	\mathcal{R}_2	N/A	3.15
2	21.9100 ± 0.0854	22.3260	-1.9	10.2	-2.1	\mathcal{R}_2	N/A	3.15
3	22.2560 ± 0.0265	22.3528	-0.4	2.2	-0.2	\mathcal{R}_2	N/A	3.15
4	14.8663 ± 0.1386	14.6585	1.4	3.3	26.4	\mathcal{R}_1	N/A	1.39
5	13.5889 ± 0.2702	13.5707	0.1	2.9	26.3	\mathcal{R}_1	N/A	1.32
6	17.5652 ± 0.2522	17.5846	-0.1	0.5	5.8	\mathcal{B}	$3.80 \cdot 10^{-1}$	2.25
7	9.0274 ± 0.0919	9.0582	-0.3	1.8	3.1	\mathcal{R}_1	N/A	1.00
8	9.4861 ± 0.1178	9.5098	-0.2	2.1	4.8	\mathcal{R}_1	N/A	1.03
9	9.0551 ± 0.1039	9.1032	-0.5	0.9	8.6	\mathcal{R}_1	N/A	1.01
10	22.3253 ± 0.0011	22.2956	0.1	4.9	-0.1	\mathcal{R}_2	N/A	3.15
11	22.3241 ± 0.0019	22.2909	0.1	5.5	-0.2	\mathcal{R}_2	N/A	3.15
12	22.3263 ± 0.0004	22.3513	-0.1	6.4	0.1	\mathcal{R}_2	N/A	3.15
13	21.5430 ± 0.0661	22.3049	-3.5	5.6	-4.6	\mathcal{R}_2	N/A	3.15
14	21.3625 ± 0.0683	22.2947	-4.4	4.1	-5.9	\mathcal{R}_2	N/A	3.15
15	22.1472 ± 0.0184	22.3512	-0.9	1.8	-0.8	\mathcal{R}_2	N/A	3.15
16	12.4034 ± 0.1270	12.5756	-1.4	1.8	32.3	\mathcal{R}_1	N/A	1.25
17	13.5195 ± 0.1270	13.6920	-1.3	1.8	36.4	\mathcal{R}_1	N/A	1.33
18	17.8801 ± 0.2830	18.9518	-6.0	4.5	-1.7	\mathcal{B}	$5.58 \cdot 10^{-1}$	2.56

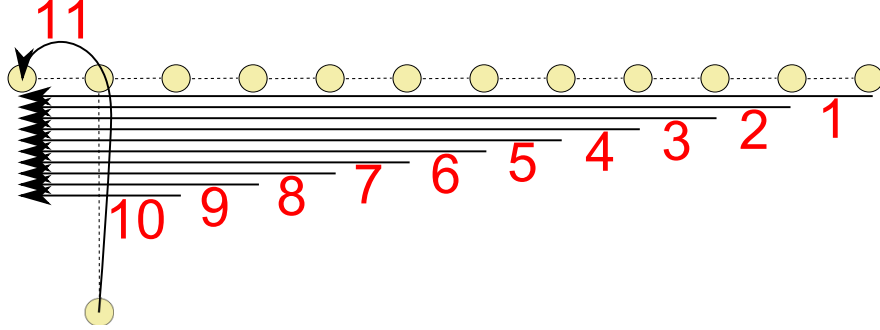


Figure 6.4: Topology A chosen for the performance evaluation of DRWN.

next section.

6.4 Performance Evaluation of EnQAWLAwH

We study two different network topologies Topology A and B depicted in Figs. 6.4 and 6.5, respectively. Topology A is an artificial one having a line-like structure whereas Topology B which is the testbed proposed in [162] to evaluate the TCP performance over an IEEE 802.11n mesh backbone has a grid-like structure. We note that the results obtained hereby for Topology B has no relevance with those of [162] since not only the underlying PHY technologies are different but also some of the fundamental assumptions made by this study such as interference-free wireless links are not valid for the reference [162]. Nodes of both topologies illustrated by yellow disks are interconnected by bidirectional DRWLs.

We identify the number of the flows, destination and source nodes of these flows, SNR level SNR_2 of each DRWL, Ω and B parameters as the dimensions to explore in evaluating the performance of the proposed EnQAWLAwH scheme. Since finding a globally optimum value for the (B, Ω) pair under this high dimensional parameter space is computationally cumbersome, we first fix all other dimensions except for Ω and B and seek a preferable operating point. For that purpose, we distribute flows of Topology A as shown in Fig. 6.4 and choose one of the scenarios realized by [162] for Topology B as shown in Fig. 6.5. The flows are

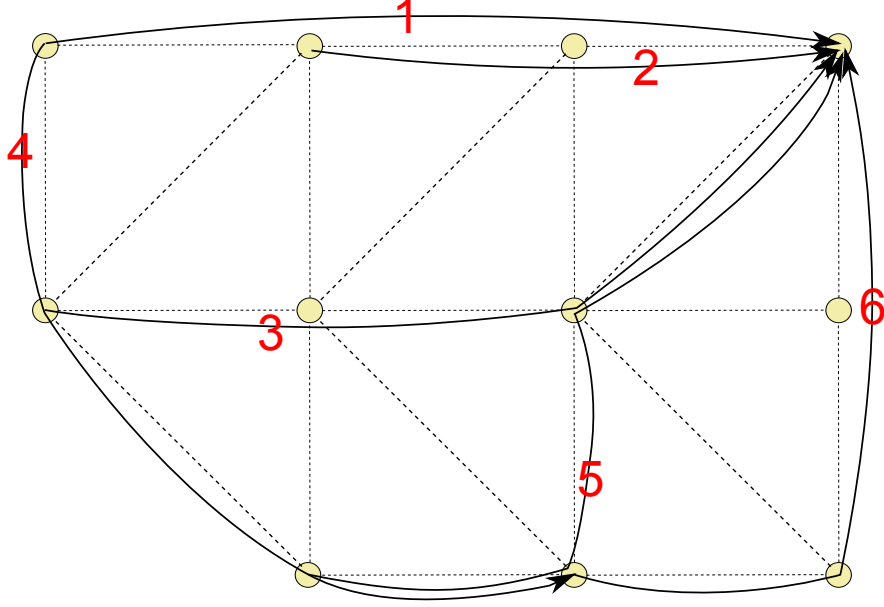


Figure 6.5: Topology B chosen for the performance evaluation of DRWN.

depicted with arrow headed lines, arrows pointing the destination node. For each value of $SNR_2 \in \{11.5, 16.0, 18.5\}$ dB, we let $\Omega \in [1, M - 1]$ where $M = 8$ and $B = 2aC$ where $a \in [1, 10]$ is an integer. In Fig. 6.6, the average value of $\Theta(0.75)$ taken over both topologies and all SNR_2 values for various values of (Ω, B) are shown. Although the average Θ peaks at $(B, \Omega) = (2C, 3)$ with a value of 7.508, we rather prefer the pair $(B, \Omega) = (4C, 3)$ for which the average Θ equals 7.479, since the gap in between is insignificant and keeping the boundary further away from empty queue is beneficial for the stability of the proposed scheme. As Ω increases, increasing values of B penalize the flows more heavily by trapping higher number of queues in \mathcal{R}_1 which in turn makes them starve for capacity. The power reduction in this case does not compensate for the loss in throughput.

Next, by keeping the same flow setting we fix $(B, \Omega) = (4C, 3)$ and let $SNR_2 \sim U(12.5, 18.5)$ with the interval of interest being sampled with 0.5 dB resolution where U represents the uniform discrete distribution. Random trials are repeated 210 times which is 5 times the total number of links of Topology B (maximum of both). In Fig. 6.7, the resultant Θ achieved by $\text{EnQAWLAWH}(B, \Omega, th_P, Z)$ scheme for various values of β is presented for both

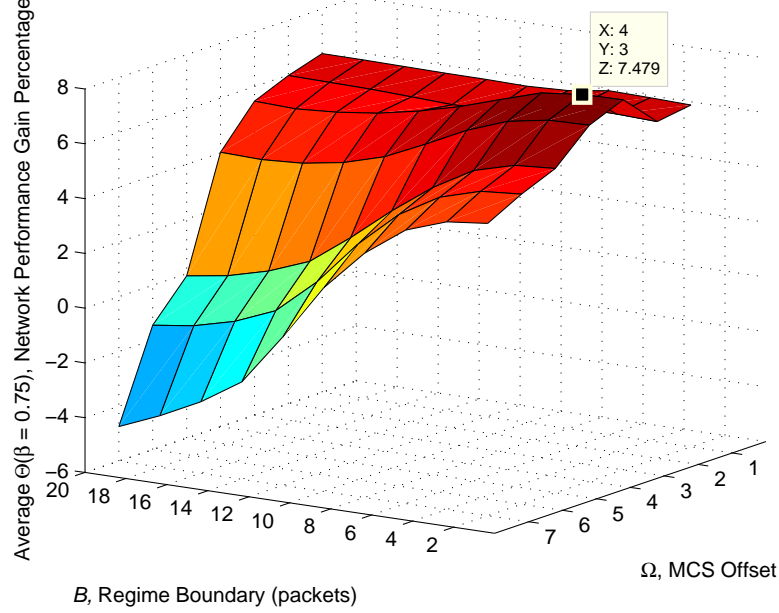


Figure 6.6: $\Theta(0.75)$ averaged over two topologies and three SNR_2 values for the $\text{EnQAWLAWH}(B, \Omega, th_P, Z) = (.,., 0.25, 3)$ scheme.

topologies. For Topology B, $NTLP$ (see $\Theta(1)$) reveals at most 7.6% degradation in throughput whereas $NPRP$ (see $\Theta(0)$) ranges from 9.5% to 37.4%. As with this example, the EnQAWLAWH scheme has a potential impact on TCP throughput by means of increasing RTT of flows getting service from links settled in \mathcal{R}_1 . We elaborate on this issue in the upcoming evaluation scenarios. Network performance results turn out to be even better for Topology A with an $NPRP$ of 22.6% to 51.6% without any throughput loss (i.e., increase in $NTLP$). As expected, intermediate values for Θ are obtained for intermediate values of β . In Fig. 6.8, $EpBRP$ for both topologies are presented. In accordance with the results of Fig. 6.7, Topology A benefits more from the EnQAWLAWH scheme. Note that there exists a slight degradation in throughput of Topology B, yet it is concealed by the $EpBRP$ metric. For that reason, we proceed with Θ and its components from that point onwards.

We now set $SNR_2 \in \{11.5, 16.0, 18.5\}$ dB of all links and randomly scatter $N \in \{4, 16, 64\}$ flows with uniformly distributed source-destination node pairs

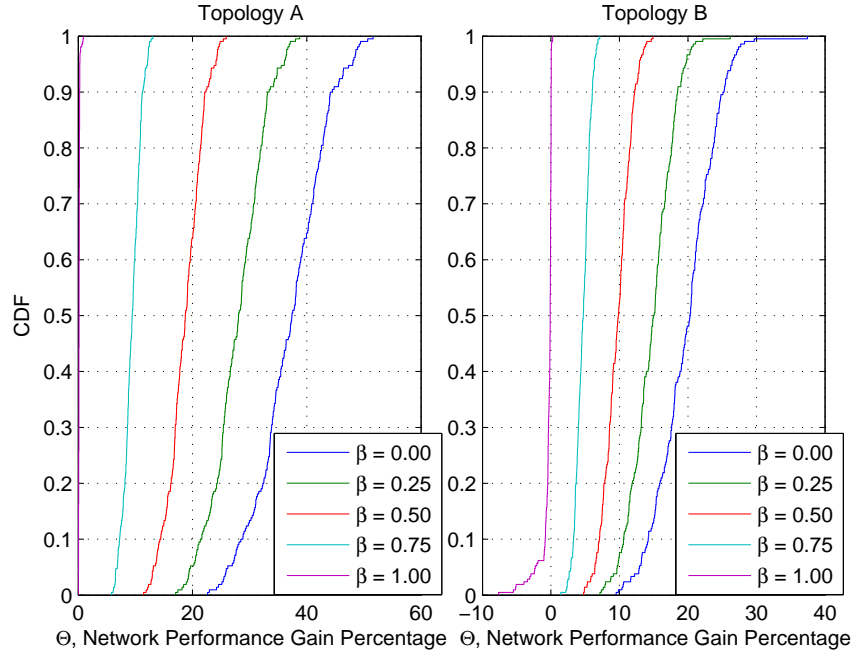


Figure 6.7: CDF of Θ of Topology A and B with links having randomized SNR_2 for various values of β for the $\text{EnQAWLA}_{\text{WH}}(B, \Omega, th_P, Z) = (4C, 3, 0.25, 3)$ scheme.

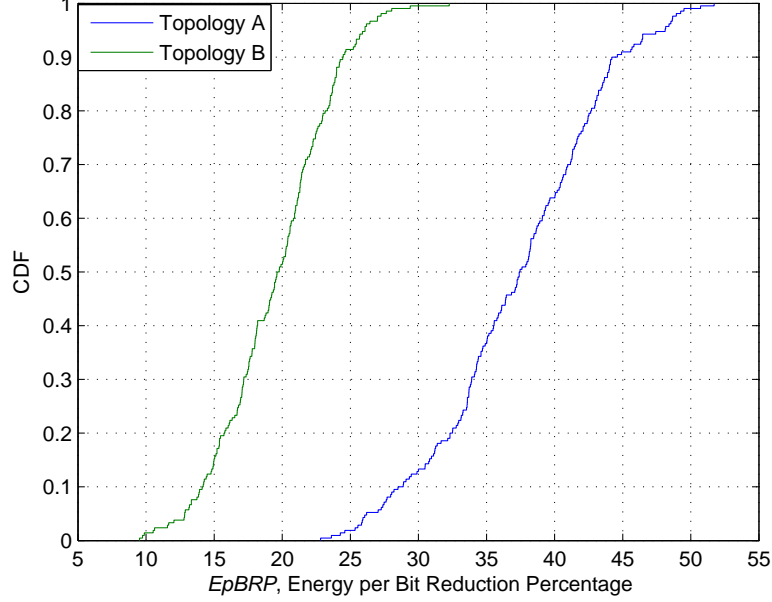


Figure 6.8: CDF of $EpBRP$ of Topology A and B with links having randomized SNR_2 for the $EnQAWLAwH(B, \Omega, th_P, Z) = (4C, 3, 0.25, 3)$ scheme.

across both topologies. For each value of N , 130 different flow configurations are realized which is 10 times the number of nodes of Topology A (maximum of both). Given a source destination pair for a flow, the route in between is determined by Dijkstra's algorithm with minimum hop routing. For this scenario, we first plot the CDF of the overall RTT of flow n denoted by $FRTT_n$ in Figs 6.9 and 6.10 for Topology A and B, respectively. $FRTT_n$ is expressed as follows:

$$FRTT_n = \sum_{j \in \mathcal{L}_n} RTT_j(x, \alpha). \quad (6.59)$$

Mean values of $FRTT_n$ annotated on these figures are consistently higher for DRWN than SRWN which is an expected consequence of using a lower bit rate MCS for \mathcal{R}_1 increasing the queuing and transmission delays for the flows serviced therein. Topology A has a higher diameter in number of hops than Topology B leading to relatively more elevated values of $FRTT_n$. Increasing N increases the congestion level for both topologies and thus $FRTT_n$. Finally, we observe cases for which the mean $FRTT_n$ of $SNR_2 = 18.5$ dB exceeds that of $SNR_2 = 16.0$ dB which may seem counter-intuitive. Because of finite SNR sampling resolution

(0.5 dB in this case) used in the PHY simulations, there exist a variability in how much $P_{m,s,0}$ of each MCS msc_m can approach a certain threshold. As evident from the validation test case with $idx = 1$ and $idx = 5$ in Table 6.2, X_2 value for $SNR_2 = 18.5$ dB turns out to be higher than that of $SNR_2 = 16.0$ dB. Projecting this difference in the resequencing delay of a single DRWL to a DRWN where multiple such links are in tandem, explains higher $FRTT_n$ values obtained for $SNR_2 = 18.5$ dB.

Overall packet loss rate the flow n suffers from denoted by $FPLR_n$ can be formulated as follows:

$$FPLR_n = 1 - \prod_{j \in \mathcal{L}_n} (1 - p_j(x, \alpha)). \quad (6.60)$$

In Figs. 6.11 and 6.12 CDFs of $FPLR_n$ are given for Topology A and B, respectively, again for $N \in \{4, 16, 64\}$, $SNR_2 \in \{11.5, 16.0, 18.5\}$ dB and for both DRWN and SRWN configurations along with the annotations for the corresponding mean values. Unlike the results for RTT_n , $FPLR_n$ of DRWN does not significantly differ from that of SRWN in statistical sense, since the packet losses stem only from GRED AQM policy which starts dropping packets only after its queue occupancy level exceeds $th_{\min} = 30C$ which is very well above $B = 4C$. Irrespective of the topology of interest, decreasing SNR_2 which in turn decreases MCS_2 and increasing N increases $FPLR_n$ values due to elevated rates of GRED AQM packet losses. Mean values of $FPLR_n$ are all below $5 \cdot 10^{-3}$ and reaches approximately 10^{-2} at maximum endorsing the upper bound χ_1 of P_{R_n} chosen for ns-3 simulations in Section 6.3.

Finally we present CDF of Θ in Figs. 6.13 and 6.14 for Topology A and B, respectively, for $N \in \{4, 16, 64\}$ and $SNR_2 \in \{11.5, 18.5\}$ dB. Mean values of Θ are annotated next to the corresponding values of β in these figures. Results reveal a general trend in Θ for increasing N . Both $NTLP$ and $NPRP$ turn out to be relatively marginal for heavily-loaded networks (e.g. $N = 64$) than for lightly loaded ones (e.g. $N = 4$), except for $SNR_2 = 11.5$ dB and Topology B. The tradeoff between throughput and power peaks when network is moderately loaded (e.g. $N = 16$) for $\beta = 0.75$ for both SNR_2 values and network topologies. Overall, mean value of Θ varies within the intervals $[4.3 \ 43.8]$, $[3.0 \ 32.4]$, $[1.8$

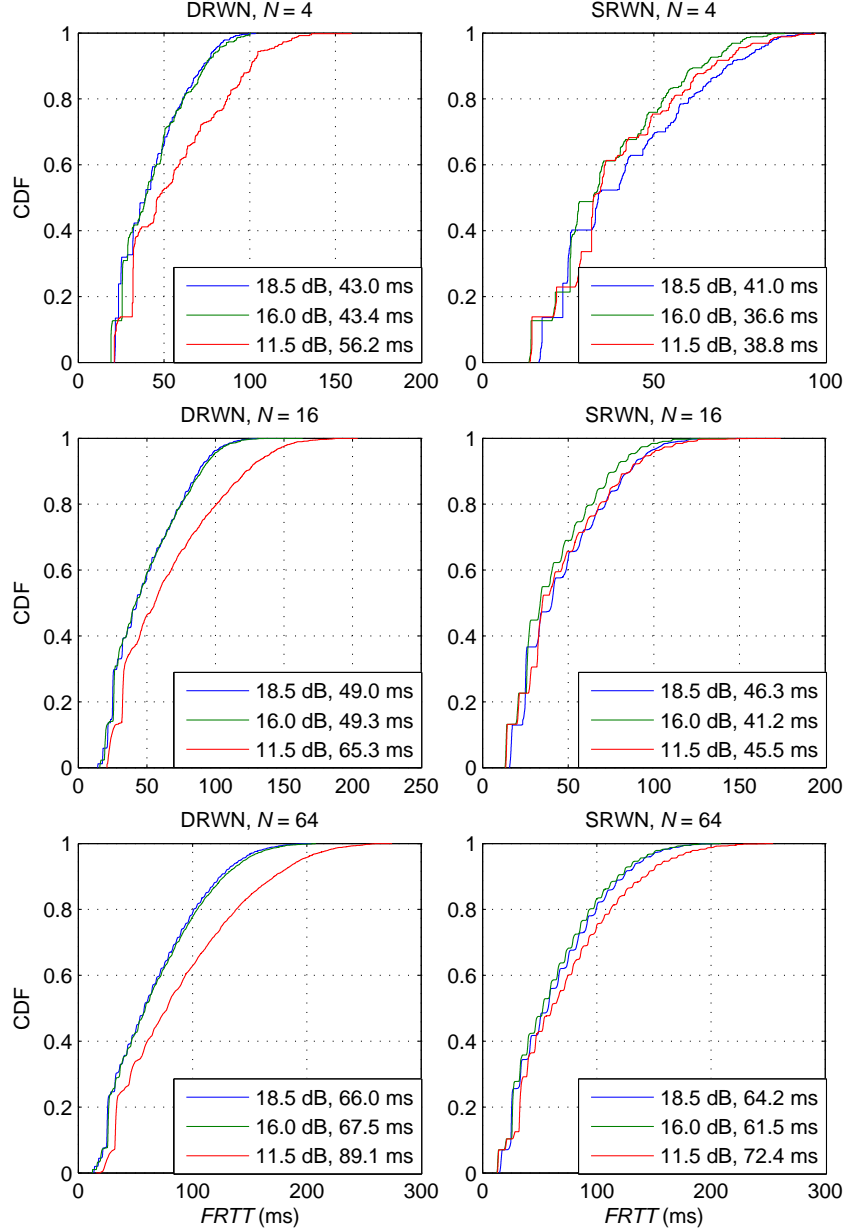


Figure 6.9: CDF of $FRTT_n$ of Topology A with randomized flow routes for various values of N and SNR_2 for the $\text{EnQAWLAwH}(B, \Omega, th_P, Z) = (4C, 3, 0.25, 3)$ scheme. Mean value of $FRTT_n$ for each CDF is annotated inside the corresponding legend box.

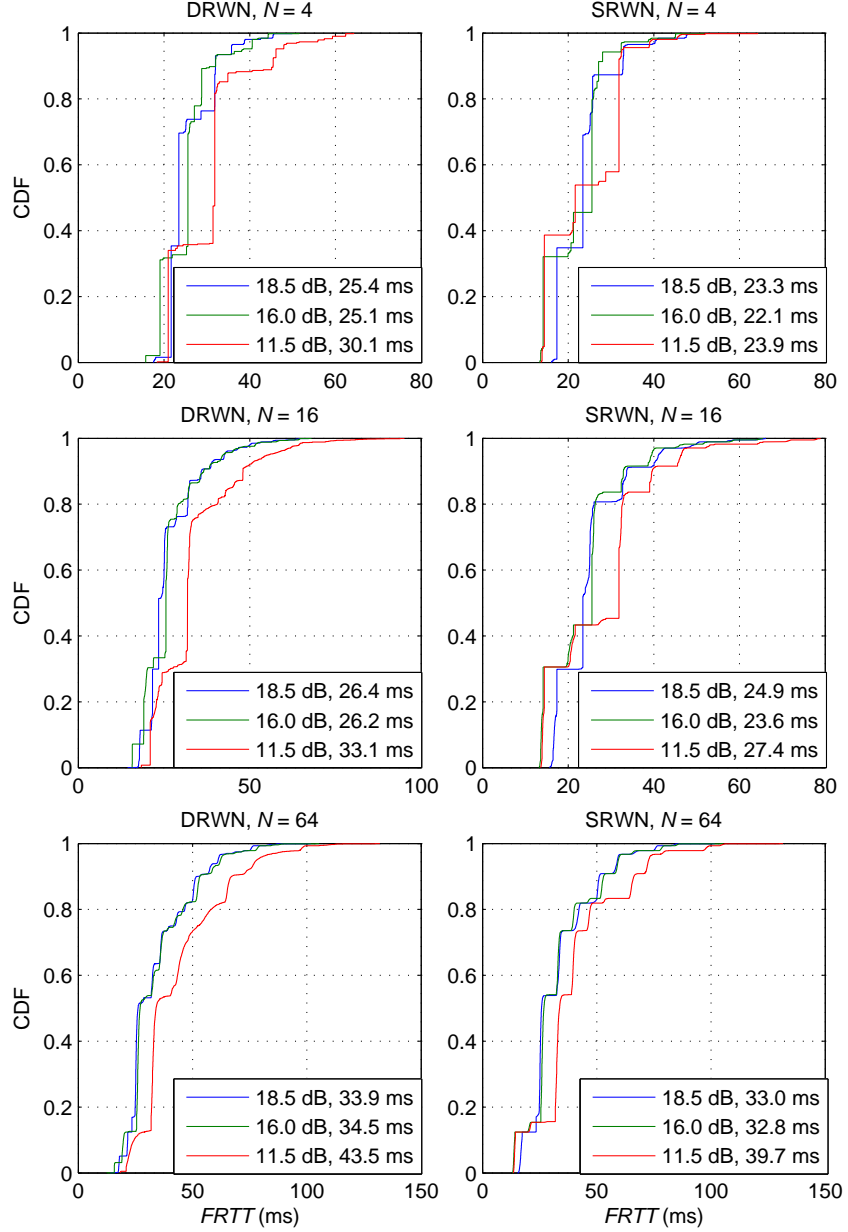


Figure 6.10: CDF of $FRTT_n$ of Topology B with randomized flow routes for various values of N and SNR_2 for the $\text{EnQAWLAwH}(B, \Omega, th_P, Z) = (4C, 3, 0.25, 3)$ scheme. Mean value of $FRTT_n$ for each CDF is annotated inside the corresponding legend box.

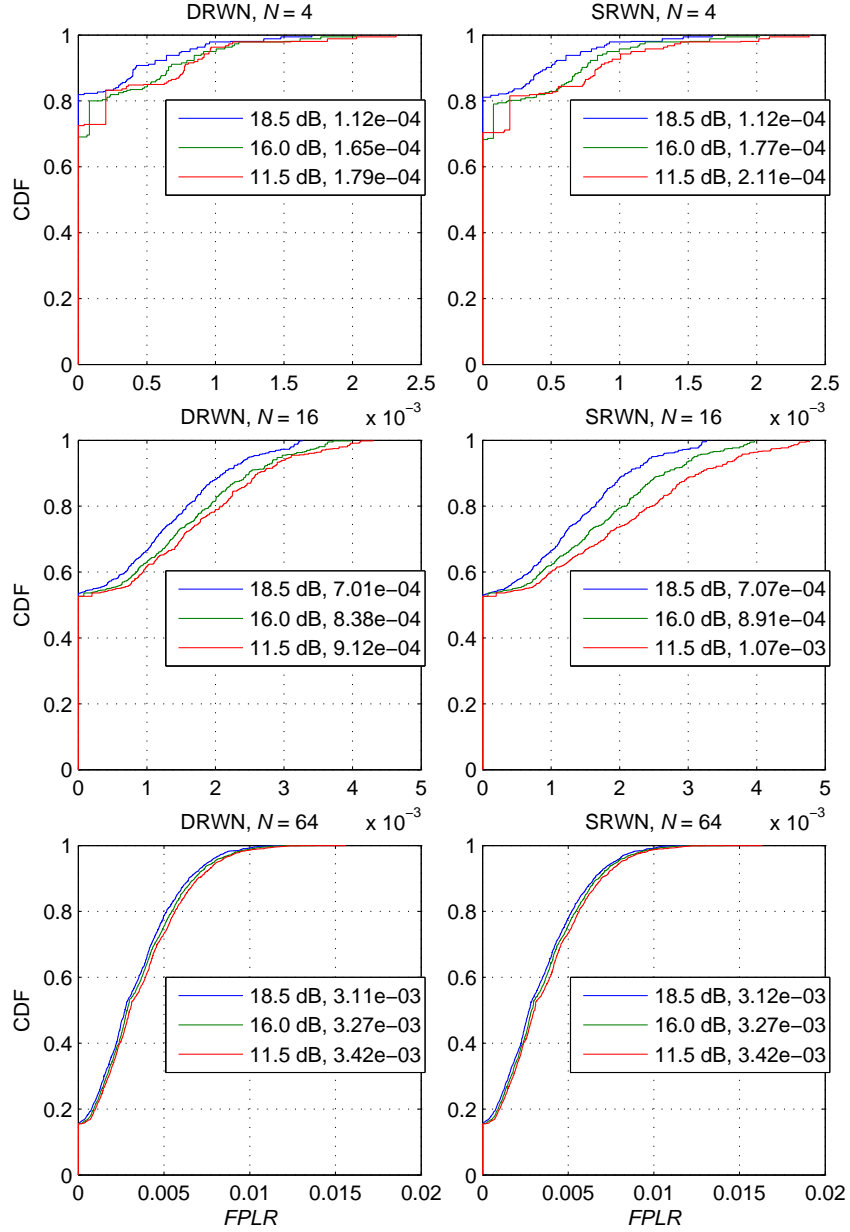


Figure 6.11: CDF of $FPLR_n$ of Topology A with randomized flow routes for various values of N and SNR_2 for the $\text{EnQAWLAwH}(B, \Omega, th_P, Z) = (4C, 3, 0.25, 3)$ scheme. Mean value of $FPLR_n$ for each CDF is annotated inside the corresponding legend box.

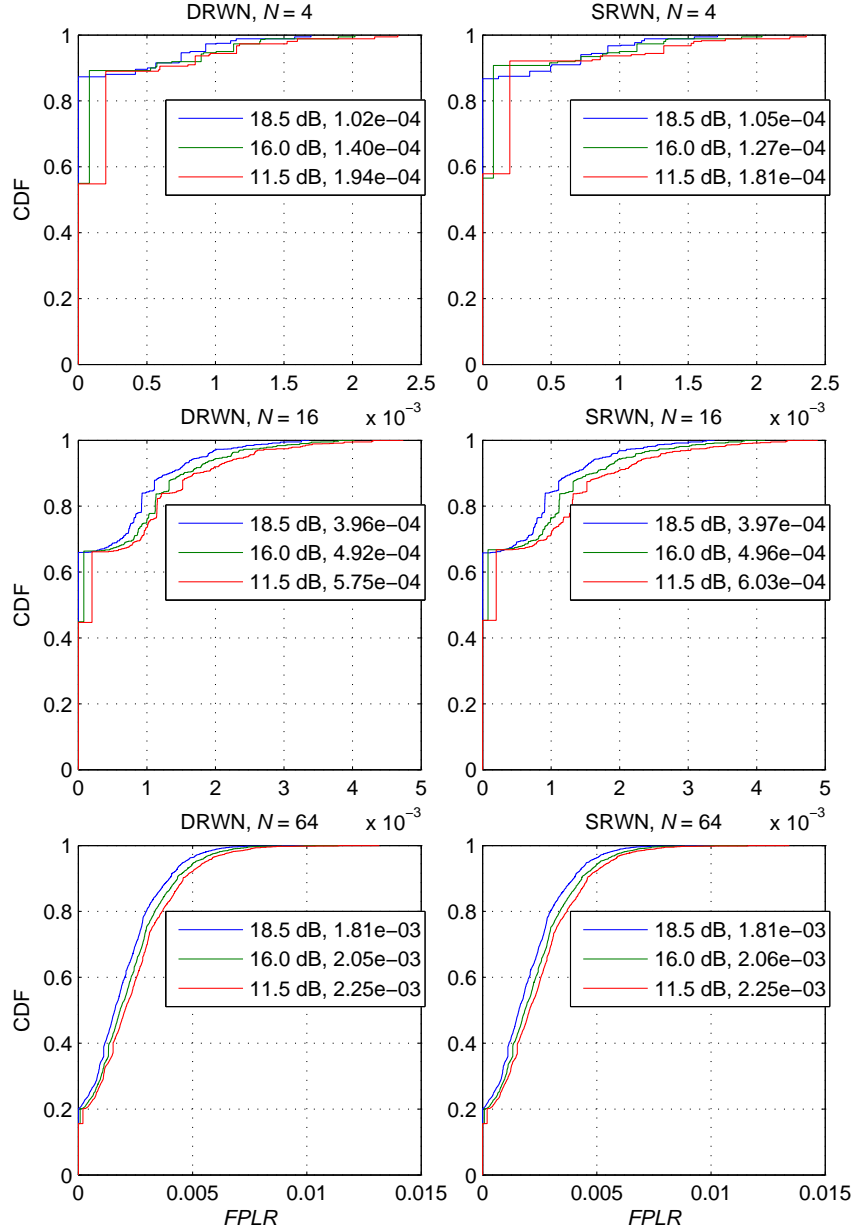


Figure 6.12: CDF of $FPLR_n$ of Topology B with randomized flow routes for various values of N and SNR_2 for the $\text{EnQAWLAwH}(B, \Omega, th_P, Z) = (4C, 3, 0.25, 3)$ scheme. Mean value of $FPLR_n$ for each CDF is annotated inside the corresponding legend box.

21.1], [0.5 9.9], [-7.7 0.1] for β equals $\{1, 0.75, 0.5, 0.25, 0\}$, respectively. Therefore, performance of the EnQAWLAwH scheme depends on the importance attributed to throughput loss and power reduction percentages by means of β .

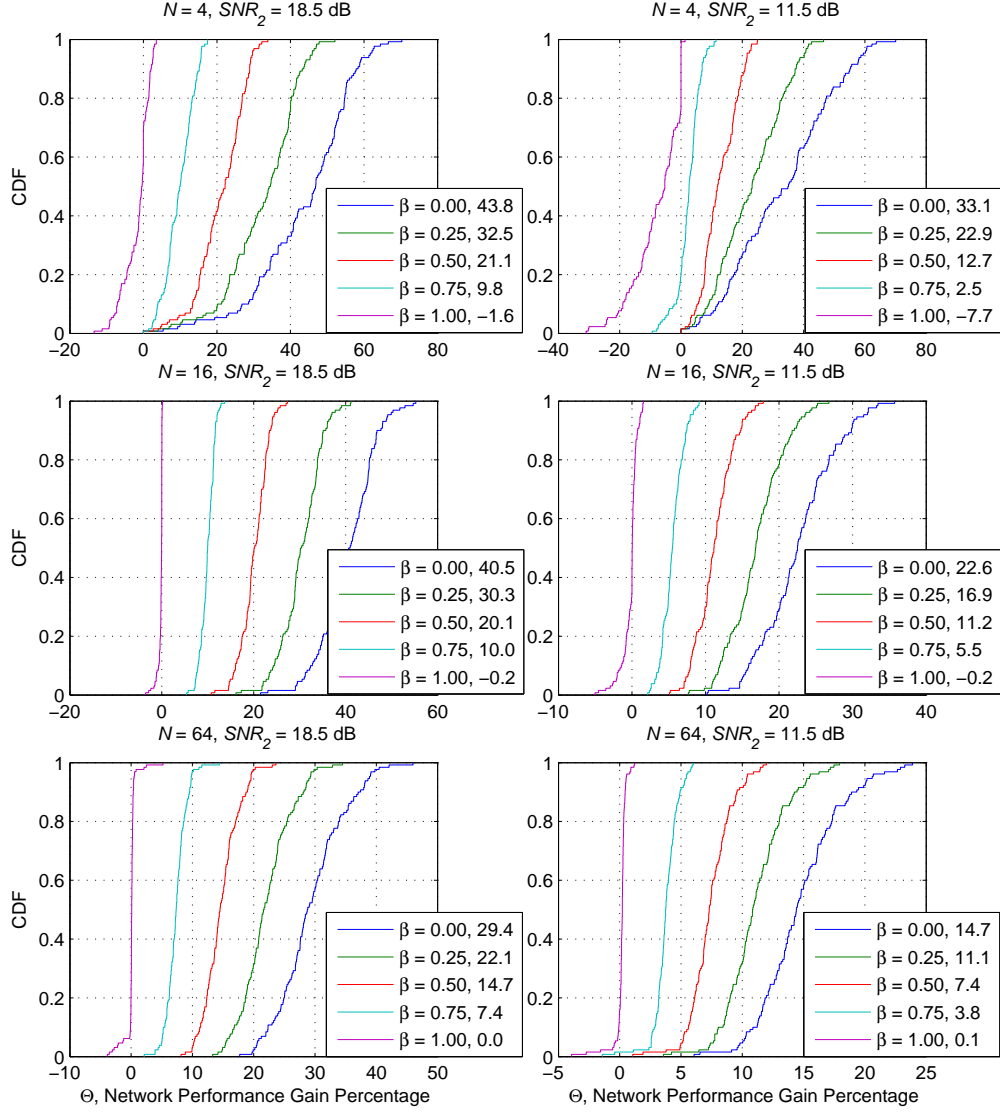


Figure 6.13: CDF of Θ of Topology A with randomized flow routes for various values of N , β and SNR_2 for the $\text{EnQAWLAwH}(B, \Omega, th_P, Z) = (4C, 3, 0.25, 3)$ scheme. Mean value of Θ for each CDF is annotated inside the corresponding legend box.

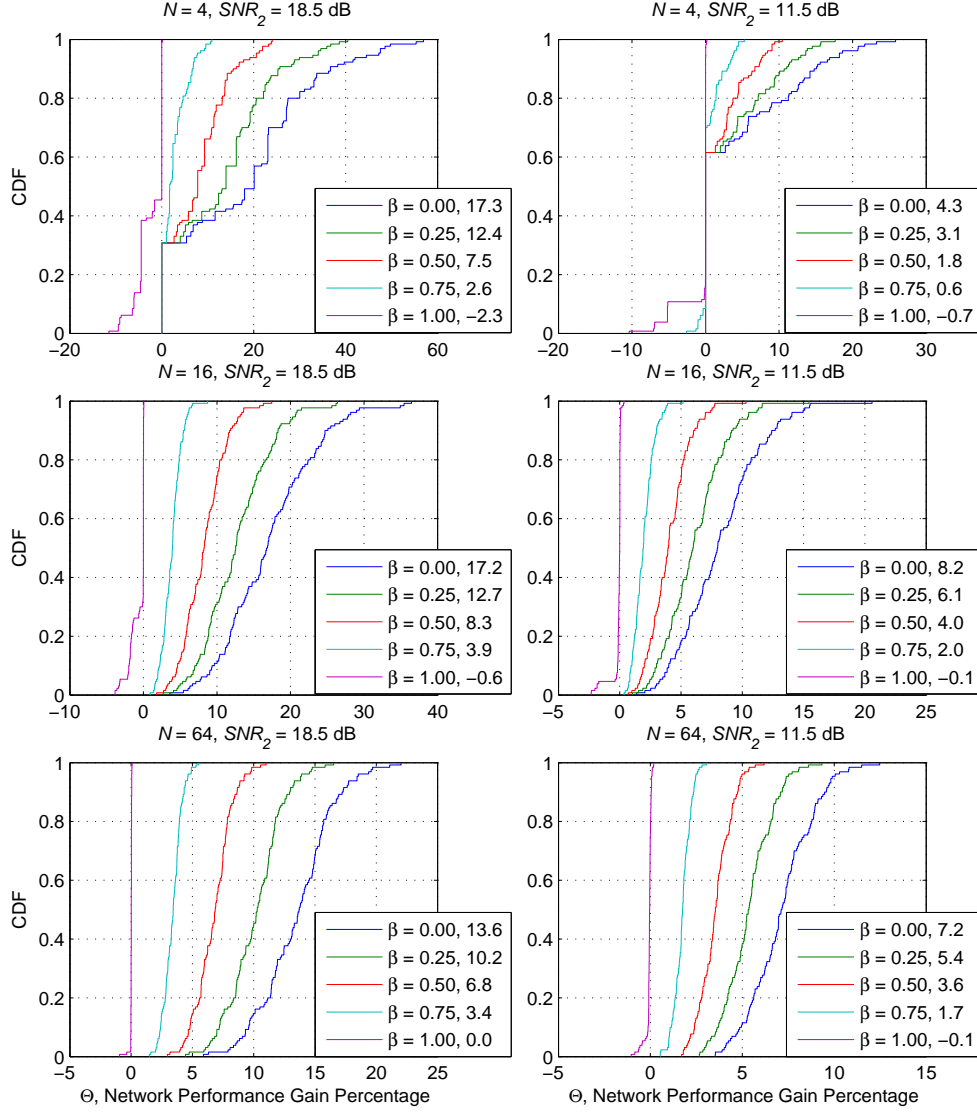


Figure 6.14: CDF of Θ of Topology B with randomized flow routes for various values of N , β and SNR_2 for the $\text{EnQAWLAwH}(B, \Omega, th_P, Z) = (4C, 3, 0.25, 3)$ scheme. Mean value of Θ for each CDF is annotated inside the corresponding legend box.

Chapter 7

Conclusion

In Chapter 3, we develop a novel workload-dependent queuing model for Active Queue Management (AQM)-controlled wireless links carrying persistent TCP flows. One of the contributions of this model is in its ability to capture the entire queue occupancy distribution as opposed to simpler performance measures of interest such as the mean queue length. The proposed queuing model is validated using ns-3 simulations in both wireline and wireless scenarios. This analytical method is then used to obtain guidelines for setting the target wireless Packet Error Rate (PER) for a PER-based link adaptation scheme, called Traffic-AGnostic Link Adaptation (TAGLA), running on a wireless bottleneck link. Assuming the wireless channel SNR to be uniformly distributed over the presented ranges of interest and packet losses to be concentrated on the wireless link (i.e., wireline losses are negligible), we show that targeting a PER around 5×10^{-3} irrespective of the underlying traffic parameters provides robust and acceptable average TCP performance for a wide range of scenarios.

In Chapter 4, we enhance the analytical method presented in Chapter 3 in order to evaluate the TCP-level throughput performance of a wireless bottleneck link deploying AMC with HARQ, called Traffic-AGnostic Link Adaptation with HARQ (TAGLAwH). To this end, we develop an approximate model for the delay caused by packet resequencing at the wireless receiver, which is validated using

MATLAB[®] simulations. It is shown that when link adaptation scheme has the opportunity to recover from wireless packet losses with the HARQ transmission technique, the overall RTTs of the contending TCP flows as well as the induced delay by the retransmissions do not have a significant effect on the resulting throughput. Based on the similar assumptions made in Chapter 3 for TAGLA scheme, we propose to maintain the probability of failure in the first transmission attempt at a value of 0.25 when the average and worst case throughput performances are considered.

In Chapter 5, a novel Queue-AWare Link Adaptation (QAWLA) mechanism is proposed for AQM-controlled wireless bottleneck links carrying persistent TCP flows. QAWLA is based on the choice of a different Modulation and Coding Scheme (MCS) depending on whether the queue occupancy is above or below a certain queue threshold at the epoch of packet transmission. A novel fixed-point analytical model is developed to accommodate discontinuous wireless packet loss rate and queue service rate of this dual-regime queuing system, which is validated with extensive ns-3 simulations. We model the boundary solution as the queue occupancy oscillating in the close vicinity of the boundary such that TCP sources perceive effectively a single queue with a “weighted average” behavior of the underlying two regimes. In this respect, the more the queue stays in one of the regimes, the more this regime contributes to the resulting packet loss rate and service rate, and the closed-loop operation of TCP establishes a balance between the two regimes. If carefully designed, dual-regime operation may have a stabilizing effect on the queue occupancy meaning that the queue rarely visits undesirable “full queue” and “empty queue” states, which is also the primary objective of the AQM schemes. The numerical studies led us to propose a target PER around 5×10^{-4} and 5×10^{-2} to the first and the second regimes of the queue, respectively, while fixing the queue threshold (i.e., regime boundary) to around twenty packets. For the harmony between QAWLA and AQM policies, we strongly recommend locating the regime boundary of QAWLA at a level lower than the queue threshold of AQM after which packets are probabilistically dropped to avoid buffer overflow. We show that performance of QAWLA exceeds that of TAGLA in terms of average and worst case TCP throughput and also in

terms of robustness with its relatively less sensitivity to the choice of the PER threshold. Such throughput improvement is shown to persist even when channel statistics are not precisely known.

In Chapter 6, we remove the bottleneck wireless link assumption made so far by developing a solver for interference-free multi-hop wireless networks with arbitrary topologies. By this solver, we present an Energy efficient and Queue-AWare Link Adaptation scheme with HARQ called EnQAWLAWH. EnQAWLAWH targets network-wide energy saving by means of decreasing transmission rates and powers of wireless links down to a level at which the contending TCP flows suffer from little or no throughput loss. To this end, we propose a dual-regime queue so as to choose a MCS with lower spectral efficiency controlled by an MCS offset parameter allowing to back-off the transmission power when the queue occupancy level stays below a certain queue threshold. We first validate the accuracy of the approximate resequencing delay for dual-regime wireless links with MATLAB® simulations and then validate the proposed analytical model for EnQAWLAWH with ns-3 simulations. We evaluate the performance of EnQAWLAWH over a wide range of scenarios with various channel SNR values, number of flows, flow distributions and network topologies. Overall results indicate that a considerable energy saving is achievable by the proposed policy at the expense of an acceptable throughput degradation depending on the associated cost. Due to curse of dimensionality, we first tailor the parameters of EnQAWLAWH for a limited set of wireless, traffic and network scenarios and then evaluate the performance of the resulting EnQAWLAWH scheme with fixed parameters for a more diverse set of scenarios. Specifically, we find the MCS offset and the queue threshold parameters of EnQAWLAWH to be 3 indices and 4 packets, respectively, which maximizes the average network performance for deterministic SNR and flow distribution scenarios and for the example 3 to 1 ratio of weights attributed to throughput and power, respectively. Subsequently, we test this pair of parameters under different network settings including random SNR and flow distributions with various numbers of flows to show varying degrees of performance gains.

In conclusion, we propose a cross-layer queuing analysis framework for TCP-level throughput performance of TAGLA and TAGLAWH link adaptation schemes

with and without HARQ, respectively, which are both traffic-agnostic. In the light of the results obtained in this thesis, we also draw some guidelines to operate TAGLA and TAGLAWH schemes in a wireless bottleneck. Moreover, we propose a novel cross-layer dual-regime queuing analysis framework upon which QAWLA, a novel queue-aware link adaptation scheme without HARQ, is developed. QAWLA improves upon TAGLA in terms of overall TCP-level throughput performance and robustness against both channel estimations and threshold selections. Finally, we generalize the aforementioned dual-regime queuing analysis framework to the network of such queues in order to study EnQAWLAWH, which is both energy efficient and queue-aware. We show varying degrees of overall network performance gains expressed as a function of both power and throughput values of the wireless links, with possible throughput degradation due to increased RTTs. Future work consists of studying EnQAWLAWH under UDP-based traffic under certain QoS constraints, which reacts neither to an increase in RTT nor to packet losses. Extending dual-regime queues of QAWLA and EnQAWLAWH schemes to multi-regime queues is another subject for future study. Modeling interference-limited networks constitutes another potential major research direction.

Bibliography

- [1] “Guidelines for evaluation of radio transmission technologies for IMT-2000,” *Recommendation ITU-R M.1225*, 1997.
- [2] “ns-3,” 2015. <http://www.nsnam.org/>.
- [3] H. Balakrishnan, V. Padmanabhan, S. Seshan, and R. Katz, “A comparison of mechanisms for improving TCP performance over wireless links,” *Networking, IEEE/ACM Transactions on*, vol. 5, no. 6, pp. 756–769, 1997.
- [4] C. Barakat and E. Altman, “Bandwidth tradeoff between TCP and link-level FEC,” *Comput. Netw.*, vol. 39, pp. 133–150, Jun. 2002.
- [5] J. Padhye, V. Firoiu, D. Towsley, and J. Kurose, “Modeling TCP throughput: A simple model and its empirical validation,” *SIGCOMM Comput. Commun. Rev.*, vol. 28, pp. 303–314, Oct. 1998.
- [6] F. Vacirca, A. De Vendictis, and A. Baiocchi, “Optimal design of hybrid FEC/ARQ schemes for TCP over wireless links with Rayleigh fading,” *IEEE Transactions on Mobile Computing*, vol. 5, pp. 289–302, Apr. 2006.
- [7] K.-C. Go, J.-R. Cha, S. K. Oh, and J.-H. Kim, “End-to-end performance analysis based on cross-layer retransmission scheme in wireless communication system,” *The International Conference on Information Networking 2013 (ICOIN)*, vol. 0, pp. 141–144, Jan. 2013.
- [8] D. Moltchanov, “A study of TCP performance in wireless environment using fixed-point approximation,” *Computer Networks*, vol. 56, pp. 1263–1285, Mar. 2012.

- [9] O. Ozturk and N. Akar, "Workload-dependent queuing model of an AQM-controlled wireless router with TCP traffic and its application to PER-based link adaptation," *EURASIP Journal on Wireless Communications and Networking*, vol. 67, Apr. 2014.
- [10] R. Bekker, S. Borst, O. Boxma, and O. Kella, "Queues with workload-dependent arrival and service rates," *Queueing Systems*, vol. 46, no. 3-4, pp. 537–556, 2004.
- [11] A. Misra, T. Ott, and J. Baras, "The window distribution of multiple TCPs with random loss queues," in *Global Telecommunications Conference, 1999. GLOBECOM '99*, vol. 3, pp. 1714–1726 vol.3, Dec. 1999.
- [12] T. Bu and D. Towsley, "Fixed point approximations for TCP behavior in an AQM network," *SIGMETRICS Perform. Eval. Rev.*, vol. 29, pp. 216–225, Jun. 2001.
- [13] "QoS: Congestion avoidance configuration guide, Cisco IOS release 15.0M," tech. rep., CISCO, 2011.
- [14] M. Wurtzler, "Analysis and simulation of Weighted Random Early Detection (WRED) queues," Master's thesis, University of Kansas, 2003.
- [15] J. Ramis and G. Femenias, "Cross-layer design of adaptive multirate wireless networks using truncated HARQ," *Vehicular Technology, IEEE Transactions on*, vol. 60, pp. 944–954, Mar. 2011.
- [16] O. Ozturk and N. Akar, "Analysis of an adaptive modulation and coding scheme with HARQ for TCP traffic," in *Wireless Telecommunications Symposium (WTS), 2015*, pp. 1–6, Apr. 2015.
- [17] J. Huang and Z. Niu, "Buffer-aware and traffic-dependent packet scheduling in wireless OFDM networks," in *Wireless Communications and Networking Conference, 2007.WCNC 2007. IEEE*, pp. 1554–1558, Mar. 2007.
- [18] Y. Lin and G. Yue, "Channel-adapted and buffer-aware packet scheduling in LTE wireless communication system," in *Wireless Communications*,

Networking and Mobile Computing, 2008. WiCOM '08. 4th International Conference on, pp. 1–4, Oct. 2008.

- [19] D. Niyato and E. Hossain, “Queue-aware uplink bandwidth allocation and rate control for polling service in IEEE 802.16 broadband wireless networks,” *Mobile Computing, IEEE Transactions on*, vol. 5, pp. 668–679, Jun. 2006.
- [20] G. Song, Y. Li, and L. Cimini, “Joint channel- and queue-aware scheduling for multiuser diversity in wireless OFDMA networks,” *Communications, IEEE Transactions on*, vol. 57, pp. 2109–2121, Jul. 2009.
- [21] E. Uysal-Biyikoglu and A. El Gamal, “On adaptive transmission for energy efficiency in wireless data networks,” *Information Theory, IEEE Transactions on*, vol. 50, pp. 3081–3094, Dec. 2004.
- [22] X. Li, X. Dong, and D. Wu, “Hierarchical queue-length-aware power control for delay-sensitive applications over wireless networks,” in *Military Communications Conference, 2008. MILCOM 2008. IEEE*, pp. 1–6, Nov. 2008.
- [23] E. C. Strinati, A. De Domenico, and L. Herault, “Green communications: an emerging challenge for mobile broadband communication networks,” *Journal of Green Engineering*, vol. 1, no. 3, pp. 267–301, 2011.
- [24] M. I. Salman, C. K. Ng, N. K. Noordin, B. M. Ali, and A. Sali, “A self-configured link adaptation for green LTE downlink transmission,” *Transactions on Emerging Telecommunications Technologies*, vol. 26, no. 2, pp. 258–275, 2015.
- [25] X. Li, X. Dong, and D. Wu, “On optimal power control for delay-constrained communication over fading channels,” *Information Theory, IEEE Transactions on*, vol. 57, pp. 3371–3389, Jun. 2011.
- [26] X. Ao, S. Jiang, and L. Tang, “Traffic-aware active link rate adaptation via power control for multi-hop multi-rate 802.11 networks,” in *Communication Technology (ICCT), 2010 12th IEEE International Conference on*, pp. 1255–1259, Nov. 2010.

- [27] M. Chiang and J. Bell, “Balancing supply and demand of bandwidth in wireless cellular networks: Utility maximization over powers and rates,” in *INFOCOM 2004. Twenty-third Annual Joint Conference of the IEEE Computer and Communications Societies*, vol. 4, pp. 2800–2811 vol.4, Mar. 2004.
- [28] M. Chiang, “Balancing transport and physical layers in wireless multihop networks: Jointly optimal congestion control and power control,” *Selected Areas in Communications, IEEE Journal on*, vol. 23, pp. 104–116, Jan. 2005.
- [29] T. M. C. Chu, H. Phan, and H.-J. Zepernick, “Adaptive modulation and coding with queue awareness in cognitive incremental decode-and-forward relay networks,” in *Communications (ICC), 2014 IEEE International Conference on*, pp. 1453–1459, Jun. 2014.
- [30] E. Eraslan, C.-Y. Wang, and B. Daneshrad, “Practical energy-aware link adaptation for MIMO-OFDM systems,” *Wireless Communications, IEEE Transactions on*, vol. 13, pp. 246–258, Jan. 2014.
- [31] P. Chevillat, J. Jelitto, and H. L. Truong, “Dynamic data rate and transmit power adjustment in IEEE 802.11 wireless LANs,” *International Journal of Wireless Information Networks*, vol. 12, no. 3, pp. 123–145, 2005.
- [32] E. Uysal-Biyikoglu, B. Prabhakar, and A. El Gamal, “Energy-efficient packet transmission over a wireless link,” *Networking, IEEE/ACM Transactions on*, vol. 10, pp. 487–499, Aug. 2002.
- [33] D. Feng, C. Jiang, G. Lim, J. Cimini, L.J., G. Feng, and G. Li, “A survey of energy-efficient wireless communications,” *Communications Surveys Tutorials, IEEE*, vol. 15, pp. 167–178, Feb. 2013.
- [34] Z. Hasan, H. Boostanimehr, and V. Bhargava, “Green cellular networks: A survey, some research issues and challenges,” *Communications Surveys Tutorials, IEEE*, vol. 13, pp. 524–540, Nov. 2011.
- [35] U. Kozat, I. Koutsopoulos, and L. Tassiulas, “A framework for cross-layer design of energy-efficient communication with QoS provisioning in multihop wireless networks,” in *INFOCOM 2004. Twenty-third Annual Joint*

- Conference of the IEEE Computer and Communications Societies*, vol. 2, pp. 1446–1456 vol.2, Mar. 2004.
- [36] M. del Rey, “Transmission control protocol,” RFC 793, RFC Editor, Sept. 1981.
 - [37] J. Postel, “User datagram protocol,” RFC 768, RFC Editor, Aug. 1980.
 - [38] R. Mok, E. Chan, and R. Chang, “Measuring the quality of experience of HTTP video streaming,” in *Integrated Network Management (IM), 2011 IFIP/IEEE International Symposium on*, pp. 485–492, May 2011.
 - [39] V. Jacobson, “Congestion avoidance and control,” *SIGCOMM Comput. Commun. Rev.*, vol. 18, pp. 314–329, Aug. 1988.
 - [40] Y. Tian, K. Xu, and N. Ansari, “TCP in wireless environments: Problems and solutions,” *Communications Magazine, IEEE*, vol. 43, pp. 27–32, Mar. 2005.
 - [41] V. Jacobson, “Modified TCP congestion avoidance algorithm,” tech. rep., Apr. 1990. end2end-interest mailing list <ftp://ftp.isi.edu/end2end/end2end-interest-1990.mail>.
 - [42] A. De Vindictis and A. Baiocchi, “Modeling a mixed TCP Vegas and TCP Reno scenario,” in *NETWORKING 2002: Networking Technologies, Services, and Protocols; Performance of Computer and Communication Networks; Mobile and Wireless Communications* (E. Gregori, M. Conti, A. Campbell, G. Omidyar, and M. Zukerman, eds.), vol. 2345 of *Lecture Notes in Computer Science*, pp. 612–623, Springer Berlin Heidelberg, 2002.
 - [43] L. Brakmo and L. Peterson, “TCP Vegas: End to end congestion avoidance on a global Internet,” *Selected Areas in Communications, IEEE Journal on*, vol. 13, pp. 1465–1480, Oct. 1995.
 - [44] K. Tan, J. Song, Q. Zhang, and M. Sridharan, “A compound TCP approach for high-speed and long distance networks,” in *INFOCOM 2006. 25th IEEE International Conference on Computer Communications. Proceedings*, pp. 1–12, Apr. 2006.

- [45] S. Ha, I. Rhee, and L. Xu, “CUBIC: A New TCP-friendly high-speed TCP variant,” *SIGOPS Oper. Syst. Rev.*, vol. 42, pp. 64–74, Jul. 2008.
- [46] P. Yang, J. Shao, W. Luo, L. Xu, J. Deogun, and Y. Lu, “TCP congestion avoidance algorithm identification,” *Networking, IEEE/ACM Transactions on*, vol. 22, pp. 1311–1324, Aug. 2014.
- [47] H. Elaarag, “Improving TCP performance over mobile networks,” *ACM Comput. Surv.*, vol. 34, pp. 357–374, Sept. 2002.
- [48] A. Bakre and B. Badrinath, “I-TCP: Indirect TCP for mobile hosts,” in *Distributed Computing Systems, 1995., Proceedings of the 15th International Conference on*, pp. 136–143, May 1995.
- [49] H. Balakrishnan, S. Seshan, and R. H. Katz, “Improving reliable transport and handoff performance in cellular wireless networks,” *Wirel. Netw.*, vol. 1, pp. 469–481, Dec. 1995.
- [50] C. P. Fu and S. Liew, “TCP Veno: TCP enhancement for transmission over wireless access networks,” *Selected Areas in Communications, IEEE Journal on*, vol. 21, pp. 216–228, Feb. 2003.
- [51] K. Xu, Y. Tian, and N. Ansari, “TCP-Jersey for wireless IP communications,” *Selected Areas in Communications, IEEE Journal on*, vol. 22, pp. 747–756, May 2004.
- [52] K. Xu, Y. Tian, and N. Ansari, “Improving TCP performance in integrated wireless communications networks,” *Computer Networks*, vol. 47, pp. 219–237, Feb. 2005.
- [53] J. Kim, J. Koo, and H. Choo, “TCP NJ+: Packet loss differentiated transmission mechanism robust to high BER environments,” in *NETWORKING 2007. Ad Hoc and Sensor Networks, Wireless Networks, Next Generation Internet* (I. Akyildiz, R. Sivakumar, E. Ekici, J. Oliveira, and J. McNair, eds.), vol. 4479 of *Lecture Notes in Computer Science*, pp. 380–390, Springer Berlin Heidelberg, 2007.

- [54] S. Henna, “A throughput analysis of TCP variants in mobile wireless networks,” in *Next Generation Mobile Applications, Services and Technologies, 2009. NGMAST '09. Third International Conference on*, pp. 279–284, Sept. 2009.
- [55] J. Sundararajan, D. Shah, M. Medard, S. Jakubczak, M. Mitzenmacher, and J. Barros, “Network coding meets TCP: Theory and implementation,” *Proceedings of the IEEE*, vol. 99, pp. 490–512, Mar. 2011.
- [56] Y. Chi and D. P. Agrawal, “TCP-Forward: Fast and reliable TCP variant for wireless networks,” *CoRR*, vol. abs/1408.2626, 2014.
- [57] M. Luby, “LT codes,” in *Foundations of Computer Science, 2002. Proceedings. The 43rd Annual IEEE Symposium on*, pp. 271–280, Nov. 2002.
- [58] J. W. Byers, M. Luby, M. Mitzenmacher, and A. Rege, “A digital fountain approach to reliable distribution of bulk data,” *SIGCOMM Comput. Commun. Rev.*, vol. 28, pp. 56–67, Oct. 1998.
- [59] V. Kokshenev and S. Suschenko, “Analytical model of the TCP Reno congestion control procedure through a discrete-time Markov chain,” in *Distributed Computer and Communication Networks* (V. Vishnevsky, D. Kozyrev, and A. Larionov, eds.), vol. 279 of *Communications in Computer and Information Science*, pp. 124–135, Springer International Publishing, 2014.
- [60] M. Mathis, J. Semke, J. Mahdavi, and T. Ott, “The macroscopic behavior of the TCP congestion avoidance algorithm,” *Computer Communication Review*, vol. 27, no. 3, pp. 67–82, 1997.
- [61] P. Lassila, H. van den Berg, M. Mandjes, and R. Kooij, “An integrated packet/flow model for TCP performance analysis,” in *Providing quality of service in heterogeneous environments* (J. Charzinski, R. Lehnert, and P. Tran-Gia, eds.), vol. 5a of *Teletraffic Science and Engineering*, (Amsterdam), pp. 651–660, Elsevier, 2003.

- [62] B. Braden, D. Clark, J. Crowcroft, B. Davie, S. Deering, D. Estrin, S. Floyd, V. Jacobson, G. Minshall, C. Partridge, L. Peterson, K. Ramakrishnan, S. Shenker, J. Wroclawski, and L. Zhang, “Recommendations on queue management and congestion avoidance in the Internet,” RFC 2309, RFC Editor, Apr. 1998.
- [63] E. S. Hashem, *Analysis of random drop for gateway congestion control*. PhD thesis, Massachusetts Institute of Technology, 1989.
- [64] S. Athuraliya, S. Low, V. Li, and Q. Yin, “REM: Active queue management,” *Network, IEEE*, vol. 15, pp. 48–53, May 2001.
- [65] M. Hassan and R. Jain, *High performance TCP/IP networking: Concepts, issues, and solutions*. US: Pearson, 2004.
- [66] S. Floyd and V. Jacobson, “Random early detection gateways for congestion avoidance,” *Networking, IEEE/ACM Transactions on*, vol. 1, pp. 397–413, Aug. 1993.
- [67] H. Abdel-jaber, F. Thabtah, A. M. Daoud, J. Ababneh, and M. Baklizi, “Performance investigations of some active queue management techniques using simulation,” *International Journal of New Computer Architectures and their Applications (IJNCAA)*, vol. 2, no. 1, pp. 286–301, 2012.
- [68] S. Floyd, “Recommendation on using the Gentle variant of RED,” tech. rep., Mar. 2000.
- [69] R. Adams, “Active queue management: A survey,” *Communications Surveys Tutorials, IEEE*, vol. 15, pp. 1425–1476, Third 2013.
- [70] J. Lakkakorpi, A. Sayenko, J. Karhula, O. Alanen, and J. Moilanen, “Active queue management for reducing downlink delays in WiMAX,” in *Vehicular Technology Conference, 2007. VTC-2007 Fall. 2007 IEEE 66th*, pp. 326–330, Sept. 2007.
- [71] “WiMAX Forum,” 2015. <http://www.wimaxforum.org/>.
- [72] K. Nichols and V. Jacobson, “Controlling queue delay,” *Commun. ACM*, vol. 55, pp. 42–50, Jul. 2012.

- [73] R. J. Gibbens, S. K. Sargood, C. V. Eijl, F. P. Kelly, H. Azmoodeh, R. N. Macfadyen, and N. W. Macfadyen, “Fixed-point models for the end-to-end performance analysis of IP networks,” in *Proceedings of the 13th ITC Specialist Seminar: IP Traffic Measurement, Modeling and Management*, Sept. 2000.
- [74] “LTE,” 2015. <http://www.3gpp.org/>.
- [75] “IEEE standard for local and metropolitan area networks part 16: Air interface for broadband wireless access systems,” *IEEE Std 802.16-2009 (Revision of IEEE Std 802.16-2004)*, pp. 1–2004, 2009.
- [76] T. Jiang and Y. Wu, “An overview: Peak-to-average power ratio reduction techniques for OFDM signals,” *Broadcasting, IEEE Transactions on*, vol. 54, pp. 257–268, Jun. 2008.
- [77] J. Joung, C. K. Ho, K. Adachi, and S. Sun, “A survey on power-amplifier-centric techniques for spectrum- and energy-efficient wireless communications,” *Communications Surveys Tutorials, IEEE*, vol. 17, pp. 315–333, Firstquarter 2015.
- [78] Y. Zhao and S. Haggman, “Sensitivity to doppler shift and carrier frequency errors in OFDM systems-the consequences and solutions,” in *Vehicle Technology Conference, 1996. Mobile Technology for the Human Race., IEEE 46th*, vol. 3, pp. 1564–1568 vol.3, Apr. 1996.
- [79] I. E. Telatar *et al.*, “Capacity of multi-antenna Gaussian channels,” *European Transactions on Telecommunications*, vol. 10, no. 6, pp. 585–595, 1999.
- [80] A. Goldsmith, S. Jafar, N. Jindal, and S. Vishwanath, “Capacity limits of MIMO channels,” *Selected Areas in Communications, IEEE Journal on*, vol. 21, pp. 684–702, Jun. 2003.
- [81] C. Oestges, V. Erceg, and A. Paulraj, “A physical scattering model for MIMO macrocellular broadband wireless channels,” *Selected Areas in Communications, IEEE Journal on*, vol. 21, pp. 721–729, Jun. 2003.

- [82] R. Heath and A. Paulraj, "Switching between diversity and multiplexing in MIMO systems," *Communications, IEEE Transactions on*, vol. 53, pp. 962–968, Jun. 2005.
- [83] S. Alamouti, "A simple transmit diversity technique for wireless communications," *Selected Areas in Communications, IEEE Journal on*, vol. 16, pp. 1451–1458, Oct. 1998.
- [84] Y. seok Choi and S. Alamouti, "A pragmatic PHY abstraction technique for link adaptation and MIMO switching," *Selected Areas in Communications, IEEE Journal on*, vol. 26, pp. 960–971, Aug. 2008.
- [85] S. Catreux, V. Erceg, D. Gesbert, and R. W. Heath, Jr., "Adaptive modulation and MIMO coding for broadband wireless data networks," *Communications Magazine, IEEE*, vol. 40, pp. 108–115, Jun. 2002.
- [86] S. T. Chung and A. Goldsmith, "Degrees of freedom in adaptive modulation: A unified view," *Communications, IEEE Transactions on*, vol. 49, pp. 1561–1571, Sept. 2001.
- [87] J. Yang, N. Tin, and A. Khandani, "Adaptive modulation and coding in 3G wireless systems," in *Vehicular Technology Conference, 2002. Proceedings. VTC 2002-Fall. 2002 IEEE 56th*, vol. 1, pp. 544–548 vol.1, 2002.
- [88] H. Chen, H. C. Chan, C.-K. Chan, and V. C. Leung, "QoS-based cross-layer scheduling for wireless multimedia transmissions with adaptive modulation and coding," *Communications, IEEE Transactions on*, vol. 61, pp. 4526–4538, Nov. 2013.
- [89] K.-C. Go and J.-H. Kim, "Application-aware MCS level selection method for cross-layered retransmission scheme," *Communications Letters, IEEE*, vol. 18, pp. 209–212, Feb. 2014.
- [90] Q. Liu, S. Zhou, and G. Giannakis, "Queuing with adaptive modulation and coding over wireless links: Cross-layer analysis and design," *Wireless Communications, IEEE Transactions on*, vol. 4, pp. 1142–1153, May 2005.

- [91] M. Lampe, T. Giebel, H. Rohling, and W. Zirwas, “PER-prediction for PHY mode selection in OFDM communication systems,” in *IEEE Global Telecommunications Conference, GLOBECOM '03*, pp. 25–29, 2003.
- [92] G. Martorell, F. Riera-Palou, and G. Femenias, “Cross-layer fast link adaptation for MIMO-OFDM based WLANs,” *Wirel. Pers. Commun.*, vol. 56, pp. 599–609, Feb. 2011.
- [93] J. Francis and N. Mehta, “EESM-based link adaptation in point-to-point and multi-cell OFDM systems: Modeling and analysis,” *Wireless Communications, IEEE Transactions on*, vol. 13, pp. 407–417, Jan. 2014.
- [94] S.-H. T. Mathias Pauli, Udo Wachsmann, “Quality determination for a wireless communications link,” Nov. 2004. Patent US20040219883.
- [95] A. K. A. Tamimi, “Exponential effective signal to noise ratio mapping (EESM) computation for WiMAX physical layer,” Master’s thesis, Sever Institute of Washington University, 2007.
- [96] S. Mumtaz, A. Gamberio, and J. Rodriguez, “EESM for IEEE 802.16e: WiMaX,” in *Computer and Information Science, 2008. ICIS 08. Seventh IEEE/ACIS International Conference on*, pp. 361–366, May 2008.
- [97] J. Fan, Q. Yin, G. Li, B. Peng, and X. Zhu, “MCS selection for throughput improvement in downlink LTE systems,” in *Computer Communications and Networks (ICCCN), 2011 Proceedings of 20th International Conference on*, pp. 1–5, Jul. 2011.
- [98] H. Liu, L. Cai, H. Yang, and D. Li, “EESM based link error prediction for adaptive MIMO-OFDM system,” in *Vehicular Technology Conference, 2007. VTC2007-Spring. IEEE 65th*, pp. 559–563, Apr. 2007.
- [99] K. Sayana, J. Zhuang, and K. Stewart, “Link performance abstraction based on mean mutual information per bit MMIB of the LLR channel,” tech. rep., Motorola, May 2007.
- [100] Y. Blankenship, P. Sartori, B. Classon, V. Desai, and K. Baum, “Link error prediction methods for multicarrier systems,” in *Vehicular Technology*

Conference, 2004. VTC2004-Fall. 2004 IEEE 60th, vol. 6, pp. 4175–4179
Vol. 6, Sept. 2004.

- [101] “Evolved Universal Terrestrial Radio Access (E-UTRA); Physical layer procedures,” *2015-3GPP TS 36.213 version 12.5.0 Release 12*, Apr. 2015.
- [102] J. Ikuno, M. Wrulich, and M. Rupp, “System level simulation of LTE networks,” in *Vehicular Technology Conference (VTC 2010-Spring)*, 2010 *IEEE 71st*, pp. 1–5, May 2010.
- [103] R. Bruno, A. Masaracchia, and A. Passarella, “Robust adaptive modulation and coding (AMC) selection in LTE systems using reinforcement learning,” in *Vehicular Technology Conference (VTC Fall), 2014 IEEE 80th*, pp. 1–6, Sept. 2014.
- [104] S. Donthi and N. Mehta, “An accurate model for EESM and its application to analysis of CQI feedback schemes and scheduling in LTE,” *Wireless Communications, IEEE Transactions on*, vol. 10, pp. 3436–3448, Oct. 2011.
- [105] A. Krishnamoorthy, Y. Blankenship, P. Sartori, K. Baum, and B. Classon, “Enhanced link adaptation methods for wireless multi-carrier systems,” in *Vehicular Technology Conference, 2007. VTC2007-Spring. IEEE 65th*, pp. 1911–1915, Apr. 2007.
- [106] R. Yaniv, D. Stopler, T. Kaitz, and K. Blum, “CINR measurements using the EESM method, C80216e-05-141r2,” tech. rep., IEEE 802.16 Broadband Wireless Access Working Group, Mar. 2005.
- [107] A. Kuhne and A. Klein, “Throughput analysis of multi-user OFDMA-systems using imperfect CQI feedback and diversity techniques,” *Selected Areas in Communications, IEEE Journal on*, vol. 26, pp. 1440–1450, Oct. 2008.
- [108] S. Guharoy and N. Mehta, “Joint evaluation of channel feedback schemes, rate adaptation, and scheduling in OFDMA downlinks with feedback delays,” *Vehicular Technology, IEEE Transactions on*, vol. 62, pp. 1719–1731, May 2013.

- [109] J. Francis and N. Mehta, “Impact of feedback delays on EESM-based wide-band link adaptation: Modeling and analysis,” in *Global Communications Conference (GLOBECOM), 2014 IEEE*, pp. 3952–3957, Dec. 2014.
- [110] H. Chen, R. Maunder, and L. Hanzo, “A survey and tutorial on low-complexity turbo coding techniques and a holistic hybrid ARQ design example,” *Communications Surveys Tutorials, IEEE*, vol. 15, pp. 1546–1566, Fourth 2013.
- [111] D. Chase, “Code combining—a maximum-likelihood decoding approach for combining an arbitrary number of noisy packets,” *Communications, IEEE Transactions on*, vol. 33, pp. 385–393, May 1985.
- [112] D. Chase, “A combined coding and modulation approach for communication over dispersive channels,” *Communications, IEEE Transactions on*, vol. 21, pp. 159–174, Mar. 1973.
- [113] T. Chaitanya and E. Larsson, “Optimal power allocation for hybrid ARQ with Chase combining in i.i.d. Rayleigh fading channels,” *Communications, IEEE Transactions on*, vol. 61, pp. 1835–1846, May 2013.
- [114] D. Mandelbaum, “An adaptive-feedback coding scheme using incremental redundancy (corresp.),” *Information Theory, IEEE Transactions on*, vol. 20, pp. 388–389, May 1974.
- [115] S. Lin and P. Yu, “A hybrid ARQ scheme with parity retransmission for error control of satellite channels,” *Communications, IEEE Transactions on*, vol. 30, pp. 1701–1719, Jul. 1982.
- [116] A. Larmo, M. Lindstrom, M. Meyer, G. Pelletier, J. Torsner, and H. Wiermann, “The LTE link-layer design,” *Communications Magazine, IEEE*, vol. 47, pp. 52–59, Apr. 2009.
- [117] M. Laor and L. Gendel, “The effect of packet reordering in a backbone link on application throughput,” *Network, IEEE*, vol. 16, pp. 28–36, Sept. 2002.

- [118] J. Li and Y. Zhao, “Resequencing analysis of Stop-and-Wait ARQ for parallel multichannel communications,” *Networking, IEEE/ACM Transactions on*, vol. 17, no. 3, pp. 817–830, 2009.
- [119] “IEEE standard for local and metropolitan area networks part 16: Air interface for broadband wireless access systems. Amendment 3: advanced air interface,” *IEEE Std 802.16m-2011 Amendment to IEEE Std 802.16-2009*, pp. 1–1064, 2011.
- [120] V. Mhatre, K. Papagiannaki, and F. Baccelli, “Interference mitigation through power control in high density 802.11 WLANs,” in *INFOCOM 2007. 26th IEEE International Conference on Computer Communications. IEEE*, pp. 535–543, May 2007.
- [121] E. Hossain, M. Rasti, H. Tabassum, and A. Abdelnasser, “Evolution toward 5G multi-tier cellular wireless networks: An interference management perspective,” *Wireless Communications, IEEE*, vol. 21, pp. 118–127, Jun. 2014.
- [122] E. Biton, A. Cohen, G. Reina, and O. Gurewitz, “Distributed inter-cell interference mitigation via joint scheduling and power control under noise rise constraints,” *Wireless Communications, IEEE Transactions on*, vol. 13, pp. 3464–3477, Jun. 2014.
- [123] J. Chen, C.-C. Yang, and S.-T. Sheu, “Downlink femtocell interference mitigation and achievable data rate maximization: Using FBS association and transmit power-control schemes,” *Vehicular Technology, IEEE Transactions on*, vol. 63, pp. 2807–2818, Jul. 2014.
- [124] G. Biczak, J. Malmudin, and A. Fehske, “Economic and ecological impact of ICT,” Tech. Rep. Energy Aware Radio and network Technologies (EARTH) Deliverable D2.1, FP7, Apr. 2011.
- [125] L. Correia, D. Zeller, O. Blume, D. Ferling, Y. Jading, I. Godor, G. Auer, and L. Van der Perre, “Challenges and enabling technologies for energy aware mobile radio networks,” *Communications Magazine, IEEE*, vol. 48, pp. 66–72, Nov. 2010.

- [126] D. Kudavithana, Q. Chaudhari, B. Krongold, and J. Evans, "On the energy efficiency of coherent communication in multipath fading channels," in *Globecom Workshops (GC Wkshps), 2014*, pp. 1087–1093, Dec. 2014.
- [127] P. Frenger, P. Moberg, J. Malmudin, Y. Jading, and I. Godor, "Reducing energy consumption in LTE with cell DTX," in *Vehicular Technology Conference (VTC Spring), 2011 IEEE 73rd*, pp. 1–5, May 2011.
- [128] C. Han, T. Harrold, S. Armour, I. Krikidis, S. Videv, P. M. Grant, H. Haas, J. Thompson, I. Ku, C.-X. Wang, T. A. Le, M. Nakhai, J. Zhang, and L. Hanzo, "Green radio: Radio techniques to enable energy-efficient wireless networks," *Communications Magazine, IEEE*, vol. 49, pp. 46–54, June 2011.
- [129] S. Videv and H. Haas, "Energy-efficient scheduling and bandwidth-energy efficiency trade-off with low load," in *Communications (ICC), 2011 IEEE International Conference on*, pp. 1–5, June 2011.
- [130] R. Vaca Ramirez, J. Thompson, E. Altman, and M. Ramos R.Victor, "A game theory framework for a distributed and energy efficient bandwidth expansion process," in *Computer Communications Workshops (INFOCOM WKSHPS), 2014 IEEE Conference on*, pp. 712–717, Apr. 2014.
- [131] O. Oyman and S. Sandhu, "Non-ergodic power-bandwidth tradeoff in linear multi-hop networks," in *Information Theory, 2006 IEEE International Symposium on*, pp. 1514–1518, Jul. 2006.
- [132] C. Bae and W. Stark, "End-to-end energy-bandwidth tradeoff in multihop wireless networks," *Information Theory, IEEE Transactions on*, vol. 55, pp. 4051–4066, Sept. 2009.
- [133] C. Xiong, G. Li, S. Zhang, Y. Chen, and S. Xu, "Energy- and spectral-efficiency tradeoff in downlink OFDMA networks," *Wireless Communications, IEEE Transactions on*, vol. 10, pp. 3874–3886, Nov. 2011.
- [134] J. Wu, G. Wang, and Y. Zheng, "Energy efficiency and spectral efficiency tradeoff in Type-I ARQ systems," *Selected Areas in Communications, IEEE Journal on*, vol. 32, pp. 356–366, Feb. 2014.

- [135] W. Su, S. Lee, D. Pados, and J. Matyjas, “Optimal power assignment for minimizing the average total transmission power in Hybrid-ARQ Rayleigh fading links,” *Communications, IEEE Transactions on*, vol. 59, pp. 1867–1877, Jul. 2011.
- [136] J. Rao and A. Fapojuwo, “A survey of energy efficient resource management techniques for multicell cellular networks,” *Communications Surveys Tutorials, IEEE*, vol. 16, pp. 154–180, Feb. 2014.
- [137] M. H. Alsharif, R. Nordin, and M. Ismail, “Survey of green radio communications networks: Techniques and recent advances,” *Journal of Computer Networks and Communications*, 2013.
- [138] A. De Domenico, E. C. Strinati, and A. Capone, “Enabling green cellular networks: A survey and outlook,” *Computer Communications*, vol. 37, pp. 5–24, Jan. 2014.
- [139] G. Li, Z. Xu, C. Xiong, C. Yang, S. Zhang, Y. Chen, and S. Xu, “Energy-efficient wireless communications: Tutorial, survey, and open issues,” *Wireless Communications, IEEE*, vol. 18, pp. 28–35, Dec. 2011.
- [140] G. Miao, N. Himayat, Y. Li, and A. Swami, “Cross-layer optimization for energy-efficient wireless communications: A survey,” *Wireless Communications and Mobile Computing*, vol. 9, pp. 529–542, Apr. 2009.
- [141] V. Vasudevan, A. Phanishayee, H. Shah, E. Krevat, D. G. Andersen, G. R. Ganger, G. A. Gibson, and B. Mueller, “Safe and effective fine-grained TCP retransmissions for datacenter communication,” *SIGCOMM Comput. Commun. Rev.*, vol. 39, pp. 303–314, Aug. 2009.
- [142] E. Kuumola, J. Resing, and J. Virtamo, “Joint distribution of instantaneous and averaged queue length in an M/M/1/K system,” in *Proceedings of the 15th ITC Specialist Seminar Internet Traffic Engineering and Traffic Management*, pp. 58–67, 2002.
- [143] A. Misra and T. Ott, “The window distribution of idealized TCP congestion avoidance with variable packet loss,” in *INFOCOM ’99. Eighteenth Annual*

Joint Conference of the IEEE Computer and Communications Societies. Proceedings. IEEE, vol. 3, pp. 1564–1572, Mar. 1999.

- [144] H. Balakrishnan, V. N. Padmanabhan, G. Fairhurst, and M. Sooriyabandara, “TCP performance implications of network path asymmetry,” RFC 3449, RFC Editor, Dec. 2002.
- [145] T. J. Speight, “Efficient TCP ACK prioritization in wireless networks,” Apr. 2008. Patent US20080080464.
- [146] S. Floyd and E. Kohler, “Internet research needs better models,” *SIGCOMM Comput. Commun. Rev.*, vol. 33, pp. 29–34, Jan. 2003.
- [147] J. Hespanha, S. Bohacek, K. Obraczka, and J. Lee, “Hybrid modeling of TCP congestion control,” in *Hybrid Systems: Computation and Control* (M. Di Benedetto and A. Sangiovanni-Vincentelli, eds.), vol. 2034 of *Lecture Notes in Computer Science*, pp. 291–304, Springer Berlin Heidelberg, 2001.
- [148] G. Carneiro, P. Fortuna, and M. Ricardo, “FlowMonitor: A network monitoring framework for the network simulator 3 (NS-3),” in *Proceedings of the Fourth International ICST Conference on Performance Evaluation Methodologies and Tools, VALUETOOLS '09*, (ICST, Brussels, Belgium, Belgium), pp. 1:1–1:10, ICST (Institute for Computer Sciences, Social-Informatics and Telecommunications Engineering), 2009.
- [149] D. Chen, “On the analysis of using 802.16e WiMAX for point-to-point wireless backhaul,” in *Radio and Wireless Symposium, IEEE*, pp. 507–510, Jan. 2007.
- [150] J. de Carvalho, H. Veiga, P. Gomes, A. Reis, and R. Costa, “A contribution to experimental performance evaluation of point-to-point WiMAX links,” in *Signal Processing and Information Technology. ISSPIT 2008. IEEE International Symposium on*, pp. 150–153, 2008.
- [151] “PTP solutions guide Motorola fixed point-to-point wireless bridges,” 2015. <http://www.motorolasolutions.com/>.
- [152] “RDL-3000 System,” 2015. <http://rdlcom.com/>.

- [153] “Coded Modulation Library (CML),” 2015.
<http://www.iterativesolutions.com/>.
- [154] “WiMAX Forum mobile system profile: Release 1.5 TDD specific part,” tech. rep., WiMAX Forum, Mar 2009.
- [155] K. Zheng, X. Jiao, M. Liu, and Z. Li, “An analysis of resequencing delay of reliable transmission protocols over multipath,” in *Communications (ICC), 2010 IEEE International Conference on*, pp. 1–5, May 2010.
- [156] J. Li and Y. Zhao, “Resequencing analysis of Stop-and-Wait ARQ for parallel multichannel communications,” *Networking, IEEE/ACM Transactions on*, vol. 17, pp. 817–830, Jun. 2009.
- [157] N. Shacham and B.-C. Shin, “A selective-repeat-ARQ protocol for parallel channels and its resequencing analysis,” *Communications, IEEE Transactions on*, vol. 40, pp. 773–782, Apr. 1992.
- [158] F. Chiti, R. Fantacci, and A. Tassi, “Evaluation of the resequencing delay for selective repeat ARQ in TDD-based wireless communication systems,” *Vehicular Technology, IEEE Transactions on*, vol. 63, pp. 2450–2455, Jun. 2014.
- [159] Q. Liu, S. Zhou, and G. Giannakis, “TCP performance in wireless access with adaptive modulation and coding,” in *Communications, 2004 IEEE International Conference on*, vol. 7, pp. 3989–3993 Vol.7, Jun. 2004.
- [160] H. Jiang and C. Dovrolis, “Passive estimation of TCP round-trip times,” *SIGCOMM Comput. Commun. Rev.*, vol. 32, pp. 75–88, Jul. 2002.
- [161] V. Paxson, M. Allman, J. Chu, and M. Sargent, “Computing TCP’s retransmission timer,” RFC 6298, RFC Editor, Jun. 2011.
- [162] S. Chakraborty and S. Nandi, “Evaluating transport protocol performance over a wireless mesh backbone,” *Performance Evaluation*, vol. 79, no. 0, pp. 198 – 215, 2014. Special Issue: Performance 2014.